Active shielding based on implicit and decentralized control

Ricardo A. Quintana Soler

Advisors: Diego A. Patiño Guevara
Departmento de ingniería electrónica, Pontificia Universidad Javeriana
Bogotá, Colombia

August 10, 2018

Acknowledgements

To my advisor Diego Patiño, who was involved in this work providing high input given in this document. His guide was very helpful at any time. Also, the three professors help me during my Internship: Luigi Piroddi at the Politecnico di Milano, Yiu Lam at the Salford University and Stephen Elliott at the University of Southampton. I learned a lot from all of them, specially from the professor Lam that help me to define the principal concept in the document. Also, my friends at the Pontificia Universidad Javeriana George, José, Cesar, Francisco and Jean (RIP) , who give a hand to anyone who need to understand new topics and enjoy the time at the Ph.D. process.

Regarding the financial suport, I want to acknowledge to the Pontificia Universidad Javeriana for the support through the project "Control activo de un campo sonoro en tres dimensiones" with ID 6316. Also, I want to acknowledge to Colciencias (Departamento Administrativo de Ciencia, Tecnología e Innovación) for financing the Ricardo Quintana's doctoral student grant.

Finally, I would like to acknowledge to my family for the support given during the whole process. Probably the most important help I received. Many thanks for all of them. This work would not be the same without them.

Contents

Chapter 1

Introduction

The noise generated by industrial machines is an environmental and health issue. In the industry, the noise induced hearing loss is an studied problem. There are cases where workers are exposed to noises until 110dB [1]. This is a high risk for hearing health. A specific case of annoyance is the exposure to low frequency noise in the industries [2]. Also, it was shown that vibrations and low frequency noise produced the similar subjective perception because they are presented simultaneously [3].

Consequently, several laws around the world have banned noise emissions with high sound pressure levels. Specifically in Colombia, the government issued a legislation called "Resolución Número 1792 de 1990" for limiting the legal maximum noise levels to exposure. This problem makes researchers to think many solutions to reduce high noise levels. First, passive techniques were developed. They consist in modifying the physical conditions, as move or put a wall. Their performance obtains good results at high frequencies, but it is opposite at low frequencies. In order to control low frequency noise, the active noise control (ANC) techniques have been created. Instead of changing physical environment, they propose to use one or several controlled noise sources and, using the wave superposition phenomenon, to create an anti-noise wave such that it cancels the noise at receiver location [4].

Objetives

In industry applications, the noise is usually attenuated using the information obtained by a sensor (usually called the error microphone). The location of this sensor determines some coefficients of the control algorithms [4]. This variable changes the secondary path. Hence, sensor location is the maximum attenuation place, but the users cannot be located at this same position. As a consequence, this work proposes the next aim:

- Attenuate noise at a desired and big size area without using a sensor inside it.

The main contribution of this thesis is focused on the active shielding method (a more detailed explanation of why this method was chosen is in the next chapter). It consists of controlling the noise at boundaries of a desired region to generate cancellation inside. In order to show the knowledge contributed to the state of art there are two aims.

- Regarding the usability of the system, there are several control algorithms, but only few of them are used as active shielding methods. Furthermore, the active

shielding algorithms are not feedback control, which is less robust. Thus, the first aim is:

- Demonstrate that any multichannel control algorithm that ensures attenuation at sensor location can be used to generate a desired attenuation in a region through an active shielding method.

- Another limitation of active shielding is characteristic of a system with high number of sensors and actuators. It implies a high computational cost, which is not necessary achieved by actual hardware. Thus, decentralized control schemes have been created, which refers to several independent ANC systems interacting between them in the same acoustic environment. The convergence of control signals and error have not been determined. The second aim is:

  - Calculate the values of convergence of error and control signals for decentralized systems.

A deeply discussion of these objectives is carried out in next chapter, including the analysis of state of the art related to these topics.

Distribution of the thesis

This document is organized as follows:

* **Chapter 2:** This chapter presents basic concepts to understand the contribution of knowledge in future chapters and advances of other documents in this field. It begins describing the active noise control. Then, it is explained how the optimization is used to solve the active control problem. Therefore, the feedback and feed-forward control schemes are defined and the most representative control algorithms for them are mentioned. Regarding the algorithms that use these schemes, problems are remarked.

* **Chapter 3:** The linearity is convenient in several context due to its simplicity. However, some authors have emphasized the use of non-linear controller for ANC as an advantage. They propose non-linear control because: *i*) the secondary path is not linear. *ii*) The controller needs a non-causal filter, then the non-linear control reduces the error using a causal control. This chapter demonstrate the possibility to use linear control and its limitations. The linearity of secondary path is tested comparing measured noise with linear models obtained through identification systems. Causality of a control system is obtained analytically for one reflection system and then approximated to several reflections.

* **Chapter 4:** The main contribution to the state of the art is shown in this chapter, which achieves the aim of using different multichannel controller as an active shielding method. It is developed in order to attenuate noise in a desired silent zone without locate sensor inside of it. Its principle is based on a new concept called implicit control, which defines the phenomenon that the attenuation of pressure of a zone necessarily implies the attenuation at another location, due to its physical relationship. Then, discretizing the wave

equation through finite difference method, it is shown that implicit control is present in the system. When the pressure at boundary of a desired silent zone is attenuated, the pressure in the area inside of it too. This chapter shows the analysis for one and two dimensional systems and simulations for one, two and three dimensional systems.

* **Chapter 5:** Regarding implementation of active shielding methods, several multichannel ANC systems are used. Thus, computational cost is a problem. Other authors have proposed decentralized control, which consists in using several independent controllers. The issue in this case is understanding the behavior in steady state conditions. For this analysis, first an analogy between game theory and decentralized control systems is proposed. Then, the Nash equilibrium is obtained to understand when all controllers do not change their associated control signals.

* **Chapter 6:** The empirical validation is carried out using the conditions necessary to achieve the phenomenon called implicit control. Directly, it is validated the linear relationship between pressure at boundary and inside the silent zone for a one dimensional system (described in chapter 4). For the three dimensional system, it is validated the mathematical model that achieved the implicit control developed in chapter four.

Bibliographic production

Related to this thesis, in conferences and congresses, the next papers have been presented:

1. Ricardo Quintana, Diego Patino, "Identificación de sistemas aplicado a un recinto reverberante", IX Congreso Iberoamericano de Acústica, Valdivia, Chile, 2014.

2. R. Quintana, L. Piroddi, D. Patino, "Virtual sensing at low computational cost for active noise control", INTER-NOISE and NOISE-CON Congress and Conference Proceedings, vol. 250, no. 4, pp. 2989-2997, San Francisco, USA, 2015.

3. M. García, D. Patiño and R. Quintana, "DSP implementation of the FxLMS algorithm for active noise control: Texas instruments TSM320C6713DSK", 2015 IEEE 2nd Colombian Conference on Automatic Control (CCAC),pp. 1-6., Manizales, Colombia, 2015.

4. R. Quintana, D. Patino, "Active shielding based on implicit control: A one dimensional approach", INTER-NOISE and NOISE-CON Congress and Conference Proceedings, vol. 253, no. 8, pp. 88-96, Hamburg, Germany 2016.

5. R. Quintana and D. Patino, "Shielding the source", Proceedings of the ICA congress (online), http://ica2016.org.ar/website/wp-content/uploads/ICA2016_Proceedings.pdf, ICA 2016, Buenos Aires, Argentina, 2016.

6. R. Quintana, D. Patino, "Active shielding based on implicit control: non-zero attenuation at boundaries", INTER-NOISE and NOISE-CON Congress and Conference Proceedings, Hong Kong, China, 2017.

In journals, the next articles have been accepted:

1. Ricardo Quintana, Yiu Lam, Diego Patino, "Fundamentals of active shielding based on implicit control", In Journal of Sound and Vibration, Volume 408, 2017, Pages 1-19, ISSN 0022-460X, doi:10.1016/j.jsv.2017. 07.006.

2. Ricardo Quintana, Diego Patino, "A game-theoretical perspective for decentralized active noise control", In Journal of Vibration and Control, Accepted.

Chapter 2

Background context

Abstract
A general background of active noise control is shown in this chapter. It begins defining active noise control and the optimization problem involved with its optimal solutions. Then, the schemes feedback and feed-forward are described. The main control algorithms are mentioned and the Filter X Least Mean Squares (FxLMS) algorithm is deeply described. A problem related to the mentioned algorithms is that they produce local control at sensor location. The proposed solutions in literature are virtual sensing and active shielding. The computational cost is a limitation for these methodologies. Thus, distributed and decentralized control are described as a possible way to decrease this cost and make applicable the solutions. This chapter concludes remarking problems not solved in reviewed literature.

2.1 Introduction

This chapter presents the background and problems that are addressed in this document. Then, the aim is to describe the noise control systems and its operation. Active noise control (ANC) is a field with several applications and restrictions. This work is focused in active noise control for high size desired silent zone without using sensors inside of it. Also, the content of this chapter presents the general concepts to understand the whole document. It is defined active noise control, Feedback ANC, Feed-forward ANC, Filtered x Least Mean Squares algorithm, silent zone, virtual sensing, active shielding, decentralized and distributed control.

The chapter is organized with the next contents: first, the active noise control is described. Second, the problem of increasing the silent zone is depicted. Furthermore, to generate high silent zone, a massive multi-channel decentralized and distributed systems are mentioned. This chapter ends with some concluding remarks and the main contribution of this work.

2.2 Background of active noise control

Active noise control is a very well-known concept defined as:

Definition 2.2.1. ***[Active noise control (ANC)]*** *is the phenomenon in which undesired sound, that want to be silenced, is attenuated using the wave superpositions at a receiver location by reproducing sounds with opposite phase [5].*

If it is shown mathematically, ANC is based in a simple concept, also depicted in figure 2.1. According to wave superposition property, the total acoustic pressure $p(\chi, t)$ at χ location can be written as the sum of the components of pressure due to each source. Supposing there are only two sources, these components are named $p_1(\chi, t)$ and $p_2(\chi, t)$ and is achieved the next equation:

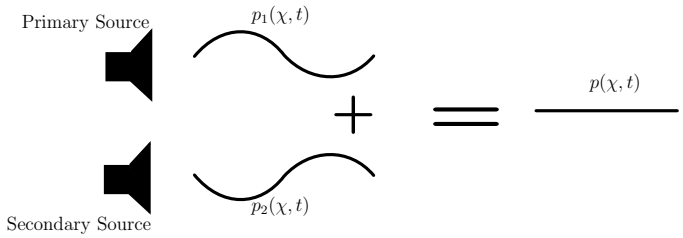

Figure 2.1: Concept of active noise control.

$$p(\chi, t) = p_1(\chi, t) + p_2(\chi, t) \tag{2.1}$$

It is easy to notice that if $p_1(\chi, t) = -p_2(\chi, t)$ then acoustic pressure is equal to zero. First approaches were published by Paul Leug and Coanda [6, 7]. The concept was explained through simple schemes. It was explained how two sine signals were canceled, if they have same frequency, amplitude and opposite phase.

Obtaining zero pressure is not always possible or getting a control signal is not simple. However, in any case, noise can be attenuated. Thus, an optimization process can be carried out (see [8] for basic concepts about optimization). There are several possible cost functions. In [9], three cost functions are compared. These functions are the integrated potential energy PE, the squared pressure SP and the energy density ED. They are defined by the next equations:

$$J_{PE} = \int_V \frac{|p(\chi, t)|^2}{4\rho_0 c_0} dX \tag{2.2}$$

$$J_{SP} = \sum_{i=1}^{I} |p(\chi_i, t)|^2 \tag{2.3}$$

$$J_{DE} = \sum_{i=1}^{I} \frac{|p(\chi_i, t)|^2}{4\rho_0 c_0} + \frac{\rho_0}{4} |V(X_i, t)|^2 \tag{2.4}$$

Where I is the number of actuators and $V(\chi_i, t) = [v_{X_1}(\chi_i, t), v_{X_2}(\chi_i, t), v_{X_3}(\chi_i, t)]$ is the particle velocity vector. It is important to remark that $p(\chi, t)$ is expressed as an complex exponential, then the magnitude is not affected by the time and simplify the analysis.

Notice that the pressure cannot be continuously measured for the whole space. It implies that J_{PE} is not measurable as well. Furthermore, the energy density allows to obtain lower sound pressure than squared pressure over different positions to the

sensors locations. Similar results are presented in [10] and [11]. Also, [12] shows that the norm l_∞ can be applied and the error is more homogeneous comparing the error value for all the microphones.

In [13] and [14], solutions for the optimization problem process in equation (2.2), using modal theory, produce the signal emitted (control signal) by controlled source (secondary source). For [13], the control signal is a transformation of the noise emitted by the primary source (uncontrolled noise source), scheme known as feed-forward control (described in definition 2.2.3). [14] gives its solution from wave equation. The modal theory has no known solutions for all shapes. Square rooms or even cylindrical are known and irregular enclosures are studied by [15]. [16] proposes a method to extract orthonormal set of structural radiation modes based on measurements and applies active control, which allows to obtain the modes for complex structures. Also, control of coupled structure to the acoustic room is studied by [17]. A deeply analysis in [18] and [19], divides the modes in clusters. [18] also finds that structural modes and acoustic modes interfere each other only if they are in the same cluster. Montazeri et al. coupled the acoustic environment not only with the structural, but also the loudspeakers of the active noise control [20, 21]. The case of an aperture such a window is analyzed by [22]. Some different modal analysis in active noise control are summarized in [23]. The modal analysis also allows to get conditions for the perfect noise cancellation [24].

Regarding the control algorithms, there are two schemes, both shown in figure 2.2, which are defined as follows:

Definition 2.2.2. ***[Feedback ANC]****: it is when the control signal of an ANC system is obtained processing only signals measured at desired attenuation location (error sensors) [4]. The figure 2.2.a shows a simple example of a feedback ANC.*

Suppose that the control signal $u(t)$ aims to cancel the noise at any location χ. Then, $u(t)$ is written as a function of the measured pressure at the attenuation location $e(t) = p(\chi, t)$:

$$u(t) = f_{fb}(e(t)) \tag{2.5}$$

Where $f_{fb}(\cdot)$ is a transformation that depends on the specific controller.

The basic common algorithms in this case are robust control [25], optimal control [26] and the Linear Quadratic Gaussian (LQG) [25]. Specifically, in active noise control applications, an early design of robust control is proposed in [27]. It identifies the transfer function which is used to obtain the feedback gain. A space state model is obtained in [28]. [29] proposes LQG control and the space state model is obtained through the modal response. A similar result is obtained in [30]. Also, an $\mathcal{H}_2$ controller is applied to a one dimensional enclosure [31]. Moreover, $\mathcal{H}_\infty$ controller is applied to a three dimensional enclosure [32].

The other scheme is defined as follows:

Definition 2.2.3. ***[Feed-forward ANC]****: it is the system which has a sensor that measures a reference signal. This signal is processed by controller to obtain the control signal. Furthermore, error microphone is used to update the process to increase control performance [4]. Figure 2.2.b shows this case.*

Suppose that the control signal $u(t)$ aims to cancel the noise at any location χ and primary source emits a noise $x(t)$. Then, $u(t)$ is written as a function of the pressure at the attenuation location:

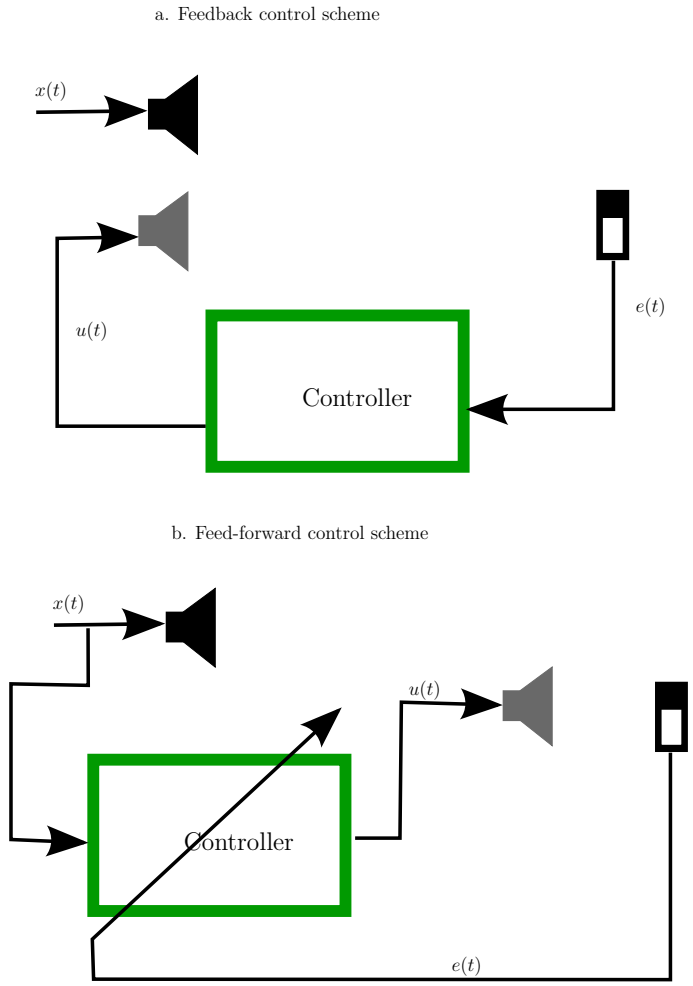

Figure 2.2: Scheme of feedfack and feed-forward controllers.

$$u(t) = f_{ff}(x(t)) \tag{2.6}$$

Where $f_{ff}(\cdot)$ is a transformation which depends on the control algorithm. This scheme is usually applied using adaptive filters and the most representative algorithm is the Filtered X Least Mean Square (FxLMS), e.g. [33, 34] and other algorithms based on it. This algorithm is deeply described in next section.

2.3 Filtered X least mean squares algorithm

The Filtered x Least Mean Squares (FxLMS) algorithm is designed specifically for hardware devices and its analysis is in discrete time k. Controller scheme is shown in figure 2.3, which is the scheme of the process inside the "controller" block in figure 2.2.b. The acoustic pressure at the receiver location $p(\chi, t)$ is measured by a sensor m which produces a discrete signal $e_m(k)$, with $m = 1, \ldots, M$ and M is the number of sensors. Mathematically, this signal can be obtained as:

$$e_m(k) = h_{p,m}(k) * x(k) + \sum_{i=1}^{I} h_{i,m}(k) * u_i(k) \tag{2.7}$$

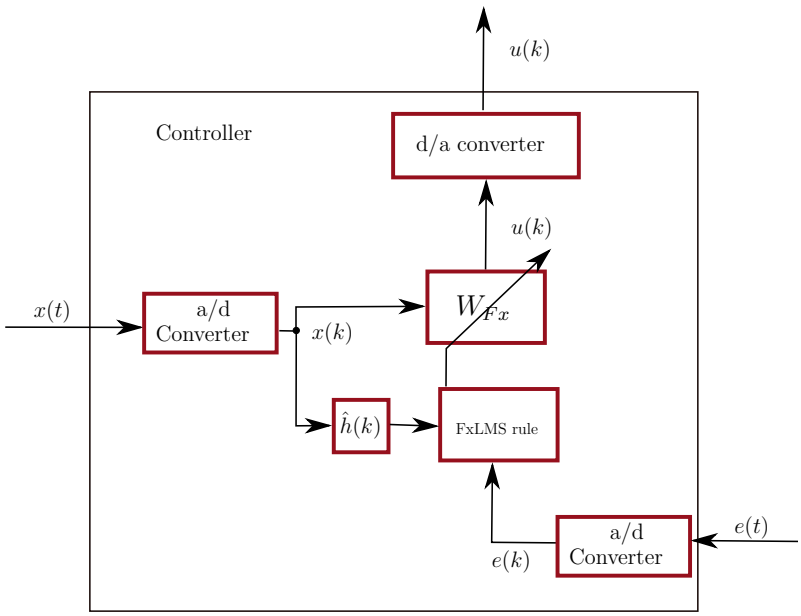

Figure 2.3: FxLMS scheme controller.

Where $*$ is the convolution operator, $h_{p,m}(k)$ is the impulse response of primary path to sensor m, $h_{i,m}$ is the secondary path from the source i to the sensor m, $u_i(k)$ is the control signal for the actuator i and I is the number of actuators. The control signals are obtained filtering the discrete samples of the emitted noise $x(k)$ as follows:

$$u_i(k) = \bar{w}_i(k)^T \bar{x}(k) \tag{2.8}$$

where:

$$\bar{x}(k) = \left[x(k), x(k-1), \cdots, x(k-L)\right]^T \tag{2.9}$$

$$\bar{w}_i(k) = \left[w_{i,0}(k), w_{i,1}(k), \cdots, w_{i,L-1}(k)\right]^T \tag{2.10}$$

$\bar{w}_i(k)$ is the vector of time variable coefficients of the adaptive filter with length L for the control signal of actuator i. The values of filter are obtained minimizing the next cost function:

$$J = ||e(k)||^2 \tag{2.11}$$

In order to find the minimum square error, the gradient descent algorithm is applied as follows:

$$\bar{w}_i(k+1) = \bar{w}_i(k) - \alpha \nabla J = \bar{w}_i(k) - 2\alpha \sum_{m=1}^{M} e_m(k) \bar{x}_{f,i,m}(k) \tag{2.12}$$

with

$$\bar{x}_{f,i,m}(k) = \left[x_{f,i,m}(k), x_{f,i,m}(k-1), \cdots, x_{f,i,m}(k-L)\right]^T \tag{2.13}$$

$$x_{f,i,m}(k) = \hat{h}_{i,m}(k) * x(k) \tag{2.14}$$

and $\hat{h}_{i,m}(k)$ is the estimation of $h_{i,m}(k)$.

A property of this algorithm is that filtering the error signal gives priority to some frequencies to be attenuated [35] , which is applied in [36] to increase the loudness. Furthermore, many algorithms have been created based on the FxLMS algorithm. [37] summarizes some of them as Filtered u Least Mean Squares (FuLMS), which modifies the structure of the filter, including past values of control signal of the filter to obtain the future output. A special case for adaptive control is shown in [38, 39], where the adaptive variables are amplitude and phase of many sinusoid signals. As the result, it reduces the noise $34dB$. In order to avoid nonlinearity due to electro-acoustic transformation, the nonlinear approach based on neural networks is shown by [40, 41, 42, 43]. Nevertheless, [43] shows that FxLMS has better performance through an experiment. The multichannel case is deeply analyzed by [44, 45, 46]. [46] concludes that the best performance is obtained using many FxLMS single channel controllers.

2.4 Increasing the silent zone

Let us center the attention in the case that sensors cannot be located at the position of the users. They cannot always carry a microphone and recalculate the secondary path to cancel the noise. Then, it is desired to obtain a zone where noise is attenuated. Strictly, this zone is defined as:

Definition 2.4.1. ***[Silent zone]****: it is the physical space where the noise is attenuated 10 dB due to the effect of the ANC system.*

Increasing the silent zone without using microphones at the user locations is a problem mentioned by several authors. A solution was proposed in [47], where an optimization problem is suggested. This mentions the possibility to optimize the sound pressure using the sensors and actuators (also called secondary sources) as optimization variables. A similar procedure is applied in [48], but it applies two consecutive optimization stages. The first stage takes into account only the sources positions, and the second the sensor locations. This can be applied using a simulation of the room. Thus, the sources and sensors are located optimally where the simulation results indicate. It has two problems, one is that user cannot be located in the optimal locations and the simulated model could have errors that produce non-optimal solutions.

2.4.1 Virtual sensing

Avoiding the problems of optimal solutions, increasing the silent zone is possible using the next definition:

Definition 2.4.2. ***[Virtual sensing]****: this is the methodology which uses a mathematical transformation of measured sound pressure at one location to estimate the one at another desired location. See the scheme in figure 2.4.*

The concept is about to make a transformation $f(\cdot)$ of M measured sensor signals $e_i(t) = p(\chi_i, t)$ at χ_i position, with $i = 1, \cdots, M$, such that the sound pressure signal $e_v(t) = p(\chi_v, t)$ at a desired position χ_v can be computed.

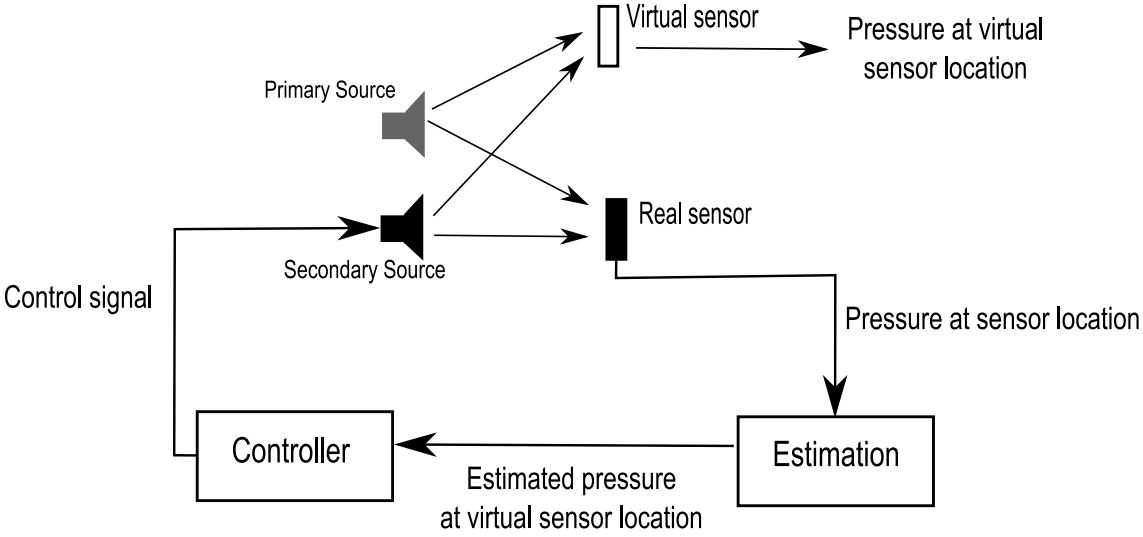

Figure 2.4: A general virtual sensing scheme.

$$e_v(t) = f(e_1(t), \cdots, e_M(t), \chi_1, \cdots, \chi_M) \tag{2.15}$$

Specifically, this methodology is carried out by first measuring the sound pressure at a different location. This signal is then transformed to obtain an approximation of the pressure at a desired location to be used as the error signal. The first algorithm is called virtual microphone arrangement [49, 50]. It takes into account the sound pressure measured by a sensor. Its limitation is due to the assumption that the sound pressure generated by the noise sources is equal for the virtual and real sensor locations (desired and measured locations respectively). A modification, called remote microphone [51], applies the same concept. However, it uses a transformation of the estimation of primary noise to avoid the assumption that the sound pressure components generated by the primary source are equal at both locations. [52] uses a Kalman filter as the estimator of the pressure, which also needs to establish a model of the system. Another proposal is based on the correlation of the pressure at different locations [53], but it is limited by the distance between real and virtual sensors. [54] introduces a nonlinear estimation to solve the problem of the non-causality relation between the measured and estimated pressure. The solution is a modification of the remote microphone algorithm. Other algorithms have been presented but only applied to one dimensional or not enclosed systems e.g. [55, 56, 57]. [58] deals with the problem that attenuating the noise using high number of virtual sensors requires high computational cost. Another issue is that the estimation is carried out using a sensor, but the real receiver is a human, which can produce a change on the estimation. To solve it, [59] proposes an approximation of a mathematical model of the identification system by using a head and torso simulator instead of human ears in the experiment.

2.4.2 Active shielding

Another important methodology for active control of sound field in a discrete region is active shielding.

Definition 2.4.3. ***[Active shielding]****: it is a method where a given region of space to be shielded from unwanted external noise by the active controls obtains the desired attenuation controlling pressure at boundary locations [60].*

Basically, there is a relationship between the acoustic pressure inside a desired silent zone and the pressure at its boundaries. Thus, mathematically this relation is written as:

$$P(\chi, t) = f(\bar{P}(\chi, t)) \tag{2.16}$$

Where $P(\chi, t) = [p(\chi_{z,1}, t), p(\chi_{z,2}, t), \cdots, p(\chi_{z,N}, t)]$ is the vector with the pressures of all locations inside the zone where the noise will be attenuated and $\bar{P}(\chi, t) = [p(\chi_{b,1}, t), p(\chi_{b,2}, t), \cdots, p(\chi_{b,M}, t)]$ is the vector with the pressures at boundary locations of this zone. Then, notice that from equation (2.16), it is possible to control $P(\chi, t)$ through controlling $\bar{P}(\chi, t)$.

The method developed by Jessel and Mangiante [61] and Canevet [62], known as the JMC method, uses Huygens' principle to formulate control of sound field in a zone with secondary sources on the boundary. Pressure and velocity detectors and monopole and dipole actuators are generally required to facilitate the sound field control [63]. Active shielding can also be derived from a formulation of Kirchhoff-Helmholtz integral equation [64]. In this case, only pressure sensors and monopole actuators are required, but the formulation suffers from the integral equation's inherent failure at the characteristic frequencies of the interior region [65]. Munjal and Erikson developed another approach based on electroacoustic analogies, but it is limited by sensor position. It cannot be located at the same position as that of a node [66]. These active shielding approaches seek to minimize the total sound pressure (noise) in the region. In some cases, it may be possible to use directional measurements to separate the unwanted and wanted sound components in the region [67], but such application is limited since in most realistic cases the wanted component cannot be completely separated out by directional measurement alone. An ability to automatically preserve wanted sound in the region while attenuating the unwanted sound coming into the region can be achieved by formulating the control problem using surface difference potentials [68, 60]. However, similar to the JMC method, this approach requires pressure and velocity sensors and monopole and dipole actuators on the boundary surface. Respect to the pressure sensors used for active shielding method, some works have shown the existence of a solution, that works even when there are nodes [69, 70, 71]. Recently, an active shielding was applied also based on virtual sensing for a cylindrical shell [72], which is a method restricted to cylindrical shape and include the problems of virtual sensing. From these methods in active shielding, it is important to remark that they have a limitation. All of them produce a solution and not a control algorithm. In order to make the control system more robust, it is desired to obtain a feedback control [73].

2.5 Decreasing computational cost

The use of a large number of sensors and actuators transforms the ANC problem into a high-dimensional multivariable control problem, which entails a large computational effort, and it is often referred to as *massive multichannel* ANC. Decentral-

ized and distributed schemes have been introduced to deal with the complexity of such problem [74, 75, 76][1].

Definition 2.5.1. ***Decentralized control:*** *this kind of control is the one characterized by using independent different controllers interacting simultaneously due to the environment. Each one has different aim (the local objective) and actuators [77].*

In figure 2.5.a, the decentralized scheme is shown. In the case of active noise control, each controller reproduces control signals to different sound sources and the process uses different error signals. The interaction between controllers is due only due to the room, because the error signals depends on all sources, including other controllers actuators.

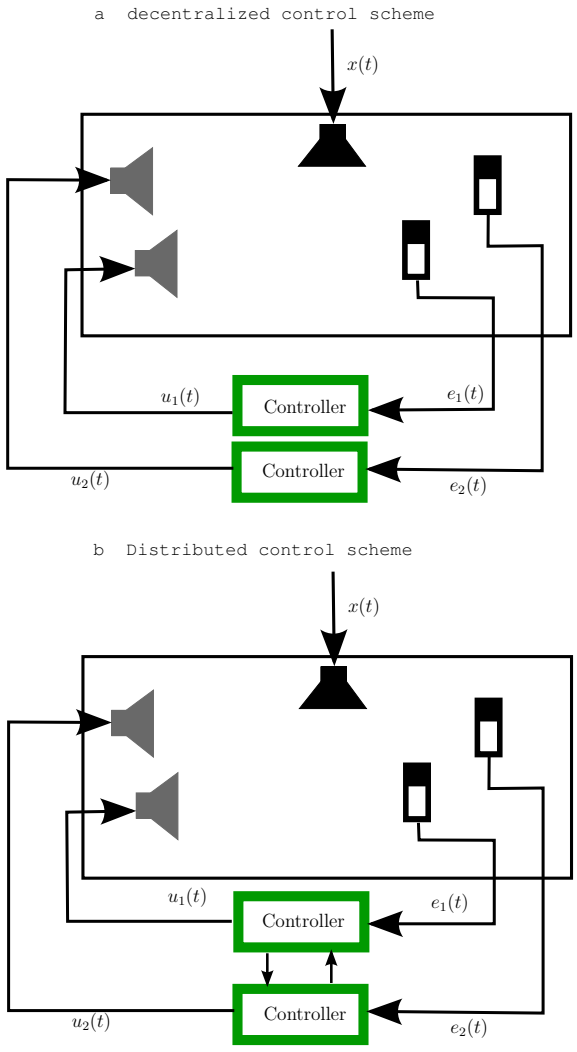

Figure 2.5: Scheme of decentralized and distributed control.

Definition 2.5.2. ***Distributed control:*** *this is the control scheme where different controllers, with different aim interact in the same environment. However, they*

[1]Regarding the concepts of decentralized and distributed control we here adopt the definitions given in [77], as opposed to those in [76].

are not complete independent and each controller shares some information with the others to acchieve its local objective [77].

This scheme is shown in figure 2.5.b. It is similar to decentralized control in many aspects, as the interaction in the room. Also, each controller has its own aim, sensors and sources. However, this scheme is differentiated because the controllers give information to other controllers.

The idea of using different control systems interacting in the same acoustic system was originally proposed in [46]. In a later work, a distributed feedback control scheme is discussed where each controller operates on a specific actuator-sensor pair, neglecting interactions between controllers inside the vibroacoustic system [78]. The performance of this scheme is reported to be satisfactory for a vibration control problem using as many as 16 sensors. A more detailed analysis of this feedback method is given in [79], while [80] applies it in an acoustic setting. A Linear Quadratic Gaussian algorithm is proposed for the same task in [81]. A system decoupling strategy studied in [75, 82] transforms the multichannel system in a series of independent single channel systems, facilitating the design of the decentralized control system. This solution involves high computational cost, or is practically applicable only to zones with a specific shape (e.g., circular). A feed-forward control scheme based on Particle Swarm Optimization proposed in [83] takes into account the interaction of different controllers' actuators and sensors. However, the error convergence is not guaranteed. Another distributed control is given in [84] for velocity and displacement of a vibrating system. It is based on H_∞ controller, ensuring attenuation and stability, but not the maximum possible attenuation. Recently, a methodology that locates the controllers according the modes of a vibrational. Furthermore, it combines two controllers (direct velocity feedback controller and negative acceleration feedback), one for specific modes, and the other for a broad band noise attenuation [85]. Also, [86] present a numerical analysis of the decentralized control based on direct velocity feedback controller. The use of a decentralized ANC scheme based on Internal Model Control and FxLMS is discussed in [87]. A decentralized ANC scheme applied to the design of a planar sound barrier is studied in [88]. It is important to remark that those studies do not focus on the comparison to the optimal attenuation or if the attenuation can be increased, but if it is achieved attenuation.

2.6 Concluding remarks and Main contribution

The active noise control was defined, it shows that it is possible to attenuate the noise using the wave superposition property. Furthermore, the total zero pressure is not always found, then an optimization problem is used to obtain a result. The solution of this optimization has different values according to the cost function and it has been reported different control signals based on measured acoustic pressure. The optimization process also produces several control algorithms. They allow to achieved attenuation even with no knowledge of primary path. However, it is common to measure the pressure at the location where the noise will be canceled. This is a limitation because the user of the active control system does not allow to located the sensor at a desired location. In literature are reported three methods to avoid the previous problem. First the optimization problem to locate the sensors and actuator, but it does not allow to ensure that the minimum is an acceptable attenuation.

Second, the virtual sensing, which estimates the pressure at a desired location, but it is limited by high computational cost and the accuracy of the prediction model which requires information of the user. An the last one is active shielding, a technique that do not produces an algorithm, but an specific control signal, which is not desired to make the control system robust. To use techniques as active shielding require massive multichannel control systems. In order to reduce the computational cost in this case, distributed and decentralized control has been proposed. They have not been deeply analyzed in active noise control applications. Hence, problems as ensure convergence of controllers and obtain minimum attenuation achieved have not been not developed for control algorithms as the Fx-LMS.

According to not solved problems in the state of the art, it is an open research field and this thesis will contribute to:

1. To give a demonstration which produces an active shielding method that allows to obtain an attenuation in a desired zone using control algorithms reported in literature.

2. Develop a method to predict the possible solutions of using decentralized active noise control.

Chapter 3

Active Noise Control linearity

Abstract

This chapter shows evidence which allows to use linear controllers. Two problems have been solved using nonlinear control systems: the non-linear secondary path and a controller which is non-causal. The linearity of secondary path is proven through experiments, then measured data is used for system identification of linear and non-linear models. These models are compared to define if linear models are closer to the behavior of measured data. Regarding causality of the controller, it is shown analytically in time space. First it is obtained the causality for a system with one reflection. Then, the solution for several reflections system is obtained using one reflection system solution. The concluding remarks are noted at the end of the chapter.

3.1 introduction

Before initial design of any active noise control system, two statements are assumed, the linearity of the system and the causality of the control system (in feed-forward scheme). However, there are some articles which deal the control system without these assumptions. Solutions for both cases imply non-linear control systems. This chapter deals with verification of these assumptions. Regarding the linearity, several authors have applied a non-linear control because "non-linearities can arise from the sensors, actuators, or amplifiers employed in the system, usually in the secondary path" [89]. In first section, a deeply description of these assumptions is formulated. In second section, in order to solve the viability to use this linearity assumption, input and output measurements of secondary path are used to obtain linear and non-linear models through identification system processes, which are evaluated and compared according to their generated error. On the other hand, [90] proposes the Filtered-s Least Mean Square algorithm to deal with non-causal secondary paths. In third section, a time analysis of a control scheme allows to describe a unique condition to make viable using a controller which assumes causality. The conclusions are summarized at the end of the chapter.

3.2 Description of assumptions

The control scheme is shown in figure 3.1. It corresponds to a control system with one sensor and one actuator. In this case, it is important to remark that after sound is emitted by sources, it is delayed by followed trajectory and attenuated by the air and reflection on surfaces. At the receiver location, the sound is a sum of several delayed and attenuated copies of emitted sound. There is also a transformation due to the electro-acoustical transducer, which could have a non-linearity. This is the transformation carried out by secondary path. Then, the linear discrete model of error signal (as it was shown in section 2.3) is represented by next equation:

$$e_1(k) = h_{p,1}(k) * x(k) + h_{1,1}(k) * u_1(k) \tag{3.1}$$

with $I = 1$.

Assumption The linearity in secondary path implies that the secondary path is modeled by the term $h_{1,1}(k) * u_1(k)$.

If it is not achieved, this convolution can not represent the secondary path and it needs another function which is restricted to be non-linear.

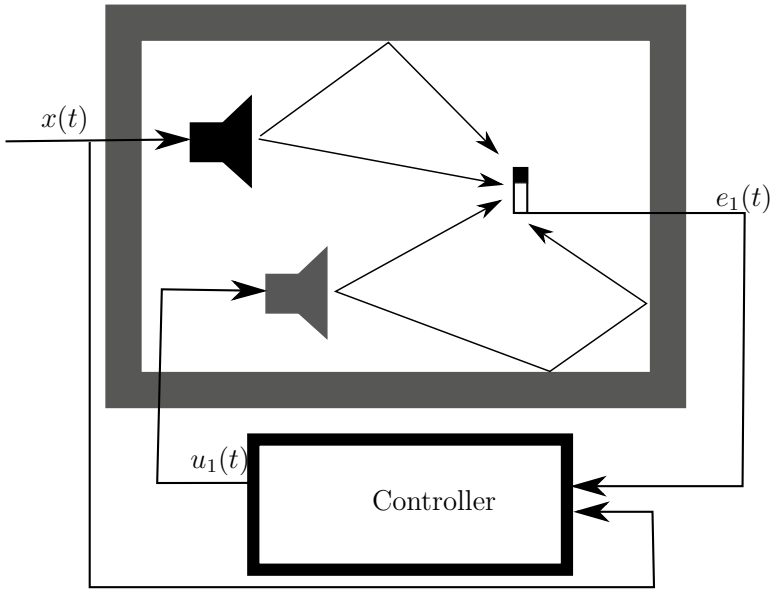

Figure 3.1: Scheme of feed-forward single input-single output active noise control inside a room.

In equation (3.1), $e_1(t)$ is not necessary zero. If it is restricted to perfect control, then it yields:

$$0 = h_{p,1}(k) * x(k) + h_{1,1}(k) * u_1(k) \tag{3.2}$$

The control signal $u_1(k)$ depends on the algorithm. Algorithms with feedback schemes come from optimization process bounded to causal controller, but they are sometimes not desired because they increase noise at not attenuated frequencies (the water bed effect [91]). Also, in all linear feed-forward control schemes in stable state, the control signal can be represented as follows:

$$u_1(k) = \tilde{w}(k) * x(k) \tag{3.3}$$

Where $\tilde{w}(k)$ is the impulse response of the controller. Replacing $u_1(k)$ in equation (3.2), it yields:

$$\begin{aligned} 0 &= h_{p,1}(k) * x(k) + h_{1,1}(k) * \tilde{w}(k) * x(k) \\ \tilde{w}(k) &= -h_{p,1}(k) h_A(k) \end{aligned} \tag{3.4}$$

Notice that $h_A(k)$ is the inverse impulse response of $h_{1,1}(k)$. This implies that $h_A(k)$ must achieve next equation:

$$\delta(k) = h_A(k) * h_{1,1}(k) \tag{3.5}$$

Where $\delta(k)$ is the Kronecker delta function. Thereupon, next assumption is assumed

Assumption $\tilde{w}(k)$ is causal and achieve the next definition:

Definition 3.2.1. *A controller is causal if and only if there exists a* $\tilde{w}(k) = 0$ *for all* $k < 0$.

Notice that this definition does not assume $\tilde{w}(k)$ as unique. This is because the impulse response of the inverse of a system, $h_{1,1}^{-1}(k)$ in this case, is not unique. More details are exposed in Appendix A.

Summarizing this section, a linear controller can be applied if the next two statements hold:

1. The signal at receiver location due to secondary path $y(k)$ can be represented by the term $y(k) = h_{1,1}(k) * u_1(k)$.

2. The control which achieves perfect cancellation accomplishes the definition 3.2.1

In next sections, these statements are proven, one empirically and the other analytically.

3.3 Secondary path linearity

This section shows an empirical evaluation of the linearity assumption (first enumerated statement in previous section). The concept behind the validation is using different possible linear models to predict the output of the secondary path given a known input signal. Then, the result is compared to measured output data and it is determined if the error of any linear model is accepted or it is better to use non-linear models.

First, linear models must be obtained and they must be fit the measured data. Thus, an identification process is carried out to get the models, which applies optimization process to minimize the difference between the predicted output and the measured one for the same input. The system identification process has three steps:

1. **Measure input and output data of system:** in this case, input signal of a speaker is also the input signal of the system. Regarding output signal, it is the one produced by a microphone at a receiver location.

2. **Choose a set of models:** this is to define all the models that will be compared and candidates to represent the system. They usually are chosen according to evident characteristics of system. e.g. linear models with short impulse response, they can be represented by space state models with order 50 or lower. Each value of state matrices produces a different model, and it can represent systems with even large impulse responses. All methods and models used in this thesis are described in Appendix B.

3. **Choose the best model:** here, it is defined which model is the best for a given rule. This rule is also defined. Usually, the rule is minimizing the difference of a set of measured data and predicted data. Then, the best model is identified.

In the direction of making available the comparison between models, obtained by different rules and different sets, a methodology to compare error $e(n) = y(n) - \hat{y}(n)$, of an simulated output $\hat{y}(n)$ respect an measured output $y(n)$, has to be implemented. There is an interesting method, which normalizes the error according the magnitude of measured output signal called FIT. Mathematically, this is written as follows:

$$FIT = 100\left[1 - \frac{||\vec{e}(n)||_2}{||\vec{y}(n) - \mathcal{E}[\vec{y}(n)]||_2}\right] \tag{3.6}$$

Where $\mathcal{E}[.]$ is the mean, $\vec{e}(n) = [e(n), e(n-1), \cdots, e(n-N_s)]$, $\vec{y}(n) = [y(n), y(n-1), \cdots, y(n-N_s)]$ and $N_s + 1$ is the number of samples used to evaluate the error.

Applying the definition of sound, and assuming the atmospheric pressure as zero, then $\hat{E}(\bar{y}(n)) = 0$. Notice that if $e(n) = 0$ for all n, then $FIT = 100$. Also, $FIT = 0$ means $||e(n)||_2 = ||\bar{y}(n)||_2$.

3.3.1 Secondary path description and measurement

In this case, a single input-single output system is considered inside a rectangular room with dimensions $[l_1, l_2, l_3]$ for the axis X_1, X_2 and X_3 respectively, with $l_1 = 2.945m, l_2 = 2.68m, l_3 = 2.35m$. The scheme is shown in Fig. 3.2. For reference location, the coordinate $[0m, 0m, 0m]$ was the corner of the room (left, bottom). The sound source (input) is a speaker Kustom KBA16, its acoustic center was located at $[1.75m, 0.30m, 0.15m]$. And, the receiver is a microphone Behringer ECM8000. It was located at $[1.54m, 1.30m, 1.2m]$. Objects are included to make an irregular acoustic field. Green color means the area covered by furniture and the black square is a column inside the room. The door is in the opposite corner to the origin, and the guide can be observed in brown color.

The input $u(n)$ is a discrete filtered white noise generated by the software audacity 1.2.6, with $44100Hz$ as sample frequency. The low-pass filter was used to get a desired frequency band for active noise control application. The magnitude of signal spectrum $U(\omega)$ can be observed in figure 3.3. Note the decay of the energy for signals higher than $300Hz$. At the receiver location, the microphone receives a

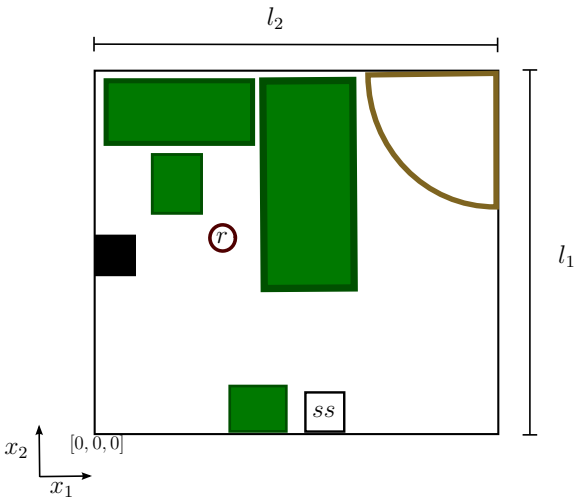

Figure 3.2: Room and measurement setup.

signal $y(n)$ (output) with spectrum $Y(\omega)$, also showed in figure 3.3. The energy of system also decreases at low frequencies. It is possibly due to transfer function of the speaker or the effect of modes of the room.

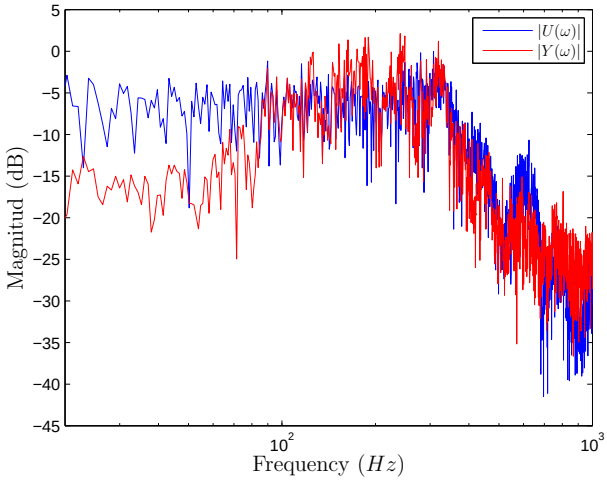

Figure 3.3: Room and measurement setup.

For the identification process, four data sets have been taken into account. The first set has the aim to train the algorithm, the length of input-output vectors is 40000, the apparent short length is due to the computational cost. Then, a validation set is needed. It consists of 20.000 samples of input and 20.000 samples of output. The initial time was chosen such that the data of these two sets are not correlated. Due to the computational cost of some methodologies, other two shorter sets have to be acquired instead of the two set mentioned before. They are decimated copies of the other two sets, this is used to obtain $2.205KHz$ as sampling frequency.

Before selecting a set of mathematical models, it is analyzed the correlation between input and output signals, see figure 3.4. The indicated figure shows the correlation from the half position of vector as zero value to 15000 samples after. The

blue line is the auto-correlation of the input R_{uu}. As it was expected, it is not an impulse because of the applied filter. The green line (R_{yu}) is the correlation between $Y(n)$ and $u(n)$. It describes the similitude between the value of each position of the vectors, due to the input signal. This must be similar to the impulse response of the system. Thereupon, from this figure it can be observed the dead time produced by the crossed distance between source and receiver. it is about 3000 samples. Then, the next 7000 samples are the most correlated to the actual output. Thus, it is expected to use them for the prediction. Thus, the estimated model must have at least 10000 samples of impulse response length for $44100Hz$ of sample frequency. The auto-correlation of the output R_{yy}, in red color, shows the similarity of the value at a time n and its past values, about 6000 past samples are correlated and are useful to predict the actual output. This is an appropriate value to define the order of the feedback models. It means that it is possible to increase the performance of an identification method if these samples are included.

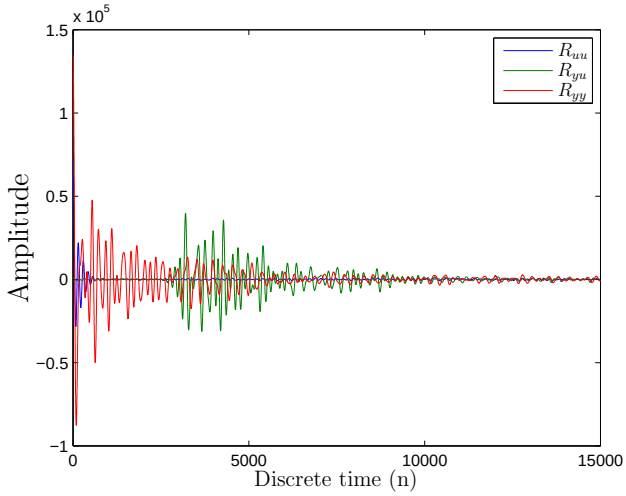

Figure 3.4: Autocorrelation and Crosscorrelation of input and output signals.

The models of the system identification system process used in this work are shown in Appendix B. Specifically, following methods have been applied: FIR filter, AR model, ARX model, N4SID, LMS filter identification and neural networks.

- **FIR:** for the sake of computational cost, only the decimated sets were used to estimate the model. In this case, the size of the order of filter is the same length as the impulse response, then, for the frequency sample of $2205Hz$, the order has to be more than 500, according to the cross correlation (Figure 3.4). The results of this method are very satisfactory, the FIT is 94.11 and 91.34 for the training data and verifications data sets.

- **AR:** as it was expected, by reason of mentioned auto-correlation R_{yy}, the value at time n can be predicted by the past values. The order of filter is 500. After simulations, outcome FIT values are 17.49 and 36.16 for training and validation data sets respectively.

- **ARX:** The method which produces an ARX model (also described in Appendix B), was simulated for the order $N_{\text{ar}} = 500$ for output past values and

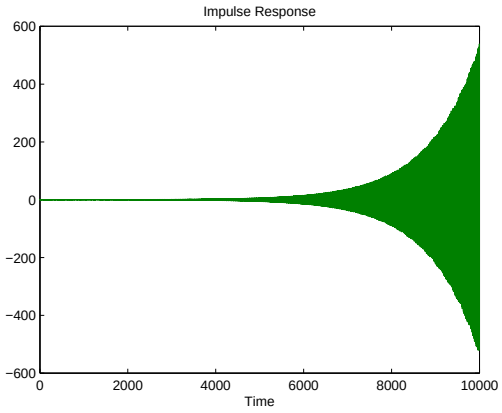

Figure 3.5: Impulse response of the ARX model.

$N_{\text{iir}} = 500$ input past values, where N_{ar} and N_{iir} are the number of coefficients that multiply past values of input and output respectively. The FIT values are 94.11 and 91.34 for training and verification data sets respectively. This outcome is similar to real transformation, which should obtain a FIT value equal to 100. However, a deepest analysis shows that this model is not stable, as it is shown by the impulse response in figure 3.5. This is not possible because the sound pressure generated inside room decreases when the source is stopped, including an impulse. The model can represent the system only for some kinds of input signals. This point is not obvious and it is not analyzed here. The inconvenient is mentioned, but it is not solved. It is proposed for future works.

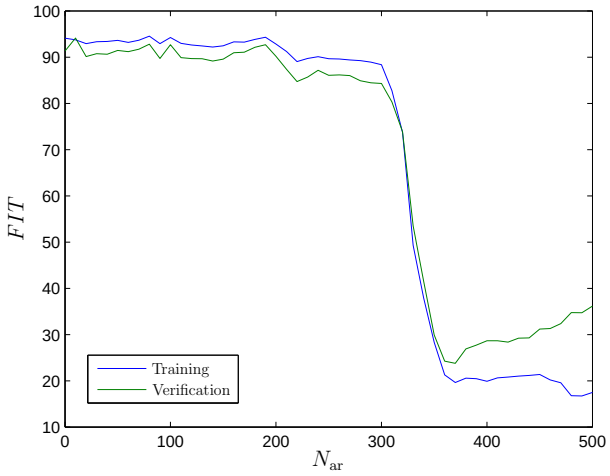

Figure 3.6: Autocorrelation and Crosscorrelation of input and output signals.

In preview examples, the order of the system uses high number of estimation variables for the identification process. Thus, the expected FIT is a high value, but it also increases the computational cost. Then, another intrinsic question about the use of this method appears: what is better?, increasing the value of N_{iir} or N_{ar}? To give an approach, variable values of N_{ar} and N_{iir} are evaluated

but maintaining the condition $N_{\text{ar}} + N_{\text{iir}} = 500$ (see figure 3.6). It shows that high values of N_{ar} has bad FIT and the behavior of error changes according to the input data set while N_{ar} increase. When $N_{\text{ar}} > 300$, then $FIT < 85$. It allows to infer that the feedback increases the FIT, but not a high value. The best measured FIT is 94.54 for the training data set when $N_{\text{ar}} = 80$ and $FIT = 94.14$ when $N_{ar} = 10$ for verification data set.

Order	**FIT (training data)**	**FIT (verification data)**
10	-2.273	-0.5335
20	1.102	4.879
30	$-1.091 * 10^{140}$	$-5.472 * 10^{63}$
40	$-3.653 * 10^{26}$	$-1.762 * 10^{13}$
50	$-1.24 * 10^{9}$	-6.806
60	$-5.68 * 10^{13}$	$-6.425 * 10^{6}$
70	$-2.693 * 10^{5}$	-8.648
80	7.822	9.103
90	$-2.337 * 10^{6}$	-241.1
100	20.87	23.6

Table 3.1: Fit for N4SID identification according to system order for trining data and nontrining data

- **N4SID:** the requirement of some kinds of controllers and estimators implies the state equation, see [30, 29, 32]. This model can be obtained by N4SID method (see Appendix B). For this case, the size of square matrix $\mathcal{A}_{n4s}$ is known as the order of the system. To obtain similar conditions and to compare the results, an order 500 model is required. However, the computational cost does not allow it. Less order models have been estimated, see table 3.1. Odd FIT values are found, negative and with high magnitude. In fact, those are consequences of the instability of the model and it cannot represent the acoustic system. The other FITs agree to the logical structure of the model. For larger impulse responses, a higher order must used to represent the system and as an a consequence, a higher FIT.

- **LMS:** From two groups of data sets (decimated and non decimated), unique characteristics can be extracted from the identification method that uses LMS filter. For the decimated data set, the error during all training iterations is shown in the figure 3.7 in the part a). The model obtained after the convergence obtains $FIT = 82.04$ and $FIT = 62.40$ for the training data set and verification data set respectively with non-amplified output. Notice that the error converges. In order to increase the FIT, the output is amplified 200 times and the result convergence is shown in the part b) of the figure 3.7. The amplified output obtains $FIT = 91.11$ for training data set and $FIT = -9.14$ for verification data set. Another FIT value can be obtained, it is when the algorithm is still updating the weights according to the equation (B.5). The result is $FIT = 90.41$ for the training data and the amplified output.

  A similar procedure is implemented for the non decimated data sets, and the results can be observed in figure 3.8. The part a) of this figure shows that the

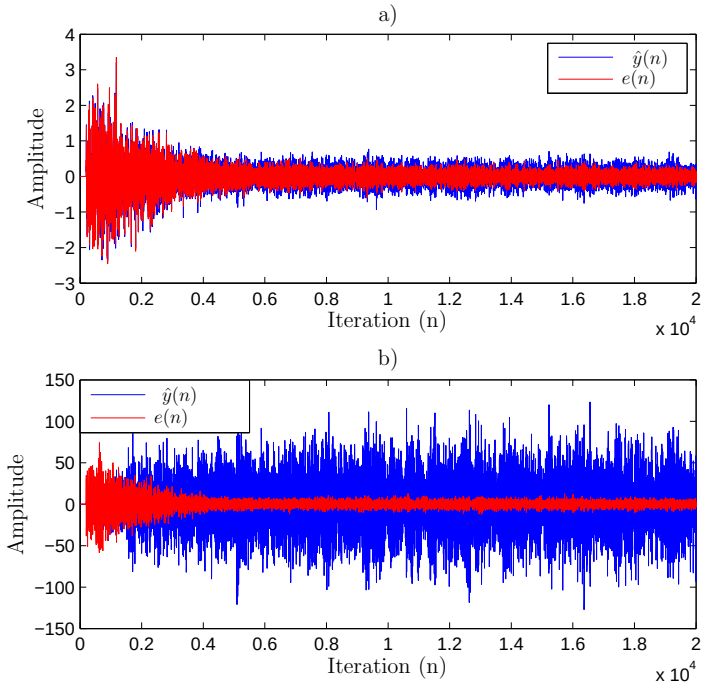

Figure 3.7: LMS error and estimated output for the decimated data set, a) estimation for non amplified output and b) estimation for amplified output.

error does not converge for non amplified data. On the other hand, the part b) shows a brief convergence for the amplified output. It means that the amplified output is needed for high sample frequency. The FIT values for the stationary filter coefficients are -459.95 and -335.3451 for the non amplified output and the training data and verification data respectively, and for amplified output 8.48 and 18.9730 for both data sets.

- **Neural Network:** In order to obtain non-linear identification, neural networks are applied. This online identification approach is applied for the secondary path in active noise control. The used neural network for this identification is composed by 40 neurons and 500 past input samples as the input. Using short data set, the acquired error and estimated output during the training phase are shown by figure 3.9. It is evident that the error does not converge to a low error magnitude. FIT values are obtained under the same condition that the LMS filter, $FIT = 57.09$ for updating weights, $FIT = -38.34$ for the training data set and $FIT = -44.04$ for the verification data set.

  Other results using neural network are obtained applying the non decimated data sets, see figure 3.10. Over sampling makes the FIT increases significantly while the weights are updating, $FIT = 87.96$. Nevertheless, the stationary behavior has $FIT = -1.62 * 10^3$ and $FIT = -1.56 * 10^3$ for training and verification data sets respectively.

All results are summarized in table 3.2. The FIR model is a good result for modeling with FIT values over 90 and the limitations are related to computational cost. On the other hand, in the AR model, the past values of $y(n)$ (unless they are

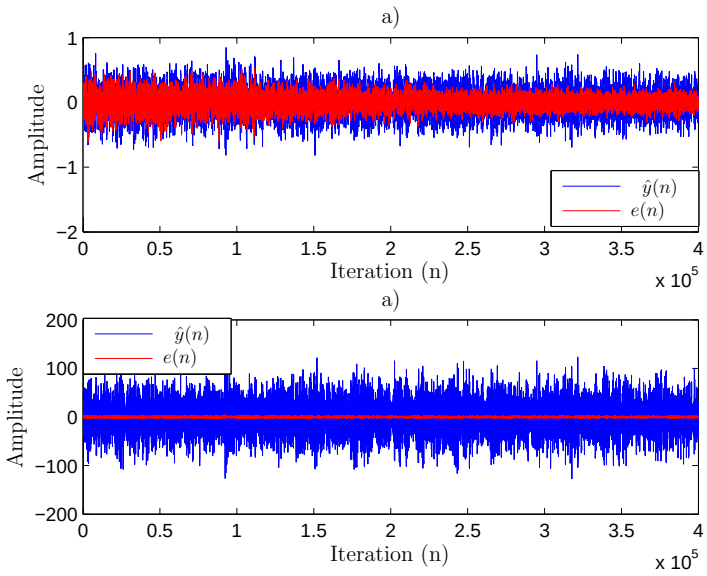

Figure 3.8: LMS error and estimated output for the non decimated data set, a) estimation for non amplified output and b) estimation for amplified output.

correlated) do not have enough information to make an estimation of future values. Thus, it has the worst results of the offline identification methods. The ARX models have the best performance, and their advantage is low difference between FIT of training data and verification data sets. Additionally, the N4SID model does not achieve a high values of FIT, probably due to the computational cost. Therefore, it is not recommended using it instead previous methods. The LMS filter has high FIT values and since it updates weights without decimate the signals, it has the best FIT of all tested methods using training data. Finally, the neural network does not decrease the error value. This is expected because the neural network does not have linear models for any kernel and the model with less error is probably linear. It agrees with the result of [42], where the linear model allows better control. This means that the secondary path can be represented by a linear model.

3.4 Causality

The section 3.2 enumerates the assumptions that allow to use a linear controller. The second one is regarding the causality and it is related to the impulse response of the controller in definition 3.2.1. Therefore, it is analyzed the impulse response in time space of a feed-forward controller for perfect control conditions (when it is attenuated 100% of noise). Taking into account the proposed system in figure 3.1, defining if the impulse response of a controller is causal is very complex. Hence, next steps are followed:

1. A simplified system of one reflection is analyzed. According to this scheme, there are two trajectories from each source to receiver.

2. Then, the result of one refection system is used to find an approximation to the impulse response.

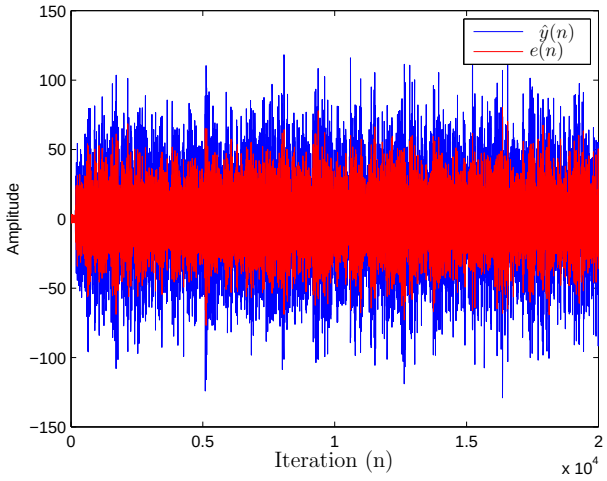

Figure 3.9: Error and estimated output for decimated data set using neural network model.

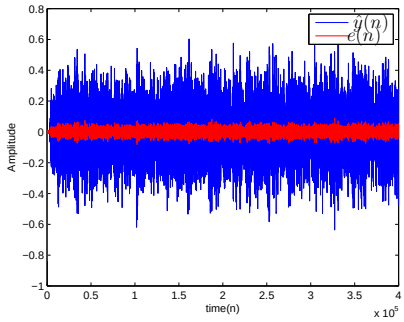

Figure 3.10: Error and estimated output for non decimated data set using neural network model.

3.4.1 One reflexion analysis

The simplified system is shown in figure 3.11, for a two dimensional system. According to this scheme, there are two trajectories from each source to receiver. The first is the trajectory with distance $d_{p,0}$ or $d_{s,0}$ (shortest trajectory to r_i), which corresponds to the direct trajectory between the primary or secondary source respectively and the receiver. The other trajectory between sources and receiver occurs due to the reflection in the surface, and its distance is $d_{p,1}$ or $d_{s,1}$ respectively for each source. Each crossed distance by the sound produces a delayed copy signal of the emitted sound pressure. The delay depends on the sound velocity c as:

$$k_{p,0} = \frac{d_{p,0}}{c}; k_{s,0} = \frac{d_{s,0}}{c}; k_{p,1} = \frac{d_{p,1}}{c}; k_{s,1} = \frac{d_{s,1}}{c}; \tag{3.7}$$

Note that due to the definitions of the crossed distances and Eq. (3.7), the next inequalities can be declared:

Method	**FIT (training data)**	**FIT (other data)**
FIR	94.11	91.34
AR	17.49	36.16
ARX ($k = 500; m = 500$)	97.89	96.19
ARX ($k = 420; m = 80$)	94.59	92.82
ARX ($k = 490; m = 10$)	93.76	94.14
N4SID	20.87	23.6
LMS(Short,Unamplified)	82.04	62.40
LMS(Short,Amplified)	91.11	-9.14
LMS (Updating, Short,Amplified)	90.41	-
LMS(Long,Unamplified)	-459.95	-335.34
LMS(Long,Amplified)	8.48	18.97
LMS (Updating, Long,Amplified)	97.44	-
NN(Updating,Short)	57.09	-
NN(Short)	-38.34	-44.04
NN(Long)	$-1.62 * 10^{-3}$	$-1.56 * 10^{-3}$
NN(Updating,Long)	87.96	-

Table 3.2: Fit according to the model for training data and non training data.

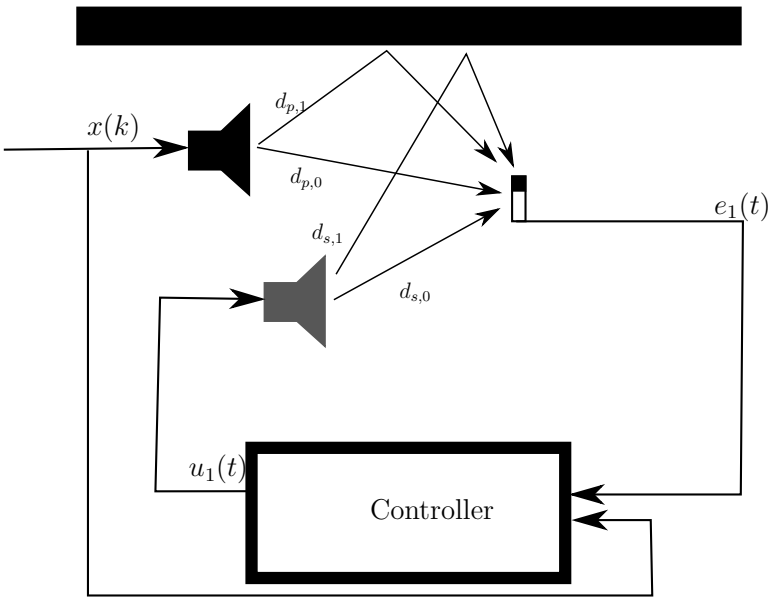

Figure 3.11: Scheme of active control with only one surface.

$$t_{p,0} < t_{p,1} \tag{3.8}$$

$$t_{s,0} < t_{s,1} \tag{3.9}$$

These conditions allow to find restrictions to the system in the analysis of $\tilde{w}(k)$. The analysis starts by defining the impulse responses for the simplified system.

According to the proposed scheme and assuming that the surface does not produce diffusion, the impulse responses $h_{p,1}(k)$ and $h_{1,1}(k)$ can be inferred as:

$$h_{p,1}(k) = \alpha_{p,0}\delta(k - k_{i,0}) + \alpha_{p,1}\delta(k - k_{p,1}) \tag{3.10}$$
$$h_{1,1}(k) = \alpha_{s,0}\delta(k - k_{s,0}) + \alpha_{s,1}\delta(k - k_{s,1}) \tag{3.11}$$

Where $\alpha_{p,0}$, $\alpha_{p,1}$, $\alpha_{s,0}$ and $\alpha_{s,1}$ are attenuation coefficients due to the crossed trajectories and its associated reflection for the distances $d_{p,0}$, $d_{p,1}$, $d_{s,0}$ and $k_{s,1}$; also $k_{p,0}$, $k_{p,1}$, $k_{s,0}$ and $k_{s,1}$ are the associated delays.

Using above equations the next lemma can be proven:

Lemma 3.4.1. *The controller with feed-forward scheme and impulse response $\tilde{w}(t)$ is causal if the impulse response of the inverse system of secondary path $h_A(k) = 0$ for $k < -k_{p,0}$.*

Proof. Substituting (3.10) in Eq. (3.2), it becomes:

$$\tilde{w}(t) = -\alpha_{p,0}h_A(k - k_{p,0}) - \alpha_{p,1}h_A(k - k_{p,1}) \tag{3.12}$$

According to Eq. (3.12), and due to the restriction $\tilde{w}(k) = 0$ for $k < 0$ (see definition 3.2.1), the next condition allows to determine the controller as causal:

$$(h_A(k - k_{p,0}) = 0) \text{ and } (h_A(k - k_{o,1}) = 0) \text{ if } (t < 0) \tag{3.13}$$

Furthermore, taking into account $(k - k_{p,0}) > (k - k_{p,1})$, if $h_A(k - k_{p,0}) = 0$ for $t < 0$, then $h_A(k - k_{p,1}) = 0$ for $k < 0$. Thus, the condition expressed in (3.13) yields to lemma 3.4.1.

□

Besides, a further analysis of $h_A(t)$ allows to obtain the next theorem:

Theorema 3.4.1. *If an acoustic system that takes into account only direct sound and one reflection, and the system is assumed as linear, then:*

if $(d_{s,0} < d_{p,0})$, then the transfer function of the controller is causal

Proof. Lemma 3.4.1 shows the conditions of $h_A(t)$ ensuring that the controller is causal. Thus, to determine $h_A(t)$ is the aim of this proof.

First, replacing (3.11) in equation (3.5) and solving the convolution, following equations are obtained:

$$\alpha_{s,0}h_A(-k_{s,0}) + \alpha_{s,1}h_A(-k_{s,1}) = 1 \quad \text{if} \quad k = 0 \tag{3.14}$$
$$\alpha_{s,0}h_A(k - k_{s,0}) + \alpha_{s,1}h_A(k - k_{s,1}) = 0 \quad \text{if} \quad k \neq 0 \tag{3.15}$$

$h_A(t)$ depends only on the attenuation and delays of secondary path (known values).

Since Eq. (3.14) and (3.15) use the same function $h_A(k)$, they are related for some k values. This interaction can be used to find a specific function $h_A(k)$ achieving the lemma 3.4.1. Furthermore, Eq. (3.14) implies that $(h_A(-k_{s,0}) \neq 0) \vee (h_A(-k_{s,1}) \neq 0)$. Thus, the next step is to know the influence of these values in (3.15).

There are two ways to replace (3.14) in (3.15). First is when $k = k_{s,0} - k_{s,1}$, then the term $h_A(-k_{s,1})$ is equal to $h_A(k - k_{s,0})$. Another form is when $k = k_{s,1} - k_{s,0}$, then $h_A(-k_{s,0})$ is equal to $h_A(k - k_{s,1})$.

From Eq. (3.14), $h_A(-k_{s,1})$ is:

$$h_A(-k_{i,1}) = \frac{1 - \alpha_{i,0} h_A(-k_{i,0})}{\alpha_{i,1}} =: h_{in,0} \tag{3.16}$$

Furthermore, an important characteristic can be obtained solving the Eq. (3.15) at time $k = \psi k_{i,0} - \psi k_{i,1}$, with $\psi \in \mathbb{Z}^+/\{0\}$.

$$h_A(\psi k_{s,0} - (\psi + 1)k_{s,1}) = \frac{-\alpha_{s,0} h_A((\psi - 1)k_{s,0} - \psi k_{s,1})}{\alpha_{s,1}} \tag{3.17}$$

From (3.17), note that $h_A(\psi k_{s,0} - (\psi + 1)k_{s,1})$ depends on the $h_A(\psi_1 k_{s,0} - (\psi_1 + 1)k_{s,1})$, where $\psi_1 = \psi - 1$.

If $\psi = 1$, $h_A(k_{s,0} - (2)k_{s,1})$ depends on $h_A(-k_{s,1})$. Thus, (3.16) can be replaced into (3.17). It yields:

$$h_A(k_{s,0} - 2k_{s,1}) = \frac{-\alpha_{s,0} h_{in,0}}{\alpha_{s,1}} \tag{3.18}$$

Equation (3.18) can be replaced into (3.17), if $\psi = 2$. This procedure can be carried out successively, increasing the value of ψ with each iteration, giving the value for $h_A(\psi k_{s,0} - (\psi + 1)k_{s,1})$:

$$h_A(\psi k_{s,0} - (\psi + 1)k_{s,1}) = \frac{(-\alpha_{s,0})^\psi h_{in,0}}{(\alpha_{s,1})^\psi} \tag{3.19}$$

On the other hand, the same analysis can be carried out, but replacing (3.14) in (3.15). From (3.14), $h_A(-k_{s,0})$ is:

$$h_A(-k_{s,0}) = \frac{1 - \alpha_{s,1} h_A(-k_{s,1})}{\alpha_{s,0}} =: h_{in,1} \tag{3.20}$$

Following a similar procedure, solving (3.15) for $k = \psi k_{s,1} - \psi k_{s,0}$, it obtains:

$$h_A(\psi k_{s,1} - (\psi + 1)k_{s,0}) = \frac{-\alpha_{s,0} h_A((\psi - 1)k_{s,1} - \psi k_{s,0})}{\alpha_{s,1}} \tag{3.21}$$

Thus, for $\psi = 1$, substituting (3.20) into (3.21), and generalizing for any value of ψ, the next equation is deduced:

$$h_A(\psi k_{i,1} - (\psi + 1)k_{i,0}) = \frac{(-\alpha_{i,1})^\psi h_{in,1}}{(\alpha_{i,0})^\psi} \tag{3.22}$$

Equations (3.16), (3.19), (3.20) and (3.22) give values of $h_A(k)$ for $k = \Psi k_{s,1} - (\Psi + 1)k_{s,0}$, but $h_A(k)$ is unknown for other time. Nevertheless, other k values do not affect Eq. (3.14), (3.19) and (3.22). Consequently, for other values of k, $h_A(k)$ is restricted to achieve (3.15). Therefore, the next proposition holds:

$$h_A(k) = 0 \text{ if } k \neq \Psi k_{s,1} - (\Psi + 1)k_{s,0} \text{ for } \Psi \in \mathbb{Z} \tag{3.23}$$

In order to prove the causality of controller, it is enough to achieve the lemma 3.4.1. The time values when $h_A(k) \neq 0$ are given by (3.16) and (3.19), (3.20), (3.22). First, taking the Eq. (3.16) and (3.19), the next condition achieves lemma 3.4.1:

$$\psi(k_{s,0} - k_{s,1}) \geq k_{s,1} - k_{p,0} \text{ for } \psi \geq 0, \psi \in \mathbb{Z} \tag{3.24}$$

From equation (3.8), it is evident that $\psi(k_{s,0}-k_{s,1})$ decreases towards $-\infty$ when ψ increases. Thus, from Eq. (3.19), $h(k) = 0$ for $k = \psi k_{s,0} - (\psi + 1)k_{s,1}$ if and only if $h_{in,0} = 0$.

According to this result, in order to achieve the lemma 3.4.1 and from Eq. (3.20) and (3.22), it implies the next constraint:

$$\psi(k_{s,1} - k_{s,0}) \geq k_{s,0} - k_{p,0} \text{ for } \psi \geq 0, \psi \in \mathbb{Z} \tag{3.25}$$

From Eq. (3.8), $\psi(k_{s,1} - k_{s,0})$ increases to ∞ when ψ also increases. It means that if (3.25) is achieved for $\psi = 0$, this is also achieved for $\psi > 0$. Then, from (3.25), a general constraint is:

$$k_{p,0} \geq k_{s,0} \tag{3.26}$$

The condition (3.26) is the only restriction to accomplish lemma 3.4.1. And, it can be replaced by a condition in space, due to equation (3.7). This condition is expressed in (3.4.1) by the theorem 3.4.1. □

Even though the previous condition is enough to ensure causality for the simplified acoustic system mentioned in this Section, it also implies two definitions for $\tilde{w}(k)$. In order to obtain them, replace $h_A(k)$ from (3.16), (3.19), (3.20), (3.22), (3.23), and $h_{in,0} = 0$ in (3.12). It can occur at two different times. i) The first, when $k = \psi k_{s,1} - (\psi + 1)k_{s,0} + k_{p,0}$, (3.20) and (3.22) can be replaced by the first term. ii) The second is when $k = \psi k_{s,1} - (\psi + 1)k_{s,0} + k_{p,1}$, (3.20) and (3.22) can be replaced by the second term. (3.16), (3.19), (3.23), and $h_{in,0} = 0$ ensures $\tilde{w}(k) = 0$ for other k. As a result, the next two equations can be obtained for $\psi \in \mathbb{N}$:

$$\begin{aligned} \tilde{w}(\psi k_{s,1} - (\psi + 1)k_{s,0} + k_{p,0}) &= -\alpha_{p,1} h_A(\psi k_{s,1} - (\psi + 1)k_{s,0} + k_{p,0} - k_{p,1}) \\ &- \alpha_{p,0} \frac{(-\alpha_{s,1})^{\psi} h_{in,1}}{(\alpha_{s,0})^{\psi}} \end{aligned} \tag{3.27}$$

$$\begin{aligned} \tilde{w}(\psi k_{s,1} - (\psi + 1)k_{s,0} + k_{p,1}) &= -\alpha_{p,0} h_A(\psi k_{s,1} - (\psi + 1)k_{s,0} + k_{p,1} - k_{p,0}) \\ &- \alpha_{p,1} \frac{(-\alpha_{s,1})^{\psi} h_{in,1}}{(\alpha_{s,0})^{\psi}} \end{aligned} \tag{3.28}$$

Let us take different values for ψ, $\psi_a \in \mathbb{Z}^+/0$ represents the value of ψ in (3.27). Also, $\psi_b \in \mathbb{Z}^+/0$ represents the value of ψ in (3.28). Note that (3.27) and (3.28) must be equal if the time is the same. It means that 3.4.1 also must achieve next preposition:

Proposition 3.4.1. *If*

$$(\psi_a k_{s,1} - (\psi_a + 1)k_{s,0} + k_{p,0}) = (\psi_b k_{s,1} - (\psi_b + 1)k_{s,0} + k_{p,1}) \tag{3.29}$$

, then

$$(\tilde{w}(\psi_A k_{s,1} - (\psi_a + 1)k_{s,0} + k_{p,0})) = (\tilde{w}(\psi_b k_{s,1} - (\psi_b + 1)k_{s,0} + k_{p,1})) \tag{3.30}$$

For this condition, $\psi_a \neq \psi_b$ also must be accomplished. Thus, the next step is to show if this is true.

In order to simplify the Eq. (3.27) and (3.28), the time equality condition, shown in proposition 3.4.1, is also simplified to:

$$(\psi_a - \psi_b)(k_{s,1} - k_{s,0}) = (k_{p,1} - k_{p,0}) \tag{3.31}$$

Then, (3.31) can be replaced inside the terms $h_A(\psi_a k_{s,1} - (\psi_a + 1)k_{s,0} + k_{p,0} - k_{p,1})$ and $h_A(\psi_b k_{s,1} - (\psi_b + 1)k_{s,0} + k_{p,1} - k_{p,1})$. Then:

$$\begin{aligned} &h_A(\psi_a k_{s,1} - (\psi_a + 1)k_{s,0} + k_{p,0} - k_{p,1}) = \\ &h_A(\psi_b k_{s,1} - (\psi_b + 1)k_{s,0}) \end{aligned} \tag{3.32}$$

$$\begin{aligned} &h_A(\psi_b k_{s,1} - (\psi_b + 1)k_{s,0} + k_{p,1} - k_{p,0}) = \\ &h_A(\psi_b k_{s,1} - (\psi_b + 1)k_{s,0}) \end{aligned} \tag{3.33}$$

According to the value of ψ_a and ψ_b, (3.32) and (3.33) can be obtained from Eq. (3.20) or (3.22). Replacing in (3.27) and (3.28), it becomes:

$$\begin{aligned} h(\psi_a k_{s,1} - (\psi_a + 1)k_{s,0} + k_{p,0}) &= \alpha_{p,0}\frac{(-\alpha_{s,1})^{\psi_a} h_{in,1}}{(\alpha_{s,0})^{\psi_a}} \\ &+\alpha_{p,1}\frac{(-\alpha_{s,1})^{\psi_b} h_{in,1}}{(\alpha_{s,0})^{\psi_b}} \end{aligned} \tag{3.34}$$

$$\begin{aligned} h(\psi_b k_{s,1} - (\psi_b + 1)k_{s,0} + k_{p,1}) &= \alpha_{p,0}\frac{(-\alpha_{s,1})^{\psi_a} h_{in,1}}{(\alpha_{s,0})^{\psi_a}} \\ &+\alpha_{p,1}\frac{(-\alpha_{s,1})^{\psi_b} h_{in,1}}{(\alpha_{s,0})^{\psi_b}} \end{aligned} \tag{3.35}$$

Notice that (3.34) and (3.35) are equal. It proves that proposition 3.4.1 is true. Then, theorem 3.4.1 is also true for all time interval.

The analysis of one reflection system was based on the analysis of the inverse of secondary path and how the controller interacts with primary path. The direct sound, represented by the first impulse of the impulse response, produces a specific meaning in theorem 3.4.1. It is that sound produced by primary source has to be delayed by the primary path as long as it allows the actuator process the reference signal with present and past values and affects acoustic pressure at receiver location. In the spatial distribution, this means that distance between primary source and error sensor has to be higher than the distance from secondary source to error sensor. Otherwise, the controller needs to predict future values to achieve the desired attenuation.

3.4.2 Several reflections

Once the one reflection analysis has been carried out, it is possible to get a several reflections analysis. The complete acoustic system includes all surfaces of an enclosure. See scheme in figure 3.1. Thus, the room has many surfaces where sound is reflected. It means that the sound at the receiver is a sum of several delayed copies of the generated sound. The impulse responses for the two locations can be inferred from the proposed model, as:

$$h_p(k) = \sum_{l=0}^{L} \alpha_{p,l}\delta(k - k_{p,l}) \tag{3.36}$$
$$h_s(k) = \sum_{l=0}^{L} \alpha_{s,l}\delta(k - k_{s,l}) \tag{3.37}$$

Where $l = 0$ represents the parameters according to the direct sound, $l \neq 0$ represents a trajectory given by one or more reflections. This is why the next inequalities are proposed:

$$k_{p,0} < k_{p,l} \quad \forall \quad l \neq 0 \tag{3.38}$$
$$k_{s,0} < k_{s,l} \quad \forall \quad l \neq 0 \tag{3.39}$$

Replacing (3.36) in (3.2), it yields:

$$\tilde{w}(k) = -\sum_{l=0}^{L} \alpha_{p,l} h_A(k - k_{p,l}) \tag{3.40}$$

In order to ensure the definition 3.2.1, the next condition must be fulfilled:

$$(k < 0) \Rightarrow (h_A(k - k_{p,l})) = 0 \text{ for } l = \{0, \cdots, L\} \tag{3.41}$$

Inequality (3.39) allows to affirm that (3.41) is achieved if lemma 3.4.1 is also achieved. Thus, the lemma 3.4.1 holds for several reflection case.

Analogous to equations (3.10) and (3.11), (3.37) is substituted in equation (3.5) produces the next equations for $h_A(k)$ in several reflections case:

$$\sum_{l=0}^{L} \alpha_{s,l} h_A(-k_{s,l}) = 1 \quad \text{if} \quad k = 0 \tag{3.42}$$
$$\sum_{l=0}^{L} \alpha_{s,l} h_A(k - k_{s,l}) = 0 \quad \text{if} \quad k \neq 0 \tag{3.43}$$

The number of variables produces several difficulties to follow the same procedure in one reflection analysis. Therefore, an approximation based on the result of one dimensional approach is proposed.

$$\hat{h}_A(k) = \bar{h}_A(k) + \mathcal{E}_1(k) + \mathcal{E}_2(k) \tag{3.44}$$

Where $\bar{h}_A(t)$ can be obtained using the result of one reflection (see Section 3.4.1). This cancels all reflections but generates error in two different origins $\mathcal{E}_1(k)$ and $\mathcal{E}_2(k)$. The impulses generated by reflections can be canceled using equation (3.22) and $h_{i,0} = 0$ as follows:

$$\bar{h}_A(k) = \frac{(-\alpha_{s,l})^{\psi}\alpha_{s,0}}{(\alpha_{s,0})^{(\psi+1)}} \text{ if } k = \psi k_{i,l} - (\psi + 1)k_{i,0} \tag{3.45}$$
$$\bar{h}_A(k) = 0 \text{ if other } k \tag{3.46}$$

However, the first error $\mathcal{E}_1(k)$ occurs if ψ is truncated to a value ψ_{max} instead of ∞, then this error can be calculated as:

$$\mathcal{E}_1(k) = \sum_{l=1}^{L} \frac{-(-\alpha_{s,l})^{(\psi_{max}+1)}\alpha_{s,0}}{(\alpha_{s,0})^{(\psi_{max}+2)}}\delta_l \tag{3.47}$$

$$\delta_l := \delta(\psi_{max}k_{S,l} - \psi_{max}k_{s,0}) \tag{3.48}$$

$$\tag{3.49}$$

On the other hand, the approximation $\bar{h}_A(k)$ produce another error $\mathcal{E}_2(k)$. It is generated because $\bar{h}_A(k)$ does not take into account the interaction between multiples impulses to achieve equation (3.5). The error can be calculated as:

$$\mathcal{E}_2(k) = \sum_{m=1}^{L}\sum_{l=1l\neq m}^{L}\sum_{k=1,k}^{k_{max}} h_{A,m,l,\psi} \tag{3.50}$$

$$h_{A,m,l,\psi} := h_A(\psi t_{s,m} - \psi t_{s,0})\alpha_{s,l}\delta(t_{s,l} + \psi t_{s,m} - \psi t_{s,0}) \tag{3.51}$$

Then, it is important to show that equation (3.44) allows to approximate a causal impulse response of the controller, using equation (3.2). Also it is important to remark that the approximation $\hat{w}(k) = -\hat{h}_A(k) * h_{p,1}$ achieves the condition in equation (3.4.1).

3.4.3 Simulation of control performance

In order to show which is the meaning of the theorem (3.4.1), several simulations are carried out. They consists on simulate the system in figure 3.1 using different impulse responses for primary and secondary path. Also, the important characteristic of both impulse responses is the time before the first value different to zero. Then, simulations take into account these parameters which are represented by the variables $k_{p,0}$ and $k_{s,0}$. The ratio between them is compared with performance of the controller.

The simulation consists in a FxLMS algorithm applied as it is shown in section 2.3. The primary and secondary paths are chosen as follows:

- The value of $k_{p,0}$ is equal to 10, 30 or 50, three cases are evaluated.
- Values of the impulse response $h_{p,1}(k)$ between $k = k_{p,0} + 1$ and $k = k_{p,0} + 15$ are randomly chosen and $h_{p,1}(k) = 0$ for $k > k_{p,0}+15$. This values are constant for any $k_{p,0}$.
- $k_{s,0}$ is evaluated for values from 1 to 100.
- Also, the values of $h_{p,1}(k)$ between $k = k_{p,0}+1$ and $k = k_{p,0}+15$ are randomly chosen and $h_{p,1}(k) = 0$ for $k > k_{p,0}+15$. This values are constant for any $k_{s,0}$.

Notice that the only parameters that changes in all simulations are $k_{p,0}$ and $k_{s,0}$, which are the only variables that affects the causality of the controller. The performance of controller is shown in figure 3.12. This result confirms the theoretical approach of the theorem (3.4.1). For the condition $k_{s,0} < k_{p,0}$, shown in values lower than one, the noise is attenuated, only the case when $k_{p,0} = 50$ the noise increases

at $k_{s,0} << k_{p,0}$ but this limitation is due to length of adaptive filter and will be investigated in future works. When the ratio is near to $k_{s,0}/k_{p,0} = 1$, the error signal increases its amplitude as $k_{s,0}$ is also increased. Thus, for high values of $k_{s,0}/k_{p,0}$ the attenuation is almost zero. Hence, these simulations of FxLMS controller achieved the theorem (3.4.1).

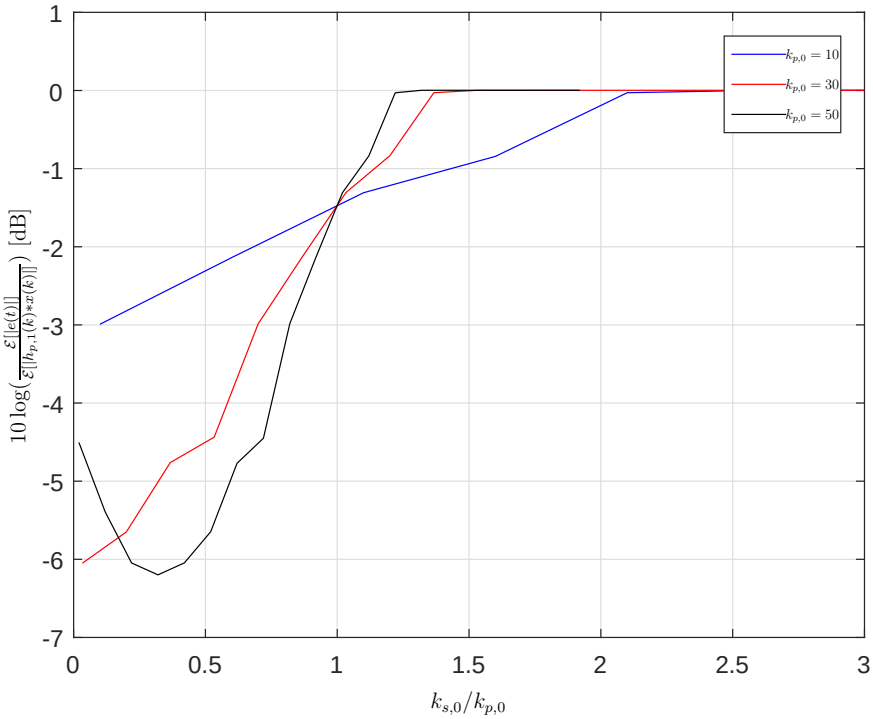

Figure 3.12: Atenuation of control system respect to the ratio $k_{s,0}/k_{p,0}$.

3.5 Conclusions

This chapter described the possibility to assume linearity in the control system. Two problems of non-linear controllers where taken into account, the non-linearity of secondary path and non-causality of the controller. The linearity was empirically proven, comparing measured data with estimated linear and non-linear models, based on identification system methods.

Regarding system identification methods, using the same data, offline methods produced a model with less error. The ARX model is the best of the chosen one for non-training data, with a FIT value equal to 96.19. Nevertheless, online identification can continuously update the model, which produces even less error, as the LMS filter that obtains a FIT equal to 97.44. Those FIT values are quite high, and non-linear proven models obtain lower FIT values. It implies that a linear model is usefull to describe the secondary path.

Analyzing causality, the one reflection system allows a simplification of the problem. Furthermore, this allows to find that location of actuator is the only variable needed to ensure causality, it must be located closer to sensor location than the

primary source. The solution for the causal controller at one reflection is used to solve the problem when several reflections are taken into account adding one error, which is possible to calculate.

The main conclusion is that it is possible. The secondary path was measured and several models were estimated. They confirmed that it can be assumed as linear and the error of estimated output is less than 10% of the energy of output signal. Furthermore, the non-linearity is also used to solve the case where the controller needs non-causal system. It was found that the controller is causal if the distance between actuator and receiver is lower than the distance between primary source and receiver.

Chapter 4

Active Shielding with Implicit Control

Abstract *The main contribution of this document is shown in this chapter, which is the active shielding method that allows to use any control algorithms ensuring attenuation using sensors located at boundaries of desired silent zone. First, it defines the concept of implicit control. Then, this definition is used to develop the proposed active shielding method. It comes from wave equation analysis. The demonstration is carried out for one and two dimensional system. Simulations are shown for one, two and three dimensional systems. At the end, a limitation regarding the distance of sensors is statistically analyzed. Using simulations, mathematical model for predicting this limit is obtained using statistical estimation. Furthermore, an active shielding system is compared to a virtual sensing model. This solves the same problem and the advantages for this case are shown.*

4.1 Introduction

In chapter 2, active noise control problems have been described. There, it is mentioned the necessity of controlling noise at locations where the sensor is not located. A solution for a high volume is active shielding (it produces a field with sensors and actuators at boundaries of a desired silent zone) and its advantage is not using estimation as virtual sensing. This chapter proposes an active shielding method, which does not produce a specific control signal, but any control algorithm can be applied to obtain desired attenuation in whole region. This allows to ensure that if a multi-channel controller attenuates the noise at boundaries of a desired silent zone, then it also attenuates sound pressure inside.

The chapter is organized as follows: the first section defines a concept called implicit control, the basis for the active shielding method. The second section shows the active shielding method and demonstrations for one and two dimensional systems (the three dimensional approach is shown in Appendix C). In third section, simulations are graphed for one, two and three dimensional cases. Then, a statistical analysis from simulations produces equations that describes the limits of theoretical approach in fourth section. The fifth section shows an example which compares and

shows the potential advantage of active shielding with respect to virtual sensing. This chapter ends with some concluding remarks.

4.2 Concept of Implicit Control

Before understanding how the proposed active shielding system works, it is necessary to define next new concept:

Definition 4.2.1. ***Implicit control****: It is the phenomenon that obtaining a specific value of variable implies getting a desired value for another variable.*

For active noise control, it occurs when attenuating (controlling) the pressure at the sensor location, implies the attenuation at other location. It is important to remark that the pressure at each location is defined as a different variable. The aim of this new concept is to be applied as a method to ensure that attenuating the boundaries of a desired silent zone, any location inside it is also attenuated.

In order to clearly show this concept, an example of an active noise control system in two dimensional free field is taken into account. See the locations in the scheme in figure 4.1. The figure shows two point sources, one generates the noise and the other is the actuator (controlled source). They are located at $\chi_1 = [\chi_{1,a}, 0]$ and $\chi_2 = [\chi_{2,a}, 0]$ respectively (for the axis $[x_1, x_2]$). The sensor is located at $\chi_l = [\chi_{l,a}, \chi_{l,b}]$ (Location which is the pressure to be controlled) with a distance d_1 and d_2 from the noise source and actuator respectively. As additional restriction $\chi_{1,a} < s_a$ and $\chi_{2,a} > s_a$. Additionally, a location χ_l' is defined as the point where the distance to both sources is equal to the distance between χ_l and the sources.

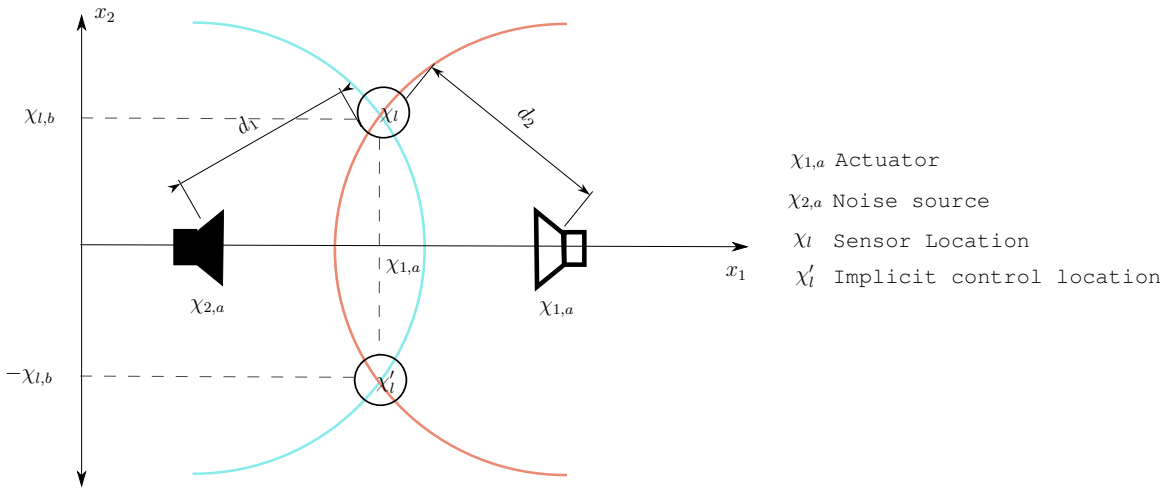

Figure 4.1: Scheme of implicit control example for a 2D acoustic system.

The total pressure $p_t(\chi, t)$, at $\chi = [\chi_1, \chi_2]$ location and time instant t, can be expressed as a function of the pressure components $p_1(\chi, t)$ and $p_2(\chi, t)$, which represent the pressure due to the noise source and the actuator respectively. Then, it can be expressed as:

$$p_t(\chi, t) = p_1(\chi, t) + p_2(\chi, t) \tag{4.1}$$

For the frequency analysis of this case, these two components of pressure can be expressed as functions of distance d_1 or d_2 between the receiver at location χ_l and source locations (each one for each source respectively), i.e.:

$$p_1(\chi_l, t) = j\rho_0 c \frac{Q_1 \eta}{4\pi d_1} e^{j(\omega t - \eta d_1)} \tag{4.2}$$

$$p_2(\chi_l, t) = j\rho_0 c \frac{Q_2 \eta}{4\pi d_2} e^{j(\omega t - \eta d_2)} \tag{4.3}$$

Where ρ_0 is the air density; c is the speed of sound; Q_1 and Q_2 are the source strength; η is the wave number; and ω is the frequency of sound.

Furthermore, the control of the pressure at χ_l is achieved if $p_t(\chi_l, t) = 0$. It means $p_1(\chi_l, t) = -p_2(\chi_l, t)$. This condition is accomplished from (4.1), (4.2) and (4.3) if:

$$Q_2 = -\frac{Q_1 d_2}{d_1} e^{j(\eta d_2 - \eta d_1)} \tag{4.4}$$

Notice that Q_2, $p_1(\chi_l, t)$ and $p_2(\chi_l, t)$ only depend on the distances d_1 and d_2 due to ρ_0, c and η, which are constants. Hence, equation (4.4) is a solution for any other location S_l' such that the distance between the sources and χ_l' are equal to χ_l, i.e. $\chi_l' = [\chi_a, -\chi_b]$ and both locations have the same value of pressure. It means that the implicit control occurs and controlling the pressure at χ_l implies to control the pressure at χ_l' because the attenuation of the pressure at one location implies the attenuation at the other location.

As a consequence of the implicit control phenomenon, a related issue appears:

Problem How to find the locations to be controlled in order to obtain implicit control in a desired silent zone?

From the definition of implicit control, the issue is to find a set of locations $\chi_{1,b}, \chi_{2,b}, \cdots, \chi_{N,b}$ such that they achieve the implicit control at another set of locations $\chi_{i,sz}$, with $i = 1, \cdots, M$ where M is the number of locations where the implicit control occurs. Defining two vectors with the pressure in frequency space for these locations as:

$$P(\omega) := [F(p_t(x_{1,sz}, t)), F(p_t(x_{2,sz}, t)), \cdots, F(p_t(x_{M,sz}, t))] \tag{4.5}$$

$$\bar{P}(\omega) := [F(p_t(x_{1,b}, t)), F(p_t(x_{2,b}, t)), \cdots, F(p_t(x_{N,b}, t))] \tag{4.6}$$

where $F(\cdot)$ is the Fourier transform.

It is evident that the implicit control can be proven for locations that achieve the following condition:

$$\left\{P(\omega) = G(\omega)\bar{P}(\omega)\right\} \text{ and } \bar{P}(\omega) \text{ is controlled} \tag{4.7}$$

Where $G(\omega)$ is any linear transform.

For the example in figure 4.1, the equation (4.4) ensures the restriction (4.7) for $[\chi_{1,s} = \chi_l]$, $[x_{1,b} = \chi_l']$ and $G(\omega) = 1$. Hence, the implicit control is accomplished in the case of figure 4.1.

4.3 Active shielding method

This section describes a novel methodology to implement an active shielding system based on implicit control. It means obtaining a controller which produces a desired silent zone using the information of the pressure at its boundaries instead the pressure inside the silent zone with the concept shown in the previous section. Basically, the aim is to solve the problem 4.2 with a set of pressure at boundaries $\bar{P}(\omega)$. For sake of simplicity, the analysis will be carried out in one and two dimensional free field systems (the analysis for three dimensional system is in Appendix C). The procedure consists of discretizing the wave equation through the finite difference method. It allows the description of the pressure at one location as a function of the pressure at contiguous locations. Thus, the relation of the pressure inside the silent zone and its boundary can be written as a space state model (This is a general form to write equations which describes linear systems, see [73] for a more detailed description), which ensures a linear relationship between them and the restriction (4.7).

Theorema 4.3.1. *Considering the sources are outside the desire silent zone, the relation between the vector of pressure at all discrete locations inside the desired silent zone $\mathcal{Z}(k)$ and the vector with pressure at the discrete locations at its boundaries $\mathcal{U}(k)$ is linear and can be written as a space state model of the form:*

$$\begin{bmatrix} \mathcal{Z}(k+1) \\ \mathcal{Z}(k) \end{bmatrix} = \begin{bmatrix} \mathcal{A} & \hat{\mathcal{A}} \\ \mathbb{I} & \mathbb{O} \end{bmatrix} \begin{bmatrix} \mathcal{Z}(k) \\ \mathcal{Z}(k-1) \end{bmatrix} + \begin{bmatrix} \mathcal{B} \\ \mathbb{O} \end{bmatrix} \mathcal{U}(k) \tag{4.8}$$

Where $\mathcal{A}$, $\hat{\mathcal{A}}$ and $\mathcal{B}$ are real matrices; $\mathbb{I}$ is an identity matrix; and $\mathbb{O}$ is a zero matrix. The size of all matrices depends on the number of discrete locations inside of desired silent zone and at its boundaries .

It means, this relation achieves the restriction (4.7).

The demonstration for one and two dimensional systems is developed below.

4.3.1 One dimensional system

In one dimensional system, the scheme taken into account is shown in figure 4.2. The desired silent zone has green color. The aim is to obtain information about the behavior of its pressure based on the behavior of the pressure at its boundaries to prove the theorem 4.3.1.

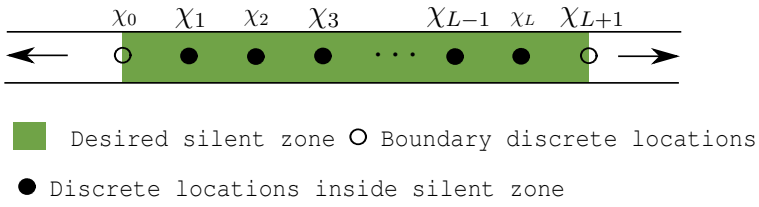

Figure 4.2: Scheme of acoustic system taken into account.

The equation that describes the behavior of pressure by the desired silent zone in figure 4.2 is the damped wave equation:

$$\frac{\partial^2 p(\chi,t)}{\partial \chi^2} - \zeta \frac{\partial p(\chi,t)}{\partial t} - \frac{1}{c^2}\frac{\partial^2 p(\chi,t)}{\partial t^2} = 0 \tag{4.9}$$

Where ζ is the damping coefficient. Notice that this equation assumes that the noise source is located away from the silent zone, where the analysis is carried out.

From equation (4.9), it is quite complex to express the pressure in a desired area based on the pressure of another location. Hence, it is discretized using the finite difference method. Specifically, the differential operator is approximated by:

$$\frac{\partial p(\chi_i,t)}{\partial t} \approx \frac{p(\chi_i,(k+1)\Delta_t) - p(\chi_i,(k-1)\Delta_t)}{2\Delta_t} \tag{4.10}$$

$$\frac{\partial^2 p(\chi_i,t)}{\partial t^2} \approx \frac{p(\chi_i,(k+1)\Delta_t) - 2p(\chi_i,k\Delta_t) + p(\chi_{i,j},(k-1)\Delta_t)}{\Delta_t^2} \tag{4.11}$$

$$\frac{\partial^2 p(\chi_i,t)}{\partial x^2} \approx \frac{p(\chi_{i+1},k\Delta_t) - 2p(\chi_i,k\Delta_t) + p(\chi_{i-1},k\Delta_t)}{\Delta_\chi^2} \tag{4.12}$$

Where Δ_t is the sampling time and Δ_χ is the distance between χ_i and χ_{i+1} for all $i \in \mathbb{Z}$. Discrete locations and time variables are identified by i and k respectively.

Replacing equations (4.10), (4.11) and (4.12) in equation (4.9) and after algebraic simplifications, the term $p(\chi_i,(k+1)\Delta_t)$ yields:

$$p(\chi_i,(k+1)\Delta_t) = \gamma_1\left[p(\chi_{i+1},k\Delta_t) + p(\chi_{i-1},k\Delta_t)\right] + \gamma_2 p(\chi_i,k\Delta_t) + \gamma_3 p(\chi_i,(k-1)\Delta_t) \tag{4.13}$$

Where:

$$\gamma_{1D,1} = \left[\frac{2c^2\Delta_t^2}{\Delta_\chi^2\left(\zeta c^2\Delta_t + 2\right)}\right] \tag{4.14}$$

$$\gamma_{1D,2} = \left[\frac{4}{\zeta c^2\Delta_t + 2}\right] - \left[\frac{4c^2\Delta_t^2}{\Delta_x^2\left(\zeta c^2\Delta_t + 2\right)}\right] \tag{4.15}$$

$$\gamma_{1D,3} = \left[\frac{\zeta c^2\Delta_t - 2}{\zeta c^2\Delta_t + 2}\right] \tag{4.16}$$

Let us consider a set of sound pressure of L successive locations of the desired silent zone such as:

$$\mathcal{Z}_{1D}(k) = \left[p(\chi_1,k\Delta_t), \quad p(\chi_2,k\Delta_t), \quad \cdots, \quad p(\chi_L,k\Delta_t)\right]^T \tag{4.17}$$

In Fig. 4.2, the discrete locations are shown by circles and the locations of the pressures that form $\mathcal{Z}_{1D}(k)$ are in black color. On the other hand, χ_0 and χ_{L+1} are empty circles. Using the equation (4.13), $\mathcal{Z}_{1D}(k)$ can be written as:

$$\mathcal{Z}_{1D}(k+1) = \mathcal{A}_{1D}\mathcal{Z}_{1D}(k) + \gamma_3\mathbb{I}_L\mathcal{Z}_{1D}(k-1) + \mathcal{B}_{1D}\begin{bmatrix} p(\chi_0,k\Delta_t) \\ p(\chi_L,k\Delta_t) \end{bmatrix} \tag{4.18}$$

Where $\mathbb{I}_L$ is an identity matrix with size $L \times L$ and

$$\mathcal{A}_{1D} = \begin{bmatrix} \gamma_2 & \gamma_1 & 0 & \cdots & \cdots & 0 \\ \gamma_1 & \gamma_2 & \gamma_1 & 0 & & \vdots \\ 0 & \gamma_1 & \gamma_2 & \gamma_1 & \ddots & \vdots \\ \vdots & 0 & \ddots & \ddots & \ddots & 0 \\ \vdots & & \ddots & \gamma_1 & \gamma_2 & \gamma_1 \\ 0 & \cdots & \cdots & 0 & \gamma_1 & \gamma_2 \end{bmatrix} \tag{4.19}$$

$$\mathcal{B}_{1D} = \begin{bmatrix} \gamma_2 & 0 \\ 0 & 0 \\ \vdots & \vdots \\ 0 & 0 \\ 0 & \gamma_2 \end{bmatrix} \tag{4.20}$$

Eq. (4.18) is rewritten as a space state model and it yields:

$$\begin{bmatrix} \mathcal{Z}_{1D}(k+1) \\ \mathcal{Z}_{1D}(k) \end{bmatrix} = \begin{bmatrix} \mathcal{A}_{1D} & \gamma_3 \mathbb{I}_L \\ \mathbb{I}_L & \mathbb{O}_L \end{bmatrix} \begin{bmatrix} \mathcal{Z}_{1D}(k) \\ \mathcal{Z}_{1D}(k-1) \end{bmatrix} + \begin{bmatrix} \mathcal{B}_{1D} \\ \mathbb{O}_{1,L} \end{bmatrix} \begin{bmatrix} p(x_0, k\Delta_t) \\ p(x_{L+1}, k\Delta_t) \end{bmatrix} \tag{4.21}$$

This model has a linear relation between $[p(\chi_0, k\Delta_t), \quad p(\chi_{L+1}, k\Delta_t)]^T$ and $\mathcal{Z}_{1D}((k)$. Notice that $p(\chi_0, (k)\Delta_t)$ and $p(\chi_{L+1}, (k)\Delta_t)$ are the pressures at the boundary of the desired silent zone. Hence, it proves the theorem 4.3.1 and ensures to achieve equation (4.7). As a consequence, if $\mathcal{A}_{1D}$ is stable, then to make $[p(\chi_0, k\Delta_t), \quad p(\chi_{L+1}, k\Delta_t)]^T = [0, \quad 0]^T$ is a sufficient condition to ensure $\mathcal{Z}_{1D}(k) = 0$. $\mathcal{A}_{1D}$ is stable if the Courant number is less than one and $0 < \zeta < 1$ and produces a correct discretization. Moreover, stability is expected because otherwise the pressure inside silent zone increases to infinity.

4.3.2 Two dimensional system

For the case of two dimensional system (shown in figure 4.3), the behavior of pressure is also described using the damped wave equation:

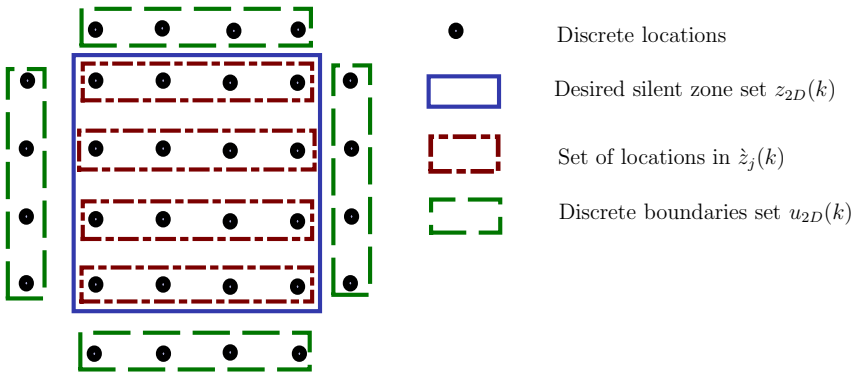

Figure 4.3: Scheme of active shielding system for two dimensional space.

$$\nabla_{2D}(p(\chi, t)) - \zeta \frac{\partial p(\chi, t)}{\partial t} - \frac{1}{c^2} \frac{\partial^2 p(\chi, t)}{\partial t^2} = 0 \tag{4.22}$$

Where $\nabla_{2D}(\cdot) := \frac{\partial^2 \cdot}{\partial \chi_1^2} + \frac{\partial^2 \cdot}{\partial \chi_2^2}$.

Using this continuous time equation, it is quite complex to express the pressure in the desired area based on the pressure at other locations. Hence, equation (4.22) is discretized using the finite difference method. Specifically, the differential operator is approximated by:

$$\frac{\partial p(\chi_{i,j},t)}{\partial t} \approx \frac{p(\chi_{i,j},(k+1)\Delta_t) - p(\chi_{i,j},(k-1)\Delta_t)}{2\Delta_t} \tag{4.23}$$

$$\frac{\partial^2 p(\chi_{i,j},t)}{\partial t^2} \approx \frac{p(\chi_{i,j},(k+1)\Delta_t) - 2p(\chi_{i,j},k\Delta_t) + p(\chi_{i,j},(k-1)\Delta_t)}{\Delta_t^2} \tag{4.24}$$

$$\frac{\partial^2 p(\chi_{i,j},t)}{\partial \chi_1^2} \approx \frac{p(\chi_{i+1,j},t) - 2p(x_{i,j},t) + p(\chi_{i-1,j},t)}{\Delta_\chi^2} \tag{4.25}$$

$$\frac{\partial^2 p(\chi_{i,j},t)}{\partial \chi_2^2} \approx \frac{p(\chi_{i,j+1},t) - 2p(x_{i,j},t) + p(\chi_{i,j-1},t)}{\Delta_\chi^2} \tag{4.26}$$

Where Δ_t is the sample time. In order to simplify the notation, $p(\chi_{i,j},k\Delta_t) =: p(\chi_{i,j},k)$, it implies $t = k\Delta_t$.

Regarding the approximation using finite difference method, it is valid when the variation of the pressure is low with respect to its variations in space. It implies that higher values of Δ_χ produces higher error and this approximation is not valid. Specifically, this discretization applied to the wave equation has been analyzed for $\zeta = 0$, e.g. [92] studies when the model is unstable and [93] deals with the phenomenon called dispersion. However, for $\zeta \neq 0$, it is not analyzed. In this chapter, a statistical analysis of the behavior of this limitation in active shielding method is carried out and presented in section 4.5. Also, it is important to notice that this limitation does not affect the one dimensional system because for any Δ_χ value always has the same two boundaries. Then, the result is the same.

Using previous approximations, the pressure at a discrete location can be written as:

$$\begin{aligned} p(\chi_{i,j},k+1) &= \gamma_{2D,a}\left[p(\chi_{i-1,j},k) + p(\chi_{i+1,j},k) + p(\chi_{i,j-1},k) + p(\chi_{i,j+1},k)\right] \\ &+ \gamma_{2D,b}p(\chi_{i,j},k) + \gamma_{2D,c}p(\chi_{i,j},k-1) \end{aligned} \tag{4.27}$$

With:

$$\gamma_{2D,a} = \frac{2c^2\Delta_t^2}{\Delta_\chi^2\left(\zeta c^2\Delta_t + 2\right)} \tag{4.28}$$

$$\gamma_{2D,b} = \left[\frac{4\left(\Delta_\chi^2 - 2c^2\Delta_t^2\right)}{\Delta_\chi^2\left(dc^2\Delta_t + 2\right)}\right] \tag{4.29}$$

$$\gamma_{2D,c} = \left[\frac{\zeta c^2\Delta_t - 2}{\left(\zeta c^2\Delta_t + 2\right)}\right] \tag{4.30}$$

It is important to remark that equation (4.27) produces a set of equations for different values for i and j. For example, for $i = 1, 2$ and $j = 1$:

$$\begin{aligned} p(x_{1,1},k+1) &= \gamma_{2,a}\left[p(x_{0,1},k)+p(x_{2,1},k)+p(x_{1,0},k)+p(x_{1,2},k)\right] \\ &+ \gamma_{2,b}p(x_{1,1},k)+\gamma_{2,c}p(x_{1,1},k-1) \qquad (4.31) \\ p(x_{2,1},k+1) &= \gamma_{2,a}\left[p(x_{1,1},k)+p(x_{3,1},k)+p(x_{2,0},k)+p(x_{2,2},k)\right] \\ &+ \gamma_{2,b}p(x_{2,1},k)+\gamma_{2,c}p(x_{2,1},k-1) \qquad (4.32) \end{aligned}$$

In order to obtain a space state model and achieve theorem 4.3.1, and assuming the silent zone is a square (as the scheme in figure 4.3), the next procedure shows how to obtain the desired model.

First, the pressures of discrete locations inside the desired silent zone form a vector. In order to organize this vector, a set of pressures along a line (for a fixed value of j) produces a vector as follows:

$$\grave{\mathcal{Z}}_j(k) := [p(\chi_{1,j},k), p(\chi_{2,j},k), \cdots, p(\chi_{I,j},k)]^T \qquad (4.33)$$

The vector $\grave{\mathcal{Z}}_j(k)$ contains the pressures at the locations inside red rectangles in figure 4.3. Each value of j produces a vector and contains the pressure of discrete locations of each line in red of the desired silent zone. These vectors $\grave{\mathcal{Z}}_j(k)$ are concatenated as:

$$\mathcal{Z}_{2D}(k) := [\grave{\mathcal{Z}}_1(k)^T \grave{\mathcal{Z}}_2(k)^T \cdots \grave{\mathcal{Z}}_J(k)^T]^T \qquad (4.34)$$

Thus, the vector $\mathcal{Z}_{2D}(k)$ is the analogous to $P(\omega)$ in discrete time space.

On the other hand, the vector of pressures at locations of the boundary of desired silent zone is formed as:

$$\begin{aligned} \grave{\mathcal{U}}_a(k) &:= [p(\chi_{1,0},k), p(\chi_{2,0},k), \cdots, p(\chi_{I,0},k)]^T \qquad (4.35) \\ \grave{\mathcal{U}}_b(k) &:= [p(\chi_{1,J+1},k), p(\chi_{2,J+1},k), \cdots, p(\chi_{I,J+1},k)]^T \qquad (4.36) \\ \grave{\mathcal{U}}_c(k) &:= [p(\chi_{0,1},k), p(\chi_{0,2},k), \cdots, p(\chi_{0,J},k)]^T \qquad (4.37) \\ \grave{\mathcal{U}}_d(k) &:= [p(\chi_{I+1,1},k), p(\chi_{I+1,2},k), \cdots, p(\chi_{I+1,J},k)]^T \qquad (4.38) \\ \mathcal{U}_{2D}(k) &:= [\grave{\mathcal{U}}_a(k)^T, \grave{\mathcal{U}}_b(k)^T, \grave{\mathcal{U}}_c(k)^T, \grave{\mathcal{U}}_d(k)^T]^T \qquad (4.39) \end{aligned}$$

Each vector of $\grave{\mathcal{U}}_a(k)$, $\grave{\mathcal{U}}_b(k)$, $\grave{\mathcal{U}}_c(k)$ and $\grave{\mathcal{U}}_d(k)$ contains the pressures of the locations inside each green rectangle in figure 4.3. Hence, $\mathcal{U}_{2D}(k)$ contains the pressure at all the discrete locations at the boundaries of the silent zone and is analogous to $\bar{P}(\omega)$. The following system of linear equations can be written to obtain $\mathcal{Z}_{2D}(k)$:

$$\mathcal{Z}_{2D}(k+1) = \mathcal{A}_{2D}\mathcal{Z}_{2D}(k) + \mathcal{B}_{2D}\mathcal{U}_{2D}(k) + \hat{\mathcal{A}}_{2D}\mathcal{Z}_{2D}(k-1) \qquad (4.40)$$

Where the matrices $\mathcal{A}_{2D}$, $\mathcal{B}_{2D}$ and $\hat{\mathcal{A}}_{2D}$ are the relations between the vectors $\mathcal{Z}_{2D}(k+1)$, $\mathcal{Z}_{2D}(k)$, $\mathcal{Z}_{2D}(k-1)$ and $\mathcal{U}_{2D}(k)$. Indeed, they come from (4.27) and they are explained below:

- $\hat{\mathcal{A}}_{2D}$: equation (4.27) expresses that $\gamma_{2D,c}$ is the coefficient which relates the values of the pressure $p(\chi_{i,j},k-1)$ with $p(\chi_{i,j},k+1)$. In equation (4.40), these pressures are located in the vectors $\mathcal{Z}_{2D}(k+1)$ and $\mathcal{Z}_{2D}(k-1)$ respectively at the same position. As a consequence, the diagonal locations of the matrix $\hat{\mathcal{A}}_{2D}$ are equal to $\gamma_{2D,c}$ and zero at any other locations. Mathematically, this is written as $\hat{\mathcal{A}}_{2D} = \gamma_{2D,c}\mathbb{I}_{IJ}$.

- $\mathcal{A}_{2D}$: lets begin analyzing the relation between $\grave{\mathcal{Z}}_j(k+1)$ and $\grave{\mathcal{Z}}_j(k)$. In order to simplify the notation, a matrix $\mathcal{A}_{b2}$ is defined as the relation between these two vectors and it is a sub-block-matrix in $\mathcal{A}_{2D}$. Its values depend on the pressures $p(\chi_{i,j}, k+1)$ and $p(\chi_{i,j}, k)$, which are at the position i inside the vectors $\grave{\mathcal{Z}}_j(k+1)$ and $\grave{\mathcal{Z}}_j(k)$. The relationship between these pressures is the multiplication of the constant $\gamma_{2D,b}$ which is the value for the locations i, i of the matrix $\mathcal{A}_{b2}$. Furthermore, the pressures $p(\chi_{i-1,j}, k)$ and $p(\chi_{i+1,j}, k)$ are also located in $\grave{\mathcal{Z}}_j(k)$ at positions $i-1$ and $i+1$, except if $i-1 \leq 0$ or $i+1 > I$ (this exception is for locations that are not inside the vector because they are out of the desired silent zone). Their relation with $p(\chi_{i,j}, k+1)$ is given by the constant $\gamma_{2D,a}$ and it is the value for all locations $i, i-1$ and $i, i+1$ in the matrix $\mathcal{A}_{b2}$. Hence, the matrix $\mathcal{A}_{b2}$ is:

$$\mathcal{A}_{b2} := \begin{pmatrix} \gamma_{2D,b} & \gamma_{2D,a} & 0 & \cdots & \cdots & 0 \\ \gamma_{2D,a} & \gamma_{2D,b} & \gamma_{2D,a} & 0 & & \vdots \\ 0 & \gamma_{2D,a} & \gamma_{2D,b} & \gamma_{2D,a} & \ddots & \vdots \\ \vdots & 0 & \ddots & \ddots & \ddots & 0 \\ \vdots & & \ddots & \gamma_{2D,a} & \gamma_{2D,b} & \gamma_{2D,a} \\ 0 & \cdots & \cdots & 0 & \gamma_{2D,a} & \gamma_{2D,b} \end{pmatrix} \tag{4.41}$$

Another relationship that needs to be taken into account is between $\grave{\mathcal{Z}}_j(k+1)$ and $\grave{\mathcal{Z}}_{j+1}(k)$. The pressure at position i in the vector $\grave{\mathcal{Z}}_j(k+1)$ is $p(\chi_{i,j}, k)$ which is related to $p(\chi_{i,j+1}, k)$ at the position i in $\grave{\mathcal{Z}}_{j+1}(k)$. Then, the matrix that relates these two vectors is $\gamma_{2D,c}\mathbb{I}_I$. The same matrix relates the vectors $\grave{\mathcal{Z}}_j(k+1)$ and $\grave{\mathcal{Z}}_{j-1}(k)$. For these two cases, it is important to remark that they do not apply for $j-1 \leq 0$ and $j+1 > J$ (it only applies for the discrete locations inside the desired silent zone). Using this result and $\mathcal{A}_{b2}$, the matrix $\mathcal{A}_{2D}$ can be constructed, due to the relationships between the vectors, as:

$$\mathcal{A}_{2D} = \begin{pmatrix} \mathcal{A}_{b2} & \gamma_{2D,a}\mathbb{I}_I & \mathbb{O}_{I,I} & \cdots & & \cdots & \mathbb{O}_{I,I} \\ \gamma_{2D,a}\mathbb{I}_I & \mathcal{A}_{b2} & \gamma_{2D,a}\mathbb{I}_I & \mathbb{O}_{I,I} & \ddots & & \vdots \\ \mathbb{O}_{I,I} & \gamma_{2D,a}\mathbb{I}_I & \mathcal{A}_{b2} & \gamma_{2D,a}\mathbb{I}_I & \ddots & \ddots & \vdots \\ \vdots & \mathbb{O}_{I,I} & \ddots & \ddots & \ddots & \mathbb{O}_{I,I} & \vdots \\ \vdots & \ddots & \ddots & \ddots & \ddots & \ddots & \mathbb{O}_{I,I} \\ \vdots & & \ddots & \mathbb{O}_{I,I} & \gamma_{2D,a}\mathbb{I}_I & \mathcal{A}_{b2} & \gamma_{2D,a}\mathbb{I}_I \\ \mathbb{O}_{I,I} & \cdots & \cdots & \cdots & \mathbb{O}_{I,I} & \gamma_{2D,a}\mathbb{I}_I & \mathcal{A}_{b2} \end{pmatrix} \tag{4.42}$$

- $\mathcal{B}_{2D}$: as it was mentioned before, the relation between the silent zone and the boundary locations has not been analyzed yet. This is because it corresponds to the matrix $\mathcal{B}_{2D}$. The vectors $\grave{\mathcal{Z}}_1(k+1)$ and $\grave{\mathcal{U}}_a(k)$ contain the pressures $p(\chi_{i,1}, k+1)$ and $p(\chi_{i,0}, k)$ respectively. Thus, the relation between these vectors is given by the matrix $\gamma_{2D,a}\mathbb{I}_L$. Notice that this matrix also relates the vectors $\grave{\mathcal{Z}}_I(k+1)$ and $\grave{\mathcal{U}}_d(k)$ and it becomes a sub-block-matrix inside $\mathcal{B}_{2D}$ at two locations.

On the other hand, $p(\chi_{1,j}, k+1)$ for $j = 1$ to J, which is the first term in the vector $\grave{\mathcal{Z}}_j(k)$, is related by the constant $\gamma_{2D,a}$ to $p(\chi_{0,j}, k)$, the pressures in $\grave{\mathcal{U}}_b(k)$. Thus, the matrix that relates $\grave{\mathcal{Z}}_j(k)$ with $p(\chi_{0,j}, k)$ is:

$$b_{2D,1} := \begin{bmatrix} \gamma_{2D,a} \\ 0 \\ \vdots \\ 0 \\ 0 \end{bmatrix} \tag{4.43}$$

The constant $\gamma_{2D,a}$ also relates the pressure $p(\chi_{I,j}, k+1)$ for $j = 1$ to J. It means, the last location in vector $\grave{\mathcal{Z}}_j(k)$ is associated to $p(\chi_{I+1,j}, k)$, which is located in the vector $\grave{\mathcal{U}}_c(k)$. Following the same analysis to obtain $b_{2D,1}$, it is obtained the matrix which multiplies $p(\chi_{I+1,j}, k)$ to obtain $\grave{\mathcal{Z}}_j(k)$. This is:

$$b_{2D,2} := \begin{bmatrix} 0 \\ 0 \\ \vdots \\ 0 \\ \gamma_{2D,a} \end{bmatrix} \tag{4.44}$$

The matrices $\gamma_{2D,a}\mathbb{I}_L$, $b_{2D,1}$ and $\gamma_{2D,a}$ are used to obtain B_{2D} as follows according to the locations of the vectors $\grave{\mathcal{Z}}_j(k+1)$, $\grave{\mathcal{U}}_a(k)$, $\grave{\mathcal{U}}_b(k)$, $\grave{\mathcal{U}}_c(k)$ and $\grave{\mathcal{U}}_d(k)$ in the vectors $\mathcal{Z}_{2D}(k+1)$ and $\mathcal{U}_{2D}(k)$:

$$\mathcal{B}_{2D} = \begin{bmatrix} \gamma_{2D,a}\mathbb{I}_I & b_{2D,1} & \mathbb{O}_{I,2} & \cdots & \cdots & \mathbb{O}_{I,1} & b_{2D,2} & \mathbb{O}_{I,1} & \cdots & \cdots & \mathbb{O}_{I,1} & \mathbb{O}_{I,I} \\ \mathbb{O}_{I,I} & \mathbb{O}_{I,1} & b_{2D,1} & \cdots & & \vdots & \mathbb{O}_{I,1} & b_{2D,2} & \mathbb{O}_{I,1} & \cdots & \vdots & \vdots \\ & & \vdots & \ddots & & \vdots & & \vdots & \ddots & & \vdots & \vdots \\ \vdots & \vdots & & & b_{2D,1} & \mathbb{O}_{I,1} & \vdots & & & b_{2D,2} & \mathbb{O}_{I,1} & \mathbb{O}_{I,I} \\ \mathbb{O}_{I,I} & \mathbb{O}_{I,1} & \cdots & & \mathbb{O}_{I,1} & b_{2D,1} & \mathbb{O}_{I,1} & \cdots & & \mathbb{O}_{I,1} & \mathbb{O}_{2D,2} & \gamma_{2D,a}\mathbb{I}_I \end{bmatrix} \tag{4.45}$$

Notice that the model (4.40) is now completed and it can be rewritten as the space state model in equation (4.22) as follows:

$$\begin{bmatrix} \mathcal{Z}_{2D}(k+1) \\ \mathcal{Z}_{2D}(k) \end{bmatrix} = \begin{bmatrix} \mathcal{A}_{2D} & \hat{\mathcal{A}}_{2D} \\ \mathbb{I}_{IJ} & \mathbb{O}_{IJ} \end{bmatrix} \begin{bmatrix} \mathcal{Z}_{2D}(k) \\ \mathcal{Z}_{2D}(k-1) \end{bmatrix} + \begin{bmatrix} \mathcal{B}_{2D} \\ 0 \end{bmatrix} \mathcal{U}_{2D}(k) \tag{4.46}$$

It means the condition in equation (4.7) and Theorem 4.3.1 are achieved. Also, it shows that the pressures in $\mathcal{Z}_{2D}(k)$ are variables where the implicit control occurs when the pressures in $\mathcal{U}_{2D}(k)$ are controlled. This also proves that controlling the noise at the boundaries of a desired square silent zone is a sufficient condition to control the noise inside this square. Furthermore, using a controller for the pressure at boundaries is an active shielding method because it does not need additional information, such as the pressure inside the desired silent zone. Also, it is important to remark that equation (4.7) has a limitation when $G(\omega)$ has poles. Nevertheless, the equation (4.7) here does not have this limitation, but the matrices $\mathcal{A}_{2D}$ and $\hat{\mathcal{A}}_{2D}$ should ensure stability. The conditions of stability is assumed because it is expected that for any constant pressure at boundaries the pressure inside does not increase to infinity.

4.4 Simulations of active shielding

Towards validating analytically the proposed Theorem 4.3.1, several simulations will be carried out. The idea is evaluating benefit of the relation between the implicit control and the active shielding method. Therefore, using an active noise control system is focused on the pressure at the boundaries, the desired silent zone is evaluated. This evaluation consists of examining the value of the attenuation, with respect to an emitted sinusoid noise signal. The attenuation only can be visualized in one dimensional system. Therefore, it is only considered the silent zone for two and three dimensional systems (satisfactory attenuation). These simulations are based on the control method proposed in Appendix D. It implies the control signal is the optimum value to minimize the pressure at boundary locations.

4.4.1 One dimensional system

According to theory in previous section, the attenuation inside the silent zone must be similar to the one obtained in the control sensor locations. It means, a control law is applied only to attenuate the noise at χ_0 and χ_{L+1}. Then, the result that confirms the theory is that the noise at χ_i with $1 = 1, \cdots, L$ is also attenuated.

The simulated system is shown in the figure 4.4. It consists of a duct with length equal to 6.8m and the reference ($\chi = 0$) is the start of the duct. Two noise sources are located at the end of both sides of the duct. Two actuators (secondary sources) are located at 0.2m and 5.7m. Also, $\chi_0 = 1.7$m and $\chi_{L+1} = 5.1$m. It is assumed the location of the control sensors and all possible location between them is the desired silent zone. The system is simulated using the ray tracing method and the reflection coefficients for the end surfaces (the surface of the noise sources) is 0.7.

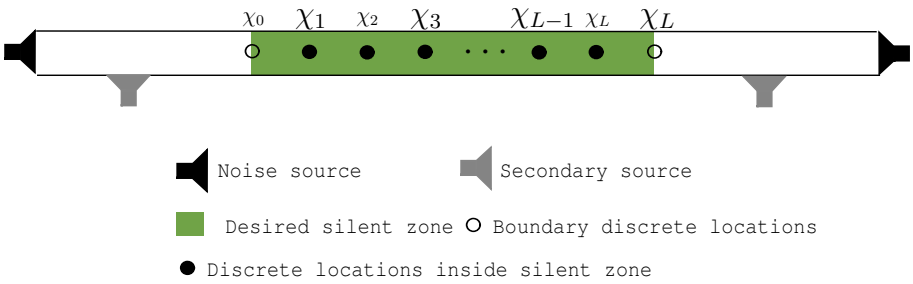

Figure 4.4: Scheme of acoustic measured system.

The attenuation achieved as function of the distance is shown in the figure 4.5. The frequencies tested in the simulation are 63Hz, 125Hz, 250Hz, 500Hz, 1KHz. For all the frequencies, the behavior of the attenuation is the same. The silent zone is achieved for all the locations between the actuators. Hence, the attenuation inside the desired silent zone is very high (more than 100dB) and similar to the obtained at χ_0 and χ_{L+1}. It means that the proposed theory is coherent with the simulation results, independent of the frequency.

4.4.2 Two dimensional system

In order to show the active shielding method in a two dimensional system, the pressure inside the desired silent zone is evaluated. To facilitate visualization, if

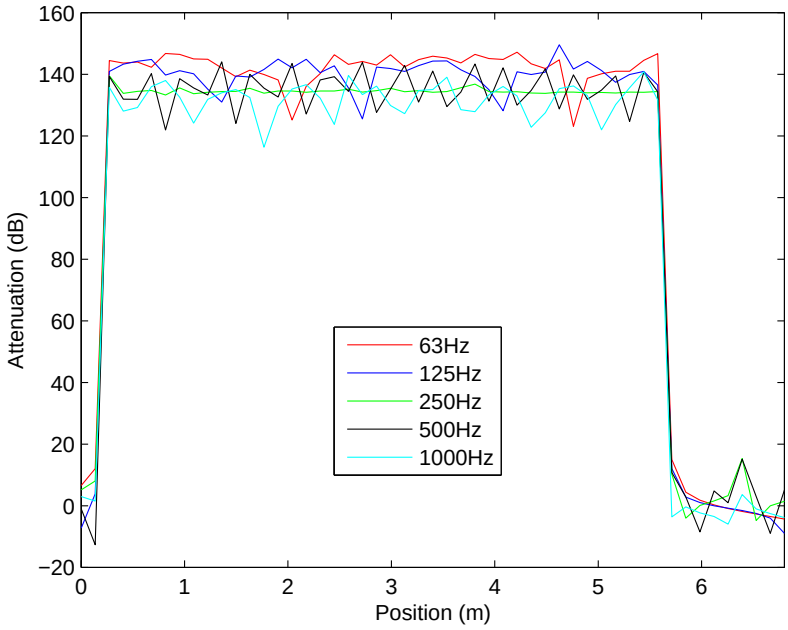

Figure 4.5: Attenuation given by each location.

it is higher than 10 dB, then these locations are plotted as a location where silent zone is achieved. If the whole desired silent zone achieves satisfactory attenuation, then it means that the implicit control is also achieved and the theory exposed in Section 4.3, for the two dimensional case, is valid. It is important to remark that attenuation higher than 10 dB is not assumed to be 100% attenuation, but this is a common limit for a desired attenuation used by other authors, e.g. [94].

In the two dimensional system, shown in figure 4.6, 408 noise sources have been taken into account in free field. They formed a circle with radius equal to 14 meters. In the figure, this circle is shown in red. In the center of it, 12 actuators form a square with each side 12 meters long and three actuators on each side. Each actuator is shown by a blue asterisk. A set of sensors forms another square with each of its sides 3 meters long. Each location of this set is shown by a black small circle and their pressures form the vector $u_{2D}(k)$. There are 12 locations and represent the sensors of the control system. For this case, the control system is focused on minimizing the square of pressure in the zone inside these 12 sensor locations. It is necessary to remark that for this case $I = J = 3$ and Δ_χ is 0.75 m.

The attenuation is hard to be visualized for a total area, instead of that, the silent zone obtained is shown in color green. In figure 4.6, it is evident that the theory works well at low frequencies, at 100Hz, 125Hz and 160Hz. For more detailed information, figure 4.7 shows the achieved percentage of the desired silent zones according to the frequency. It is evident, if the frequency is increased, the achieved silent zone decreases. At frequencies lower than 125Hz, 100% of the silent zone is achieved. For higher frequencies, lower values of this percentage are obtained until less than 10% at 500Hz. It implies that the attenuation decreases inside the silent zone when the frequency is increased. These results show that implicit control is achieved for low frequencies, where it is expected to work according to the finite difference discretization. This is a limitation of the theoretical approach in previous

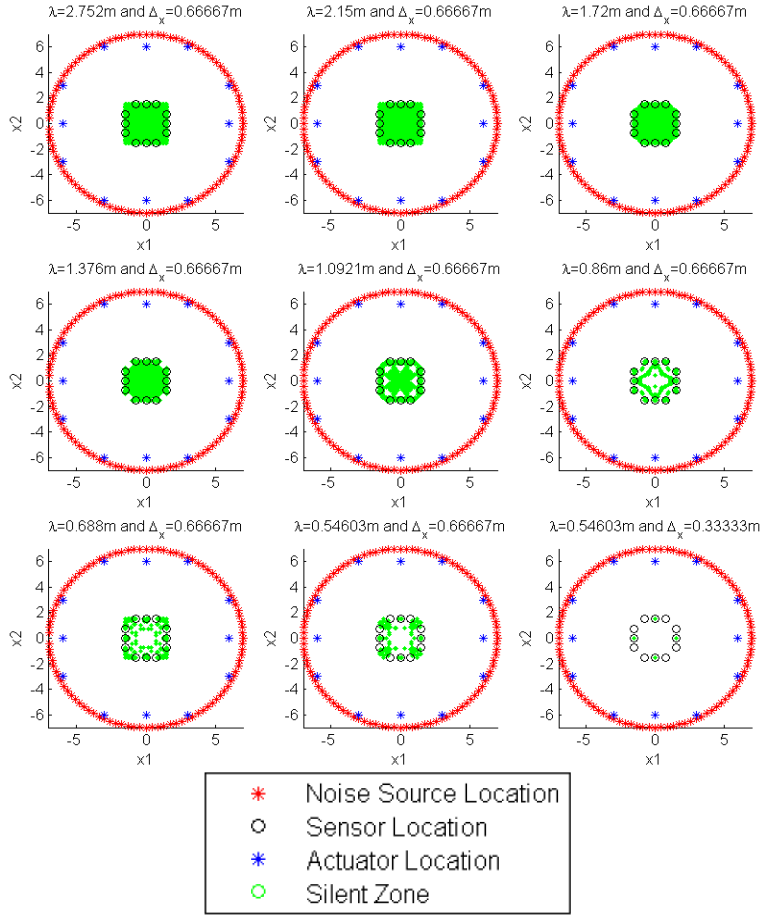

Figure 4.6: Scheme of acoustic active shielding 2D system and its generated silent zone.

section. The value of Δ_x, which is less than the wave length at 125Hz (1.72m), means that the theory is assured if Δ_x is lower than 1/3 of the wave length for this scheme. Thus, the implicit control is achieved. This agrees with the theorem 4.3.1.

4.4.3 Three dimensional system

After the simulations obtained using the two dimensional systems, the three dimensional system is also simulated (see the theory in the Appendix C). Analogous to the simulations in two dimensions, the three dimensional system replaces the circle of noise sources by a shell of a sphere with 14 meters of radius and 114 sources, as it is shown in figure 4.8 in the part a. The squares (two formed by actuators and sensors each one) are replaced by the shell of cubes. Each one has 54 positions for actuators or sensors according it corresponds. The biggest cubic shell in the figure (formed by dots in black color) locates the actuators. Each side of this cube is a square of 3x3 actuators, the size of each side of the squares is 12 m. The other cubic shell (formed by dots in blue color) contains the locations where the control is achieved. It is similar to the other cube, the only difference is the size of each side that is 3 m. The pressures of these locations are contained in $\mathcal{U}_{3D}(k)$. For this case, also Δ_χ is 0.75m and $I = J = L = 3$.

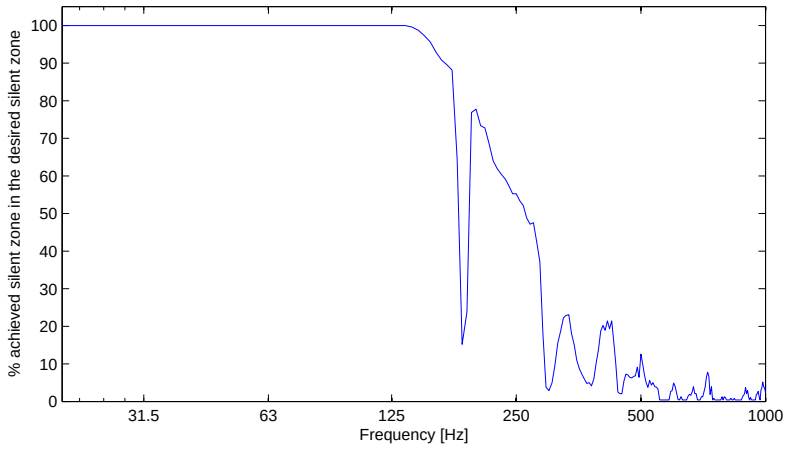

Figure 4.7: Percent of the desired silent zone achieved with respect to the frequency in a two dimensional system.

The 3D results are very similar to the two dimensional system as they are shown in figure 4.8 b. This figure shows a front view of the scheme with the generated silent zone. The frequencies of 100Hz, 125Hz and 160Hz produce the target attenuation, but it cannot be achieved at higher frequencies. A more detailed analysis of the achieved silent zone is shown in figure 4.9. It confirms the high percentage of the attenuation for the mentioned frequencies. However, at 160Hz, 100% of the silent zone is not achieved. This silent zone is achieved at the frequencies lower than 125Hz. In order to obtain the desired silent zone, it implies that Δ_χ must be lower than 1/3 of the wave length.

The results using a three dimensional system totally agree with the results for two dimensional system. They also lead in the direction of the theoretical approach of the theorem 4.3.1, which is proven for three dimensional system in Appendix C.

4.5 Limits of theoretical approach

According to previous simulations, one of the questions to be solved is: which value for Δ_χ is valid to achieve the desired silent zone? This is important because it defines the number of sensors at boundary locations for two and three dimensional systems. It is important to notice that Δ_χ does not affect the number of sensors at one dimensional system. This is the reason why, at higher frequencies, the attenuation is not decreased in the simulation. Using similar simulations to those shown previously for two and three dimensional systems, different values of Δ_χ are tested. Using a boundary formed by the sensors with the same length from previous simulations, the values of I, J and L are changed. This produces the variation for Δ_χ. Also, this variation is evaluated for different frequencies and the parameter to compare the different cases is the percentage of area achieved of the desired silent zone.

For simulations with two dimensional and three dimensional systems, the figures 4.10 and 4.11 show the percentage of the desired silent zone which achieves the attenuation higher than 10 dB with respect to the relation between the distance Δ_x and the wave length λ. For all the frequencies and from both systems, the result produces the same performance. For low values of Δ_χ/λ, the silent zone is not

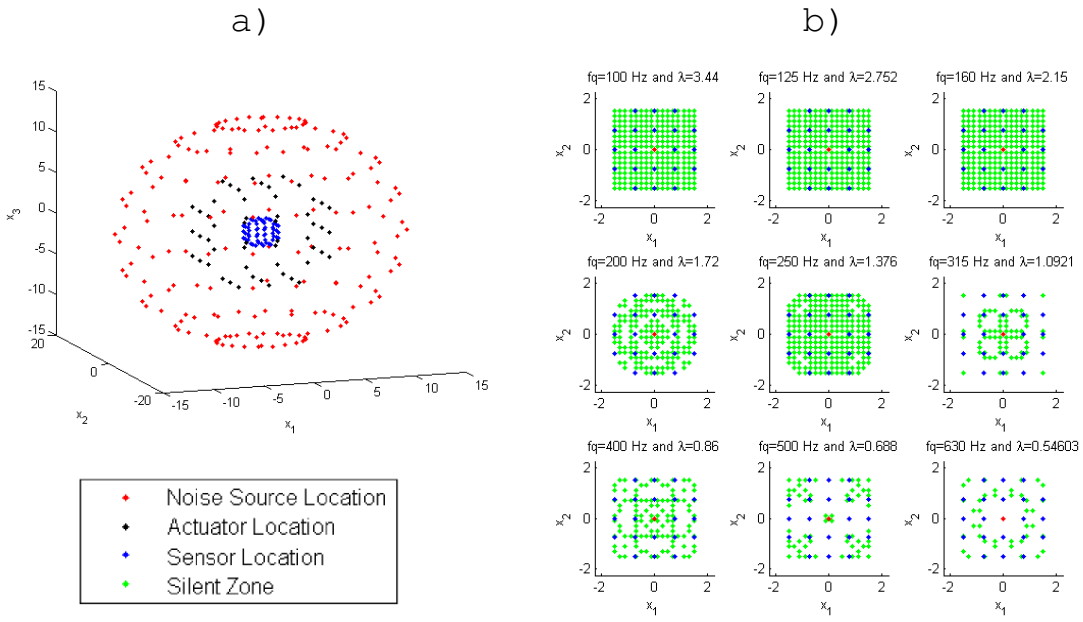

Figure 4.8: Scheme of acoustic active shielding 3D system with the generated silent zone.

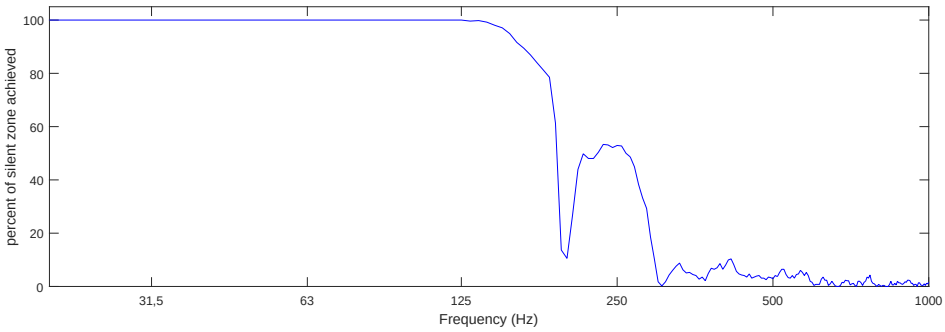

Figure 4.9: Percent of the desired silent zone achieved with respect to the frequency in a three dimensional system.

achieved because the controller produces undetermined mathematical operations. This controller needs to calculate the pseudo-inverse matrix of secondary paths, which is not possible when they are very similar. Hence, sensors must be separated enough with respect to the wave length or the control signal cannot be calculated, for more information see Appendix D (This interval is not shown in figures 4.7 and 4.9 because it occurs at very lower frequency to be shown). As result, the attenuation is not obtained at the boundaries. Therefore, the implicit control is not achieved. This first interval is due to the controller, not to the proposed theory. In spite of it, this interval is taken into account to ensure completeness in the analysis. Then, according figures 4.10 and 4.11, there is an interval of values of Δ_χ/λ where the control system obtains the complete silent zone. The second interval is explained due to the theory exposed in theorem 4.3.1. Other values of Δ_χ/λ produce an interval which shows that the attenuation is not achieved. This is when the implicit control is not achieved. The third interval is due to the limitation when the finite

difference step is not sufficiently fine to discretize the wave equation. Moreover, it is important to remark on the variation of these intervals when the frequency also varies. For higher frequencies, the desired silent zone is obtained even for higher values of Δ_χ/λ.

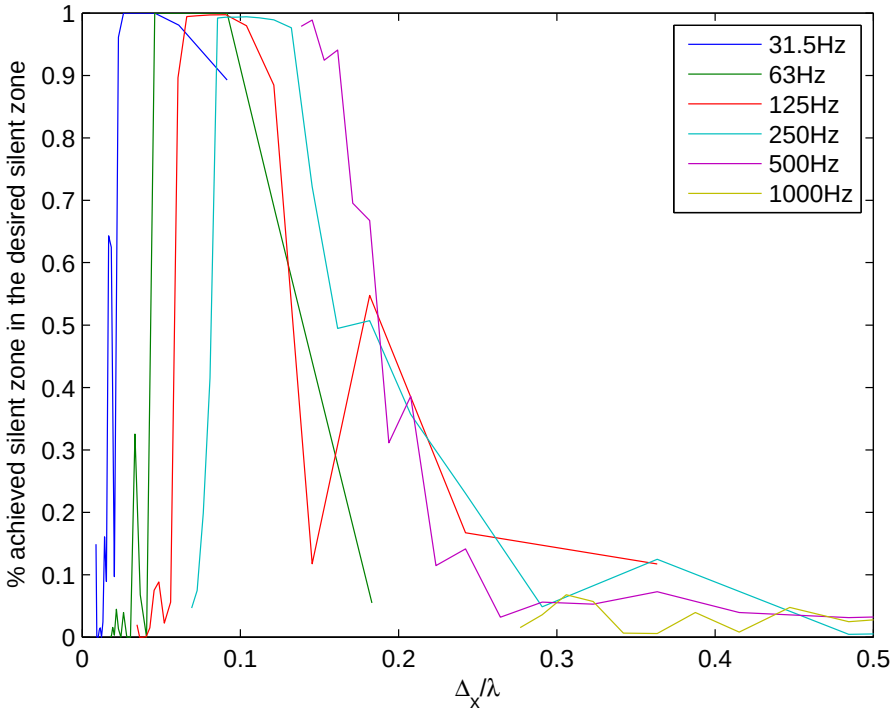

Figure 4.10: Effectiveness of implicit control varying Δ_χ and frequency for the 2D system.

For a more detailed analysis, figures 4.12 and 4.13 plot the maximum and minimum values of Δ_χ/λ where the 90% of the desired silent zone is achieved. In figure 4.12, these maximum and minimum values of Δ_χ/λ are shown with respect to the frequency for the two dimensional system, while figure 4.13 shows the same information, but obtained using the three dimensional system. These figures also show the estimated models used to relate the parameters Δ_χ/λ and the percentage of the achieved silent zone. For the estimated models, the next equations are proposed:

$$\psi_M = \xi_{M,1}(\ln(\omega)) + \xi_{M,0} \tag{4.47}$$

$$\psi_m = \xi_{m,1}(\ln(\omega)^2) + \xi_{m,0} \tag{4.48}$$

Where ψ_M and ψ_m are the maximum and minimum values of Δ_χ/λ where the achieved silent is expected to be higher than 90% of the desired silent zone, $\xi_{M,0}$, $\xi_{M,1}$, $\xi_{m,0}$ and $\xi_{m,1}$ are coefficients obtained through an optimization process which minimizes the mean square error between the data obtained and their corresponding model. The values obtained for these coefficients are shown in the table 4.1

The most important result of this section is that there exists a relation between the frequency of the sound, Δ_χ and the achieved silent zone. Additionally, this relation agrees with the case where the approximations (4.23), (4.24), (4.25) and

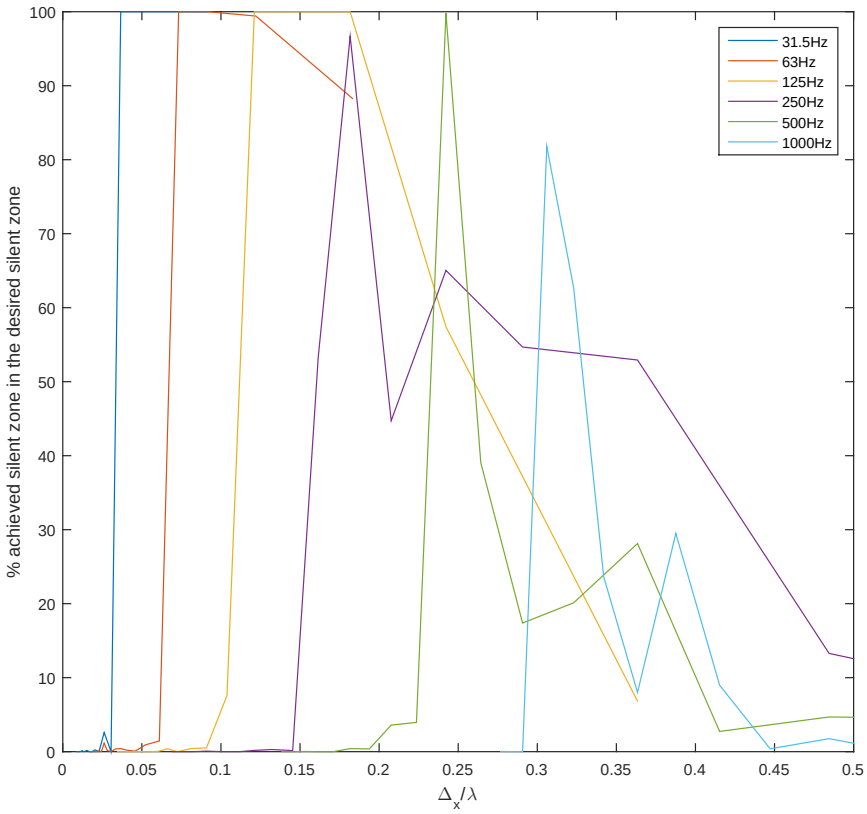

Figure 4.11: Effectiveness of implicit control varying Δ_χ and frequency for the 3D system.

(4.26) are expected to be valid. The figures 4.12 and 4.13 confirm this statement. Furthermore, this section obtains the equation (4.47) which describes the maximum relation Δ_χ/λ to obtain the 90% of the desired zone while the controller attenuates the discrete boundaries.

4.6 Comparison with respect to virtual sensing

In this document, the active shielding is proposed as an alternative solution for virtual sensing. Thus, a simulation between these two methodologies is carried out in this section. Here, it is presented simulations for different frequencies using same locations for sensors and actuators for active shielding and virtual sensing. This comparison is carried out to show advantages of active shielding through an example. However, this is not conclusive. Indeed, this is just to show an example as a first step for future works.

For this simulation, it uses a similar scheme to the one proposed in section 4.4.2. The results can be visualized in figures 4.14 and 4.15. 408 noise sources form a circle with 6 m of radius. The array of 12 actuators is the boundary of a square, which each side is a three meters line. The sensors are located forming the boundaries of another square with two meters side length. In order to apply the virtual sensing method, the desired silent zone is full of a square of 5×5 virtual sensors (25 virtual sensors

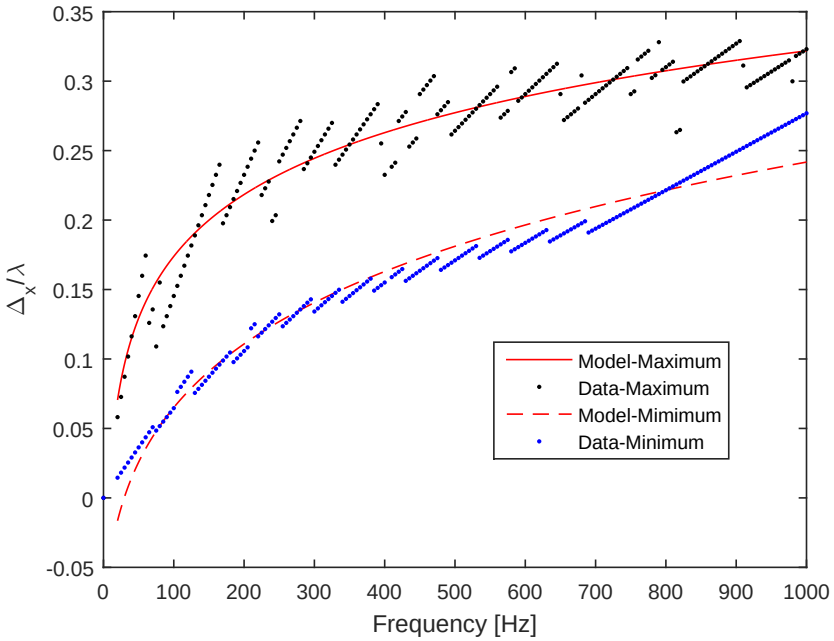

Figure 4.12: Maximum and minimum values of Δ_χ/λ where the active shielding method achieves 90% of the silent zone for a two dimensional system.

Coefficient	2D data	3D data
$\xi_{M,0}$	0.0235	0.0224
$\xi_{M,1}$	0.4727	0.2778
$\xi_{m,0}$	-0.1220	-0.2288
$\xi_{m,1}$	0.0642	0.0947

Table 4.1: Coefficient values of the mathematical models.

are located). The control signal for active shielding is the method in Appendix D. While, for virtual sensing, it is obtained using the optimum value to decrease noise energy according to [94].

The generated silent zone, for frequencies 63, 100, 160 and 250 Hz, is visualized in figures 4.14 and 4.15 for active shielding and virtual sensing respectively. Both methodologies obtain a desired silent zone when the frequency is very low (63 and 100 Hz). At the frequencies of 160 and 250 Hz, attenuating the whole silent zone is not achieved. Previous section explains the reason why attenuation of active shielding is limited, but it is interesting that the virtual sensing method also does not obtain a significant difference in the achieved silent zone. It can be remarked that although the virtual sensing is the optimum at sensor locations based on an estimation, there is a similitude in the silent zone generated between the optimum at the virtual sensors locations and the optimum using active shielding at silent zone boundary.

Regarding the computational cost, it is one of the most important issues to decide which technique is convenient according to hardware limitation. Generalizing, the computational cost of an active shielding system is the computational cost of the controller specified for the number of sensors. It means, depends on the control algorithm, the size of the boundaries and Δ_χ, which must achieve the restriction

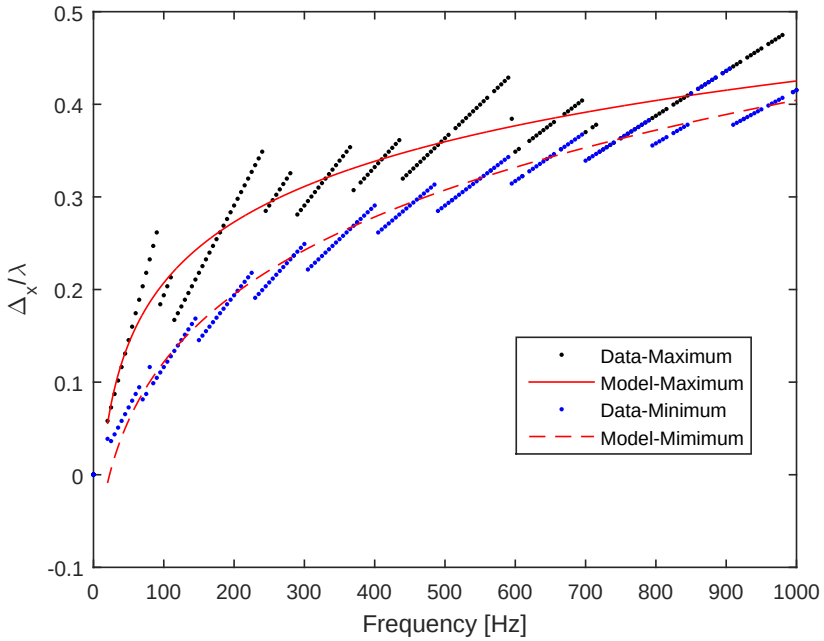

Figure 4.13: Maximum and minimum values of Δ_χ/λ where the active shielding method achieves 90% of the silent zone for a three dimensional system.

in equation (4.47). On the other hand, virtual sensing implies more operations by sensor location due to the transformation to the measured signals to obtain the estimated pressure at virtual sensor locations. The number of operation varies for each virtual sensing algorithm according to the transformation, e.g. it has different value for a Kalman filter [52] than a filter as the method in [51]. Using this analysis, it is evident that the active shielding methods are convenient when the sensor locations at boundary of silent zone are less than the needed by virtual sensors to cover the same area inside. Specifically, in the example shown in this section, active shielding method uses a multichannel controller with 12 sensors and 12 actuators. On the other hand, virtual sensing uses a multichannel control algorithm with 25 sensors and 12 actuators. Moreover, it requires the computational cost for the estimation of the error signal at this locations. Then, it is shown that the computational cost is satisfactorily reduced. A more detailed cases will be the subject of future work.

4.7 Conclusions

This chapter showed a method for active shielding using the definition of implicit control. In section 4.2, the implicit control concept was defined and explained through an example. This section ended up proposing a linear relation to ensure that the implicit control occurs. Then, the wave equation was discretized to obtain a discrete model. It yields a space state model which relates the pressure at the boundaries of a desired silent zone with the pressure inside it. Based on this, an active shielding method was proposed. Later, the simulations presented the silent zone achieved for the proposed active shielding method. This result allows to conclude that if the finite difference approximation is valid, controlling the pressure at the boundaries of the desired silent zone implies controlling the pressure inside it.

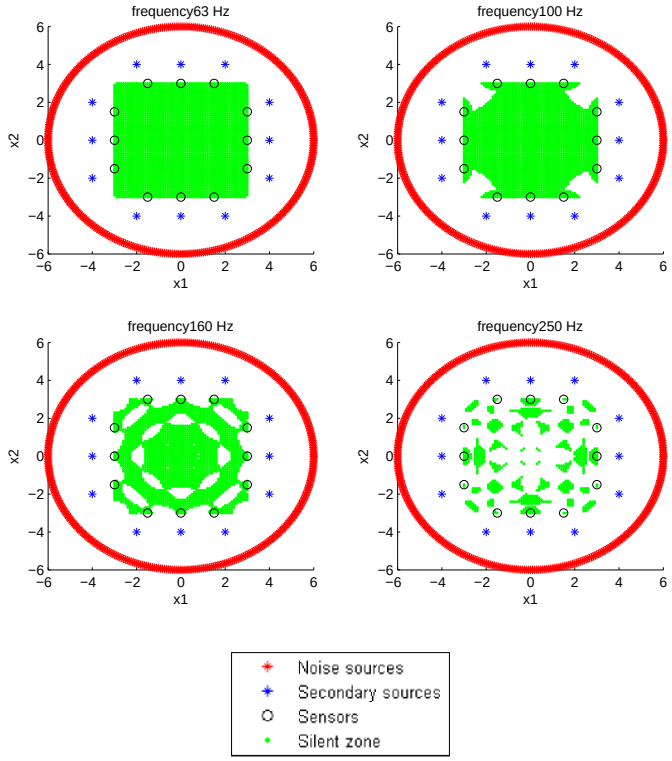

Figure 4.14: Silent zone generated by an active shielding system.

It means, it is an implicit control case. Moreover, it was concluded that applying an active control system to this case is an active shielding system, because it is only needed to control the pressure at the boundaries. It does not need more information to obtain the desired silent zone. From the simulated data, it can be inferred the same conclusion validating the theoretical approach for one, two and three dimensional systems. It is valid for all frequencies for one dimensional systems because Δ_χ does not affects the number and locations of sensors. The simulations for two and three dimensional systems also showed that it happens for frequencies lower than 1/3 of the wave length in the proposed scheme. However, an even more detailed analysis shows that changing the frequency also produces a variation between the maximum value for Δ_χ to achieve the implicit control. When the frequency is higher, the relation Δ_χ/λ can be increased without loosing the attenuation effect inside the silent zone. Besides, the maximum acceptable relation between Δ_χ/λ to achieve 90% of the desired silent zone with respect to the frequency was modeled by equation (4.47), which is the last contribution of this chapter.

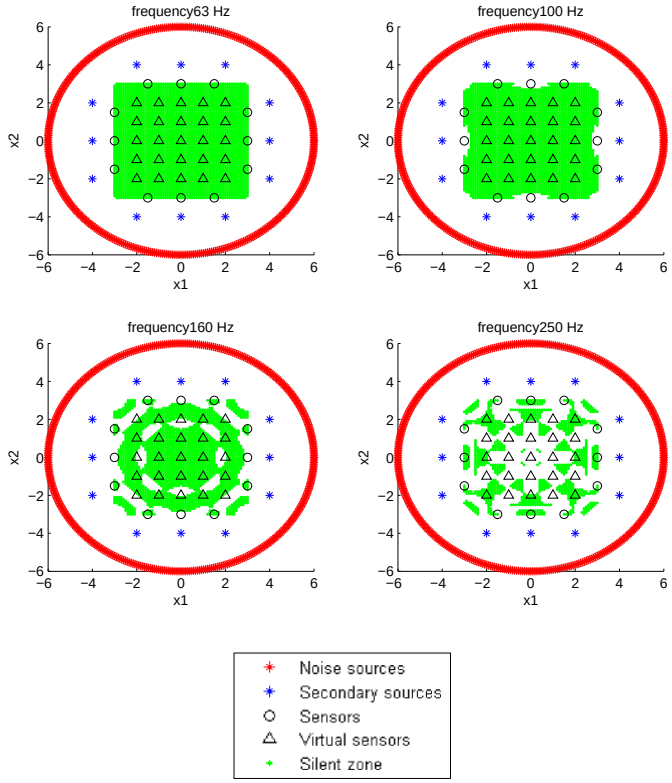

Figure 4.15: Silent zone generated by a virtual sensing system.

Chapter 5

Gaming viewpoint of ANC

Abstract
This chapter is focused on the decentralized control as a solution for massive multichannel active noise control. It begins describing the centralized and decentralized active noise control schemes applied to feed-forward and feedback schemes. Then, an analogy between these schemes and the game theory is proposed. This analogy allows to determine the points where the controller does not have incentive to change the control signal, called Nash Equilibrium. This is analyzed in frequency and time spaces. Furthermore, the Filtered x Least Mean Squares (FxLMS) algorithm with single input and single output is applied as local control as an special case of decentralized control.

5.1 Introduction

In chapter 4, an active shielding method that uses any controller that attenuates the pressure at boundaries is proposed. In order to cover all boundaries as the method requires, several sensors and actuators have to be used. Furthermore, the chapter 2 shows that decentralized and distributed control are methodologies to decrease the computational cost applied to multichannel active noise control, but its convergence and evolution have not been analyzed. In this chapter, the decentralized control is deeply described, analyzed as a game and control signal where the controllers convergence is found using the Nash equilibrium, which gives the values of control signals where the system is in equilibrium and controllers do not have incentive to change the control signal.

5.2 Description of control systems

Taking as reference the definitions given in section 2.5 for decentralized control, this section describes feedback and feed-forward schemes on this context. Figure 5.1 depicts a multichannel feedback ANC scheme, with a fully centralized and a decentralized structure (see Figure 5.1.a and 5.1.b, respectively). It is important to notice that all sources affect the acoustic pressure at all sensor locations in both schemes, but the sensor signals do not affect the control signals in the same way. This section

describes the interaction going on inside the enclosure among the various signals and formulates a general optimization problem to address the ANC task with reference to decentralized scheme.

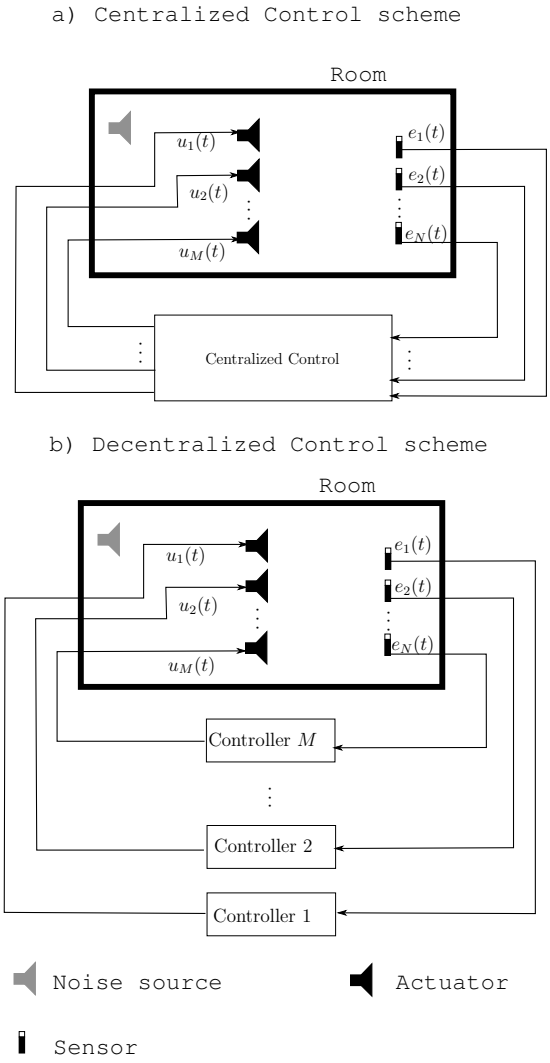

Figure 5.1: Multichannel feedback ANC control inside an enclosure: centralized (Above) and decentralized (Below) schemes.

5.2.1 Sound transmission in the enclosure

The characteristics of the enclosure affect sound transmission in the same way in both schemes in Figure 5.1. For simplicity, we assume that only one noise source is present in the room, shown in gray color. The generalization to the case with multiple noise sources can be easily carried out as shown by [94]. The noise emitted is transmitted directly, through the air, and indirectly, by reflection on the surfaces, finally reaching the receiver microphones. The transfer function between the noise source and the receivers is referred to as primary path. A set of M actuators generates the control signals $\{u_1(t), u_2(t), \ldots, u_M(t)\}$ designed to attenuate the noise. The transfer function from the secondary sources to the receivers (involving again both direct and indirect sound transmission) is called the secondary path. The sound at

the receiver locations is the sum of all the sounds generated and transformed inside the room. At each receiver location, a microphone measures the acoustic pressure signal $e_i(t)$, with $i = 1, \ldots, N$. To simplify the explanation and comparison, it is assumed that the number of sensors equals the number of actuators. Formally, the sound transmission from sources to receivers can be written as:

$$E_i(\omega) = D_i(\omega) + \sum_{j=1}^{M} H_{i,j}(\omega) U_j(\omega) \; ; \; i = 1, \ldots, N, \tag{5.1}$$

where $E_i(\omega)$ and $U_j(\omega)$ are the Fourier transforms of the error signal $e_i(t)$ and control signal $u_j(t)$, respectively, and $D_i(\omega)$ is the Fourier transform of the noise due to the primary source at the location of sensor i. Letting $E(\omega) = [E_1(\omega), E_2(\omega), \ldots, E_N(\omega)]^T$, $D(\omega) = [D_1(\omega), D_2(\omega), \ldots, D_N(\omega)]^T$ and $U(\omega) = [U_1(\omega), U_2(\omega), \ldots, U_M(\omega)]^T$, and defining the matrix

$$H(\omega) = \begin{bmatrix} H_{1,1}(\omega) & H_{1,2}(\omega) & \cdots & H_{1,M}(\omega) \\ H_{2,1}(\omega) & H_{2,2}(\omega) & & H_{2,M}(\omega) \\ \vdots & \vdots & \ddots & \vdots \\ H_{N,1}(\omega) & H_{N,2}(\omega) & \cdots & H_{N,M}(\omega) \end{bmatrix} \tag{5.2}$$

The previous expression can be written in the following compact form:

$$E(\omega) = D(\omega) + H(\omega)U(\omega). \tag{5.3}$$

5.2.2 Feedback Decentralized control

The decentralized control scheme employs several controllers, each one pursuing its own objective and generating one control signal. Here, it is assumed for simplicity that $M = N$. Then, similarly to the control scheme in appendix D, the cost function for the ith controller is the energy of the acoustic pressure at the location of sensor i:

$$J_{D,i}(U_i(\omega)) = E_i^{\mathcal{H}}(\omega) E_i(\omega) \quad i = 1, \ldots, N \tag{5.4}$$

The control signal is obtained by solving the following optimization problem:

$$U^*_{DB,i}(\omega) = \underset{U_i(\omega)}{\operatorname{argmin}} \, J_i(U_i(\omega))$$

$$= -H_{i,i}(\omega)^{-1} \left(D_i(\omega) + \sum_{j=1; j \neq i}^{N} H_{i,j}(\omega) U_{DB,j}(\omega) \right), \tag{5.5}$$

where the subscript $_{DB,i}$ indicates that this solution refers to the decentralized feedback control scheme and the ith actuator. The solution in Equation (5.5) shows clearly that the optimum control signal of an individual controller depends on the values of the control signals of the others, which makes calculation difficult in practice when all controllers operate simultaneously and all the control signals are changing over time.

A gradient descent algorithm can be designed to find the optimum, in the same way to the one carried out by [88], as follows:

$$\begin{aligned} U_{D,i}^{k+1}(\omega) &= U_{D,i}^{k}(\omega) - \mu \nabla J_{D,i}(U_{D,i}^{k}(\omega)) \\ &= U_{D,i}^{k}(\omega) - 2\mu E_i^k(\omega) H_{i,i}(\omega)^H, \end{aligned} \tag{5.6}$$

where the superscript ^{k} indicates the iteration number and $\nabla J_{D,i}(U_{D,i}^{k}(\omega))$ denotes the gradient of $J_{D,i}$ with respect to the value of $U_{D,i}(\omega)$ at iteration k. This method may be employed during online operation, but it may take several iterations to converge to the minimum. Furthermore, even if the optimization algorithm converges, there is no method to evaluate if the cost functions can reduce the error signal value for all locations.

5.2.3 Feed-forward Decentralized control

In feed-forward scheme, the control signals are obtained through a transformation of reference signal $x(t)$, with notation $X(\omega)$ in frequency space. Thus, next relationship is achieved:

$$D_i(\omega) = X(\omega) H_{p,i} \tag{5.7}$$

Where $H_{p,i}$ is the primary path transformation to sensor i. Hence, control signal is written as:

$$\bar{U}_{DF,j}(\omega) = W_i(\omega) X(\omega) \tag{5.8}$$

Where $W_i(\omega)$ is the transfer function associated to controller i.

The value of $W_i(\omega)$ is the decision variable of the optimization problem as follows:

$$\begin{aligned} W_{D,i}^{*}(\omega) &= \arg\min_{W_i(\omega)} E_i^{\mathcal{H}}(\omega) E_i(\omega) \text{ with } j \neq i \\ &= -h_{i,i}(\omega)^{-1} \left(h_{p,i}(\omega) + \sum_{j=1, j\neq i}^{I} h_{j,i}(\omega) W_{D,j}(\omega) \right) \end{aligned} \tag{5.9}$$

The subscript D, i indicates the actuator i and the decentralized scheme.

Analogous to the feedback scheme, the gradient descent algorithm also can find the minimum as follows:

$$\begin{aligned} W_{D,i}^{k+1}(\omega) &= W_{D,i}^{k}(\omega) - \mu \nabla J_{D,i}(W_{D,i}^{k}(\omega)) \\ &= W_{D,i}^{k}(\omega) - 2\mu E_i^k(\omega) \left[H_{i,i}(\omega) X(\omega) \right]^H, \end{aligned} \tag{5.10}$$

where $\nabla J_{D,i}(W_{DB,i}^{k}(\omega))$ denotes the gradient of $J_{D,i}$ with respect to the value of $W_{D,i}(\omega)$ at iteration k.

Again, gradient descent method may be used during online operation. However, the value of the transfer function $W_{D,i}(\omega)$ after algorithm convergence is not known. Thus, next sections center attention on determining its value of convergence, as well as $U_{DB,i}(\omega)$ for feedback scheme.

5.3 Game theoretical perspective

Game theory studies the interaction of different agents with different aims under the same rules ([95]). Each agent uses one option of a set of strategies to obtain its aim. In the analysis of a game, it is important to establish what is the benefit gained by each agent according to its preference. This section formulates the decentralized multichannel ANC problem as a game and uses the concept of Nash Equilibrium to evaluate the amount of attenuation obtained inside the enclosure as a result of the interaction of the different controllers.

A game consists of more than one agent, a relation of preference for each agent, and a set of strategies for each agent. The decentralized multichannel ANC problem configures a game where the agents are the independent controllers operating on different input/ouput pairs. The relation of preference is represented by the aim of each agent, which amounts to the sound pressure minimization at its own sensor location. The strategy is the decision variable of the optimization process, i.e. $U_i(\omega)$ for the ith feedback controller and $W_i(\omega)$ for the ith feed-forward controller. Since the control signal or control filter take values in a real interval, infinite strategies are possible, and the game is characterized as a *continuous* one. See the evolution of each controller in equations (5.6) and (5.10), which do not employ information related to the other controllers. Table 5.1 summarizes the similarities between the game and the control problem described in this section.

Game	**Feedback ANC**	**Feed-forward ANC**
Environment	Physical acoustic system	Physical acoustic system
Agents	Controllers	Controllers
Relation of preference	J_i	J_i
Strategy	$U_i(\omega)$	$W_i(\omega)$

Table 5.1: Reformulation of the decentralized multichannel ANC problem as a game.

5.4 Nash Equilibrium in frequency space

A solution for games is the Nash equilibrium [95], which describes the chosen strategies for all agents such that no controller has incentive to use another strategy. In the Nash equilibrium, there does not exist an alternative strategy for any given agent that may increase its benefit (that is, if all the other agents keep the same strategy). In other words, it represents a condition where all the agents simultaneously find a minimum. With reference to the decentralized multichannel ANC problem, the fact that the Nash equilibrium condition provides a minimum for each controller is important because it implies that at this point a gradient-based algorithm such as the one proposed in equation (5.6) will not alter the control signal. In other words, the Nash equilibrium constitutes a (local) convergence point for the optimization problem. If $J_i(U_i|\{U_j|j = 1, \ldots, N; j \neq i\})$ (for feedback control) denotes the cost incurred by the ith controller for applying the strategy U_i, given that the other controllers apply the control signals U_j, with $j \neq i$, then the formal definition of the Nash equilibrium for this case is given as follows:

Definition 5.4.1. ***Nash Equilibrium for the decentralized multichannel ANC problem:*** *this is the set of possible strategies* $\{U_1^*, U_2^*, \ldots, U_N^*\}$ *such that* $J_i(U_i^*|\{U_j^*|j = 1, \ldots, N; j \neq i\}) \leq J_i(U_i|\{U_j^*|j = 1, \ldots, N; j \neq i\})$ *for* $i = 1, \ldots, N$.

It is important to remark that , for feed-forward control, $U_i^*(\omega) = W_i^*(\omega)X(\omega)$. Then, the same definition applies for both schemes.

5.4.1 Nash Equilibrium for feedback scheme

When a local controller follows (5.6), it can be assumed that it converges to the solution in (5.5). If all the controllers converge, then the Nash equilibrium must be achieved and it can be expressed as

$$U_{D,i}^*(\omega) = -H_{i,i}(\omega)^{-1} \times \left(D_i(\omega) + \sum_{j=1;j\neq i}^{N} H_{i,j}(\omega) U_{D,j}^*(\omega) \right). \tag{5.11}$$

When (5.11) holds for all value of i between 1 and N. In matrix form, this is

$$\begin{aligned} U_D^*(\omega) &= -H_d(\omega)^{-1} D(\omega) - H_d(\omega)^{-1} \tilde{H}(\omega) U_D^*(\omega) \\ &= -\left[I_N + H_d(\omega)^{-1} \tilde{H}(\omega) \right]^{-1} H_d(\omega)^{-1} D(\omega), \end{aligned} \tag{5.12}$$

where

$$H_d(\omega) = \operatorname{diag}\left(H_{1,1}(\omega), H_{2,2}(\omega), \ldots, H_{N,N}(\omega) \right), \tag{5.13}$$

and

$$\begin{aligned} \tilde{H}(\omega) &= H(\omega) - H_d(\omega) \\ &= \begin{bmatrix} 0 & H_{1,2}(\omega) & \cdots & H_{1,N}(\omega) \\ H_{2,1}(\omega) & 0 & & H_{2,N}(\omega) \\ \vdots & \vdots & \ddots & \vdots \\ H_{N,1}(\omega) & H_{N,2}(\omega) & \cdots & 0 \end{bmatrix}. \end{aligned} \tag{5.14}$$

The corresponding error signal is calculated as follows:

$$\begin{aligned} E(\omega) &= D(\omega) + H(\omega) U_D^*(\omega) \\ &= D(\omega) + H(\omega) \left[-\left(I_N + H_d(\omega)^{-1} \tilde{H}(\omega) \right)^{-1} \right. \\ &\times \left. H_d(\omega)^{-1} D(\omega) \right] \\ &= \left[I_N - H(\omega) \left(I_N + H_d(\omega)^{-1} \tilde{H}(\omega) \right)^{-1} \right. \\ &\times \left. H_d(\omega)^{-1} \right] D(\omega). \end{aligned} \tag{5.15}$$

Now, exploiting expressions $I_N = H_d(\omega)^{-1} H_d(\omega)$ and $\tilde{H}(\omega) + H_d(\omega) = H(\omega)$, it can be shown that

$$\begin{aligned} & H(\omega)(I_N + H_d(\omega)^{-1}\tilde{H}(\omega))^{-1}H_d(\omega)^{-1} \\ = \; & H(\omega)(H_d(\omega)^{-1}H_d(\omega) + H_d(\omega)^{-1}\tilde{H}(\omega))^{-1}H_d(\omega)^{-1} \\ = \; & H(\omega)(H_d(\omega)^{-1}H(\omega))^{-1}H_d(\omega)^{-1} \\ = \; & H(\omega)H(\omega)^{-1}H_d(\omega)H_d(\omega)^{-1} \\ = \; & I_N \end{aligned} \tag{5.16}$$

Substituting expression (5.16) in Equation (5.15), one obtains the zero error condition, as for the centralized case. This is an important result because it shows that the Nash equilibrium associated to the N independent controllers, with the aim to minimize (5.4), produces the same error compared to the centralized controller with control signal (E.1) (see the error of centralized control in appendix E). In other words, the decentralized control system described in this section is in principle capable of achieving the same result as the centralized control one.

Remark Taking into account the several controllers that updates the control signal with equation (5.6), if the decentralized control does not achieve the same minimum as the centralized control(see equation (5.12)), then at least one of the controllers has not obtained the minimum.

5.4.2 Nash Equilibrium for feed-forward scheme

For Nash equilibrium in feed-forward case, the equation (5.9) is analyzed when the minimum is obtained for all controllers using $W^*_{D,j}(\omega)$ as follows:

$$W^*_{D,i}(\omega) = -h_{i,i}(\omega)^{-1}\left(h_{p,i}(\omega) + \sum_{j=1,j\neq i}^{I} h_{j,i}(\omega)W^*_{D,j}(\omega)\right) \tag{5.17}$$

To solve this equation, it is proposed the next array:

$$\bar{W}^*_D(\omega) = \left[\bar{W}^*_{D,i}(\omega), \bar{W}^*_{D,i}(\omega), \cdots, \bar{W}^*_{D,i}(\omega)\right]^T \tag{5.18}$$

Rewriting equation (5.17) as the form of $\bar{W}^*_D(\omega)$, it yields:

$$\bar{W}^*_D(\omega) = -\tilde{H}_d^{-1}\left[H_p(\omega) + \tilde{H}\bar{W}^*_D(\omega)\right] \tag{5.19}$$

$$= -\left[\mathcal{I}_I + \tilde{H}_d^{-1}\tilde{H}\right]^{-1}\tilde{H}_d^{-1}H_p(\omega) \tag{5.20}$$

where

$$H_d(\omega) = \mathrm{diag}\left(H_{1,1}(\omega), H_{2,2}(\omega), \ldots, H_{J,J}(\omega)\right), \tag{5.21}$$

and

$$\tilde{H}(\omega) = H(\omega) - H_d(\omega) = \begin{bmatrix} 0 & H_{1,2}(\omega) & \cdots & H_{1,J}(\omega) \\ H_{2,1}(\omega) & 0 & & H_{2,J}(\omega) \\ \vdots & \vdots & \ddots & \vdots \\ H_{J,1}(\omega) & H_{J,2}(\omega) & \cdots & 0 \end{bmatrix}. \tag{5.22}$$

Obtaining the pressure at the sensor locations, it yields:

$$\begin{aligned} E(\omega) &= H_p(\omega)\nu(\omega) + H(\omega)\nu(\omega)\bar{W}_D^*(\omega) \\ &= -\left[\mathcal{I}_I - H(\omega)\left(\mathcal{I}_I + \tilde{H}_d^{-1}\tilde{H}\right)^{-1}\tilde{H}_d^{-1}\right] H_p(\omega)\nu(\omega) \end{aligned} \tag{5.23}$$

Notice that the term in rectangular brackets of this result has the same form of equation (5.16), it means the error is equal to zero. It shows that if the controllers converge, then the control signals go in the direction of centralized control solution, see the appendix E for the error when centralized control is applied. Moreover, if they do not obtain the centralized control solution, then, the decentralized control system will not converge.

Summarizing this section, it was found that the decentralized control can be analyzed as a game. This analysis is not based on the control algorithm, but the optimization problems of all controllers. Thus, it is necessary to assume that the control algorithm obtains the solution of the minimum error signal energy at its local sensor. When this simultaneously happens to all controllers, it is known as the Nash Equilibrium. This value coincide with the control signals where there is no controller that can decrease further its local cost function without changing the control signal of another controller. For the decentralized active noise control, using local control of one actuator and one sensor, the Nash equilibrium yields the same control signal as the centralized case.

5.5 Nash Equilibrium in time space

For the decentralized control, in time analysis, error signals are written as follows

$$e_i(k) = x(k) * h_{p,i}(k) + \sum_{j=1}^{J} h_{j,i}(k) * u_j(k) \tag{5.24}$$

This is an expression analogous to equation (5.1). Furthermore, control signal is a filter which can be represented by multiplication of vectors.

$$u_j(k) = \bar{x}^T(k)\bar{W}_j \tag{5.25}$$

where $\bar{x}(k) = [x(k), x(k-1), x(k-2), \cdots, x(k-N_f)]^T$ is a vector with the actual and past values of noise signal, $\bar{W}_i = [w_{j,0}, w_{j,1}, w_{j,2}, \cdots, w_{j,N_f}]^T$ is the vector with the coefficients filter and N_f is the size of the filter.

Replacing $u_j(k)$ in (5.24), the error signal becomes:

$$e_i(k) = \bar{x}^T(k)\bar{h}_{p,i} + \sum_{j=1}^{J} \bar{h}_{j,i}^T\tilde{x}(k)\bar{W}_j \tag{5.26}$$

With $\bar{h}_{p,i} = [h_{p,i}(0), h_{p,i}(1), h_{p,i}(2), \cdots, h_{p,i}(N_1)]^T$,
$\bar{h}_{j,i} = [h_{j,i}(0), h_{j,i}(1), h_{j,i}(2), \cdots, h_{j,i}(N_2)]^T$, N_1 and N_2 are the size of the impulse response of primary and secondary paths respectively and:

$$\tilde{x}(k) = \begin{bmatrix} \bar{x}^T(k) \\ \bar{x}^T(k-1) \\ \bar{x}^T(k-2) \\ \vdots \\ \bar{x}^T(k-N_2) \end{bmatrix} \tag{5.27}$$

Furthermore, the aim of all controllers is to minimize the energy of the control signal, which is assumed as a random variable. Then, the cost function is:

$$\mathcal{J}_i = \mathcal{E}\left[e_i^2(k)\right] \tag{5.28}$$

Where $\mathcal{E}[\cdot]$ is the expected value operator.

The equilibrium of previous decentralized control system described is summarized in the next theorem:

Theorema 5.5.1. *More than one independent control systems that interact in same acoustic field, and if they ensures the local optimal value of the cost function in equation* (5.28) *and if the next constraints are achieved:*

1. *One sample is an estimation of the mean.*
2. $[\breve{h}_{x,i,i}^T(k)\breve{h}_{x,i,i}(k)]^{-1}$ *exists and the inverse can be calculated. Where:*

$$\breve{h}_{x,i,j}(k) := \bar{h}_{j,i}^T\tilde{x}(k) \tag{5.29}$$

Then, only has one value of control signals that ensures equilibrium and they obtain minimum pressure (zero).

Proof. Using equation (5.26), the gradient $\nabla_W\mathcal{J}$ of $\mathcal{J}_i$ respect to the filter coefficients yields:

$$\begin{aligned} \nabla_{\bar{W}_i}\mathcal{J}_i &= \frac{\partial}{\partial\bar{W}_i}[\mathcal{J}_i] \\ &= 2\mathcal{E}\left[\tilde{x}^T(k)\bar{h}_{i,i}\bar{h}_{i,i}^T\tilde{x}(k)\bar{W}_i + \tilde{x}^T(k)\bar{h}_{i,i}\bar{h}_{p,i}^T\bar{x}(k)\right. \\ &+ \left.\tilde{x}^T(k)\bar{h}_{i,i}\left(\sum_{j=1,j\neq i}^{J}\bar{h}_{j,i}^T\tilde{x}(k)\bar{W}_j\right)\right] \end{aligned} \tag{5.30}$$

Making $\nabla_{\bar{W}_i}\mathcal{J}_i = 0$ it can be obtained the optimum value of the filter coefficients.

$$\bar{W}_i^* = -\mathcal{E}\left[\tilde{x}^T(k)\bar{h}_{i,i}\bar{h}_{i,i}^T\tilde{x}(k)\right]^{-1}\mathcal{E}\left[\tilde{x}^T(k)\bar{h}_{i,i}\left(\bar{h}_{p,i}^T\bar{x}(k) + \sum_{j=1,j\neq i}^{J}\bar{h}_{j,i}^T\tilde{x}(k)\bar{W}_j\right)\right] \tag{5.31}$$

Then, the expected value operator does not allow to simplify the previous equation. Thus, in order to avoid this limitation, it is assumed that one sample of the signals involved are estimations of its mean. This assumption is used by the Least Mean Squares (LMS) algorithm [96] and subsequently by algorithms based on it, as the FxLMS [97]. It allows to solve the next array:

$$\tilde{W}^* = \begin{bmatrix} \bar{W}_1^* \\ \bar{W}_2^* \\ \vdots \\ \bar{W}_N^* \end{bmatrix} = -\tilde{H}_x^{-1}(k)\tilde{H}_{x,p}(k) - \tilde{H}_x^{-1}(k)\breve{H}_x(k)\tilde{W}^* \tag{5.32}$$

Where

$$\tilde{H}_x^{-1}(k) = \begin{bmatrix} \grave{h}_{x,1,1}(k) & \mathbb{O} & \cdots & \mathbb{O} \\ \mathbb{O} & \grave{h}_{x,2,2}(k) & & \vdots \\ \vdots & & \ddots & \mathbb{O} \\ \mathbb{O} & & \mathbb{O} & \grave{h}_{x,N,N}(k) \end{bmatrix} \tag{5.33}$$

$$\grave{h}_{x,i,i}(k) = [\breve{h}_{x,i,i}^T(k)\breve{h}_{x,i,i}(k)]^{-1}\breve{h}_{x,i,i}(k) \tag{5.34}$$

$$\tilde{H}_{x,p}(k) = \begin{bmatrix} \bar{h}_{p,1}^T\bar{x}(k) \\ \bar{h}_{p,2}^T\bar{x}(k) \\ \vdots \\ \bar{h}_{p,N}^T\bar{x}(k) \end{bmatrix} \tag{5.35}$$

and

$$\breve{H}_x(k) = \begin{bmatrix} \mathbb{O} & \breve{h}_{x,1,2}(k) & \cdots & \breve{h}_{x,1,N}(k) \\ \breve{h}_{x,2,1}(k) & \mathbb{O} & \ddots & \vdots \\ \vdots & \ddots & \ddots & \breve{h}_{x,N-1,N}(k) \\ \breve{h}_{x,N,1}(k) & \cdots & \breve{h}_{x,N,N-1}(k) & \mathbb{O} \end{bmatrix} \tag{5.36}$$

Thus, the Nash equilibrium is:

$$\tilde{W}^* = -\left[\mathbb{I} + \tilde{H}_x^{-1}(k)\breve{H}_x(k)\right]^{-1}\tilde{H}_x^{-1}(k)\tilde{H}_{x,p}(k) \tag{5.37}$$

In order to know the error signal generated by controllers at Nash Equilibrium, equation (5.26) is written in matrix form as follows:

$$\bar{e}(k) = \tilde{H}_{x,p}(k) + H_x(k)\tilde{W}^* \tag{5.38}$$

with

$$\bar{e}(k) = [e_1(k), \cdots, e_N(k)]^T \tag{5.39}$$

$$H_x(k) = \tilde{H}_x(k) + \breve{H}_x(k) \tag{5.40}$$

And

$$\tilde{H}_x(k) = \begin{bmatrix} \breve{h}_{x,1,1}(k) & \mathbb{O} & \cdots & \mathbb{O} \\ \mathbb{O} & \breve{h}_{x,2,2}(k) & & \vdots \\ \vdots & & \ddots & \mathbb{O} \\ \mathbb{O} & & \mathbb{O} & \breve{h}_{x,N,N}(k) \end{bmatrix} \tag{5.41}$$

Furthermore, analogous to equation (5.16), one can show:

$$H_x(k)\left[\mathbb{I} + \tilde{H}_x^{-1}(k)\breve{H}_x(k)\right]^{-1}\tilde{H}_x^{-1}(k) = \mathbb{I} \tag{5.42}$$

Then, replacing $\tilde{W}^*$ in (5.43), it yields:

$$\begin{aligned}\bar{e}(k) &= \tilde{H}_{x,p}(k) - H_x(k)\left[\mathbb{I} + \tilde{H}_x^{-1}(k)\check{H}_x(k)\right]^{-1}\tilde{H}_x^{-1}(k)\tilde{H}_{x,p}(k) \\ &= \tilde{H}_{x,p}(k) - \mathbb{I}\tilde{H}_{x,p}(k) = \mathbb{O} \end{aligned} \tag{5.43}$$

Summarizing this section, the Nash equilibrium can be applied to controllers in time domain. This analysis shows that using two restrictions, the attenuation of decentralized control is zero. It implies some restrictions for the input signal. □

5.6 Analysis of convergence of Distributed FxLMS

The FxLMS is one case of the controllers that minimizes function in equation (5.28) using a control signal of the form (5.25). Thus, this section depicts the behavior of this algorithm and the conditions to obtain the Nash equilibrium. First, it is evaluated the behavior respect to the local optimum. Then, it is evaluated if the local minimum varies its value faster than the filter coefficients. This allows to define if at infinity time, the algorithm obtains the minimum.

To obtain the filter coefficients, a gradient descent algorithm is used in the optimization process as follows:

$$\bar{W}_i(k+1) = \bar{W}_i(k) - \mu_{i,0}\nabla_{\bar{W}_i}\mathcal{J}_i \tag{5.44}$$

$$\bar{W}_i(k+1) = \bar{W}_i(k) - \mu_i\bar{x}_{f,i}(k)e_i(k) \tag{5.45}$$

Where $\mu_{i,0}$ is the size of the step, $\mu_i = 2\mu_{i,0}$ and:

$$\bar{x}_{f,i}(k) = [x_{f,i}(k), x_{f,i}(k-1), \cdots, x_{f,i}(k-N_f+1)]^T \tag{5.46}$$

$$x_{f,i}(k) = \bar{h}_{i,i}\bar{x}(k) \tag{5.47}$$

In order to analyze the evolution of each coefficient of the filter $w_{i,l}(k)$, They are compared respect to its optimum value $w_{i,l}^*$. According to their difference, the next lemma is proposed:

Lemma 5.6.1. *The difference $\varepsilon_i(k) = \bar{W}_i(k) - \bar{W}_i^*(k)$ can be related with the optimum error $e_i(k)^*$ as a linear time variant system of the form:*

$$\mathbf{z}(k+1) = \mathbf{A}(k)\mathbf{z}(k) + \mathbf{B}_1(k)\mathbf{E}(k) + \mathbf{B}_2(k)\bar{\Delta}_{w^*}(k) \tag{5.48}$$

Where:

$$\bar{\varepsilon}(k) = [\varepsilon_1^T(k), \varepsilon_2^T(k), \cdots, \varepsilon_N^T(k)]^T \tag{5.49}$$

$$\mathbf{z}(k) = [\bar{\varepsilon}^T(k), \bar{\varepsilon}^T(k-1), \cdots, \bar{\varepsilon}^T(k-N_2)]^T \tag{5.50}$$

$$\mathbf{E}(k) = [e_1^*(k), e_2^*(k), \cdots, e_N^*(k)]^T \tag{5.51}$$

$$\bar{\Delta}_{w^*}(k) = [\Delta_{w_1^*}^T(k), \Delta_{w_2^*}^T(k), \cdots, \Delta_{w_N^*}^T(k)]^T \tag{5.52}$$

Where $\Delta_{w_i^*}(k) = \bar{W}_i^*(k+1) - \bar{W}_i^*(k)$ and $e_1^*(k)$ is the error when the filter $\bar{W}_i^*(k)$ is applied.[1]

[1] $\bar{W}_i^*(k)$ is the local minimum shown in equation (5.31), then it is not necessary the Nash equilibrium.

Proof. Let's begin focusing on the value of $e_i(k)$ described in equation (5.26). It is writing in terms of $\varepsilon_i(k)$ as follows:

$$\begin{aligned} e_i(k) &= \bar{x}^T(k)\bar{h}_{p,i} + \sum_{j=1}^{J}\left[\sum_{n=0}^{N_2} h_{j,i}(n)\bar{x}^T(k-n)\left(\bar{W}_j(k-n) + \bar{W}_j^*(k-n) - \bar{W}_j^*(k-n)\right)\right] \\ e_i(k) &= e_i^*(k) + \sum_{j=1}^{J}\left[\sum_{n=0}^{N_2} h_{j,i}(n)\bar{x}^T(k-n)\left(\varepsilon_j(k-n)\right)\right] \end{aligned} \tag{5.53}$$

with:

$$e_i^*(k) = \bar{x}^T(k)\bar{h}_{p,i} + \sum_{j=1}^{J}\left[\sum_{n=0}^{N_2} h_{j,i}(n)\bar{x}^T(k-n)\bar{W}_j^*(k-n)\right] \tag{5.54}$$

It is important to remark that $\bar{W}_j^*(k)$ is the one given by equation (5.31). It implies that the local minimum for the instant k given non-optimal values for $\bar{W}_i(k)$ with $i \neq j$. Furthermore, it is assumed as a dynamical variable, due to the variation of $\bar{W}_i(k)$. Hence, it cannot be simplified using $\tilde{x}(k)$.

Also, the equation (5.47) allows to obtain the evolution of $\varepsilon_i(k)$ adding the term $\bar{W}_i^*(k+1) = \bar{W}_i^*(k) + \Delta_{w_i^*}(k)$.

$$\begin{aligned} \bar{W}_i(k+1) - \bar{W}_i^*(k+1) &= \bar{W}_i(k) - \bar{W}_i^*(k) + \Delta_{w_i^*}(k) + \mu_i\bar{X}_{f,i}(k)e_i(k) \\ \varepsilon_i(k+1) &= \varepsilon_i(k) + \Delta_{w_i^*}(k) + \mu_i\bar{X}_{f,i}(k)e_i(k) \end{aligned} \tag{5.55}$$

Then, substituting equation (5.53), it yields:

$$\begin{aligned} \varepsilon_i(k+1) &= \varepsilon_i(k) + \Delta_{w_i^*}(k) + \mu_i\bar{X}_{f,i}(k) \\ &\times \left[e_i^*(k) + \sum_{j=1}^{J}\left(\sum_{n=0}^{N_2} h_{j,i}(n)\bar{x}^T(k-n)\left(\varepsilon_j(k-n)\right)\right)\right] \end{aligned} \tag{5.56}$$

Thus, taken into account $\bar{\epsilon}(k)$, defined in equation (5.49), this is used to express equation (5.56) in matrix form.

$$\bar{\epsilon}(k+1) = \bar{\epsilon}(k) + \sum_{n=1}^{N_2}\bar{\mathbf{A}}(k,n)\bar{\epsilon}(k-n) + \bar{\Delta}_{w^*}(k) + \bar{\mathbf{B}}\bar{e}^*(k) \tag{5.57}$$

Where:

$$\bar{\mathbf{A}}(k,n) = \begin{bmatrix} \bar{\mathbf{a}}_{1,1}(k,n) & \cdots & \bar{\mathbf{a}}_{1,N}(k,n) \\ \vdots & \ddots & \vdots \\ \bar{\mathbf{a}}_{N,1}(k,n) & \cdots & \bar{\mathbf{a}}_{N,N}(k,n) \end{bmatrix} \tag{5.58}$$

$$\bar{\mathbf{a}}_{1,1}(k,n) = \mu_i\bar{X}_{f,i}(k)h_{j,i}(n)\bar{x}^T(k-n) \tag{5.59}$$

$$\bar{\mathbf{B}} = \begin{bmatrix} \mu_i\bar{X}_{f,1}(k) & \mathbb{O} & \cdots & \mathbb{O} \\ \mathbb{O} & \ddots & \ddots & \vdots \\ \vdots & \ddots & \ddots & \mathbb{O} \\ \mathbb{O} & \cdots & \mathbb{O} & \mu_i\bar{X}_{f,N}(k) \end{bmatrix} \tag{5.60}$$

Equation (5.57) has an analogous form in equation (5.48). It is obtained when sum in the second term of the right side is written as a multiplication of vector, where $\mathbf{z}(k)$ appear and the next matrices are defined:

$$\mathbf{A} = \left[\begin{array}{ccc|c} \mathbb{I} + \bar{\mathbf{A}}(k,0) & \bar{\mathbf{A}}(k,1) & \cdots & \bar{\mathbf{A}}(k,n) \\ \hline \multicolumn{3}{c|}{\mathbb{I}} & \mathbb{O} \end{array}\right] \tag{5.61}$$

$$\bar{\mathbf{B}}_1 = \begin{bmatrix} \bar{\mathbf{B}} \\ \mathbb{O} \end{bmatrix} \tag{5.62}$$

$$\mathbf{B}_2 = \begin{bmatrix} \mathbb{I} \\ \mathbb{O} \end{bmatrix} \tag{5.63}$$

□

Lemma 5.6.1 proves that the evolution of the difference between actual value of the coefficient of filter and optimal values can be written as a linear time varying system. Furthermore, convergence can be achieved if the value of μ_i produces a stable system. Stability of time variant systems has been studied e.g. [98] which produces specific characteristics for the matrix $\mathbf{A}(k)$, but more specific characteristics for μ_i will be analyzed in future works. It is interesting to see that there are two disturbances that do not allow to obtain the local minimum, even though $\mathbf{A}(k)$ achieves stable conditions:

1. The minimum possible error $e_i^*(k)$ is a disturbance to the number of the optimization algorithm used as controller. If it is high, then the difference between the optimal adaptive filter and its optimal value is increased. Also, it is important to note that the number of actuators affects $e_i^*(k)$, as it is shown in equation (5.54). Then, it is obvious that more actuators increases the disturbance of the optimization algorithm.

2. The other disturbance is the variation of the local optimum $\Delta_{w_i^*}(k)$, which can be obtained using equation (5.31) for the coefficients in (5.45).

5.7 Simulated examples

In the previous sections, the Nash equilibrium concept was used to obtain an analytical solution for the decentralized multichannel feedback and feed-forward ANC schemes. This section illustrates this result with the aid of some simulation examples.

5.7.1 Free field system with two decentralized controllers

We first consider the free field system depicted in Figure 5.2. Only one noise source is presented, located at the origin. This source emits a noise signal $D(100) = -0.8311 - j0.2004$. Two actuators are located at $[0.5, 0.5]$ and $[0.5, 1]$, respectively. The initial values of the control signals are chosen at random: $U_{D,1}^0(100) = -0.4803 - j0.6001$ and $U_{D,2}^0(100) = -0.1372 - j0.8213$. Additionally, one sensor is located one meter to the right of each actuator. The simulation frequency is $\omega = 100$ and $\mu = 0.5$. The error in frequency space is calculated using equation (5.3).

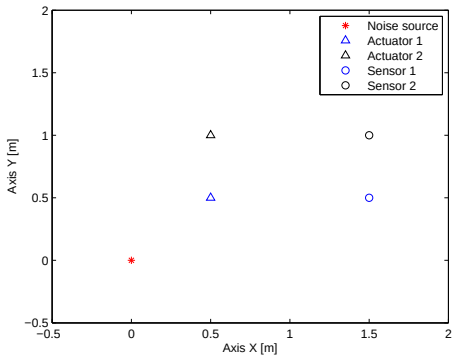

Figure 5.2: Scheme of the locations of sources and sensors.

Equation (5.6) is used to compute the control signals at each iteration k. The corresponding error and control signals are plotted in Figure 5.3. After 600 iterations of the algorithm, the values of the cost functions of both controllers have decreased below 10^{-15}, with a logarithmic evolution with respect to the number of iterations (after iteration 25). Notice that even the number of iterations before convergence is high, the error decreases with only few iterations, with $E_i < 10^{-2}\ \forall\ i = 1, 2$ with 30 iterations. The control signal values converge to $U_{D,1}^{300}(\omega) = 0.5953 + j0.0846$ and $U_{D,2}^{300}(\omega) = -0.0605 - j0.0558i$, respectively. These values are very close to the Nash equilibrium, calculated to be $U_D^*(\omega) = [0.5952 + j0.0847, -0.0604 - j0.0559]^T$. Besides convergence of the two controllers to the Nash Equilibrium, we can also observe that, as expected, the cost function decreases almost to zero.

5.7.2 Nash equilibrium for an active shielding system

Active shielding is one of the most common applications of massive multichannel ANC systems. In order to evaluate the Nash equilibrium for this case, we consider the active shielding scheme proposed by [99], depicted in Figure 5.4.a. The system consists of two squares around the noise source, the internal one formed by actuators and the external by sensors. Each side of the internal square is 5m long and contains eight actuators. The external square has the same number of sensors per side (of length 6m). Both squares are centered on the origin. The noise source is positioned inside both squares, but not necessarily at the origin. In the example case considered here, the noise source is located at $[0.5, 0]$. The emitted noise is a tonal component at 100Hz.

The control signals produced in equilibrium of the optimization process entailed by (E.1) are shown in Figure 5.4.b. For comparison purposes, the corresponding values calculated by means of (5.12) are also represented in the figure. As expected from the theory developed in the previous sections, there is a good correspondence between the results obtained for the error of centralized control and Nash equilibrium. Indeed, the obtained attenuation performance (see Figure 5.4.c) is extremely good, with an essentially null residual error (the magnitude of the error signals is below 1×10^{-14}), and the apparent differences between the two methods can be ascribed to numerical errors and safely considered negligible.

The evolution of control signal of gradient descent algorithm is obtained using (5.6). Figure 5.5 shows the error and control signals for two controllers, its actuators

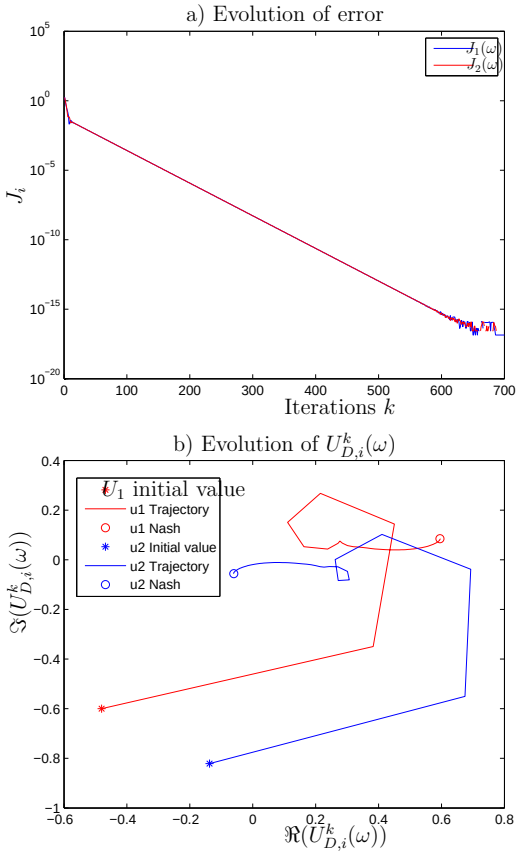

Figure 5.3: Evolution of the error (top) and control (bottom) signals.

and sensors are shown in triangles in figure 5.4 part a. The value of cost function shown in figure 5.5 part a decreases exponentially until less than 10^{-30}, even lower than the obtained using the centralized control using the open loop control with the equation (E.1) (cont function value very close to zero, the difference is probably due to computational limitations). It takes around 1600 iterations to converge to the same value of centralized error and agrees with figure 5.4. The control signals confirm the same as the theoretical approach and previous simulation, that it converges to Nash equilibrium even though there are 32 controllers. This simulation confirms that the minimum energy inside the controlled zone can be obtained either through the centralized control scheme or using a decentralized control scheme provided that convergence to the Nash equilibrium is achieved.

5.8 Conclusions

This chapter reformulates the decentralized multichannel ANC problem into a non-cooperative continuous game. This allows to compute explicitly the Nash equilibrium which represents the optimal solution for the decentralized control, the control signals where no controller can decrease further its cost function without access to the control signals of the other controllers. Furthermore, for the proposed scheme, the Nash equilibrium also corresponds to the optimal solution of the centralized control, which remarkably implies that the same attenuation performance can be achieved using a decentralized scheme. A simulation example with a 32×32 system

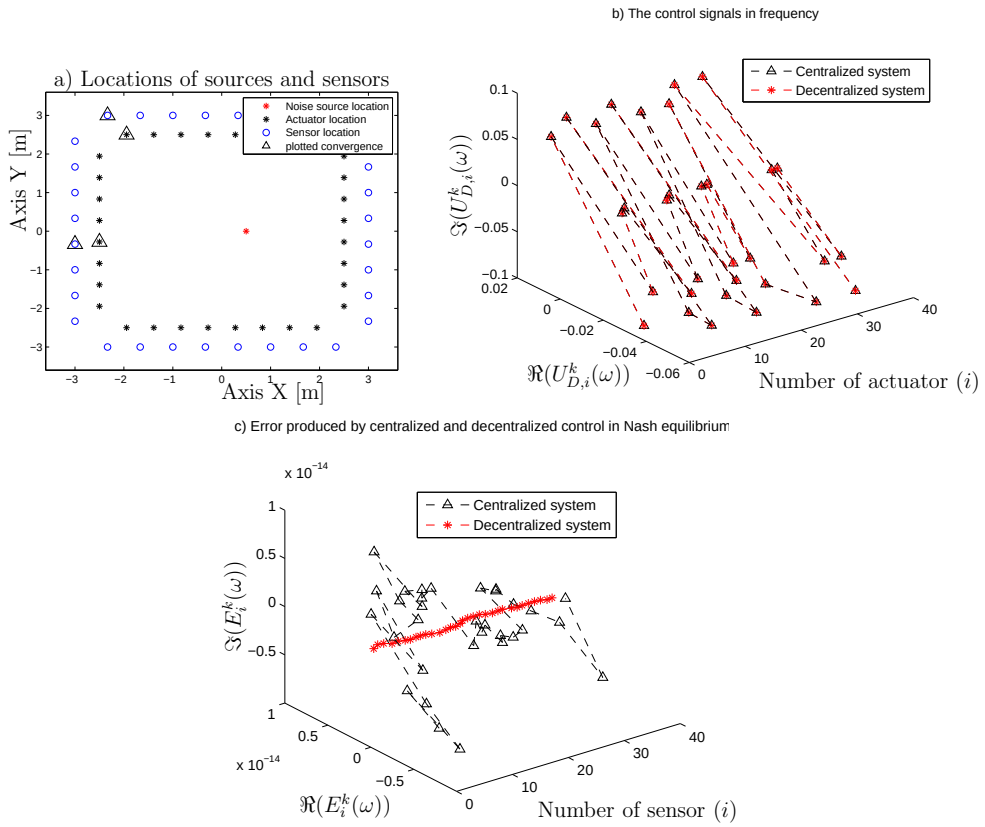

Figure 5.4: Active shielding system simulated for centralized control and distributed at Nash equilibrium.

shows that with an appropriate learning algorithm the controllers can independently converge to the Nash equilibrium.

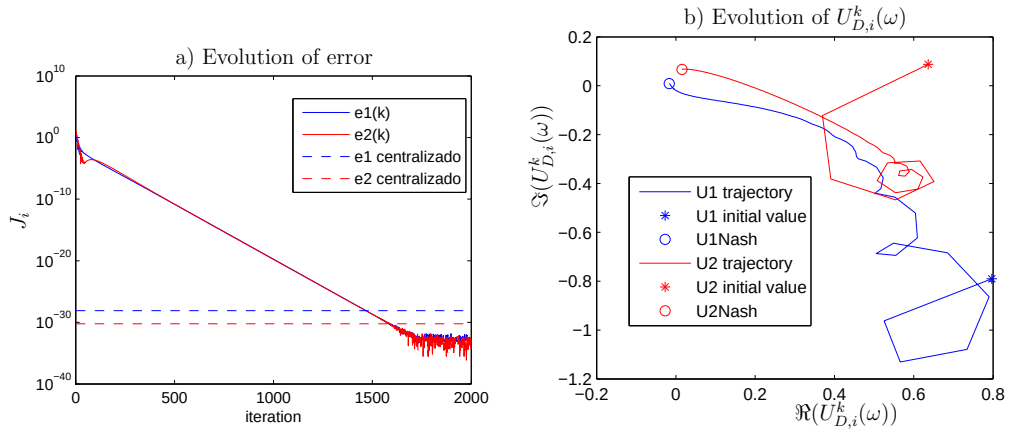

Figure 5.5: Evolution of the error (top) and control (bottom) signals of active shielding system.

Chapter 6

Experimental Verification

Abstract

In previews chapters, it has been described the active noise control, This Chapter depict the procedure to make experimental validations of the active shielding method. A linear relation between boundaries and discrete locations are directly validated using a comparison between an identified linear model with measured data. On the other hand, the 3D dimensional systems are more complex and prove it implies more sensors. Thus, the model (the dicretized wave equation), which allows demonstrate the implicit control, is evaluated and compared to empirical evidence, validating the necessary conditions to obtain the active shielding method. Furthermore, a discussion about the implementation and a scheme of the active shielding method is carried out.

This chapter shows the empirical evidence that the discrete model in chapter 4 occurs in experimental environment. The procedure to prove this relation is similar to the one followed in Chapter 3. In order to prove that the model of silent zone achieve equation (4.7), the model is identified and compared to experimental data. Specifically, the linear relationship between the pressure at one location and discrete contiguous positions is analyzed.

6.1 Validation of linear relation in 1D system

This section shows a proposal to obtain empiric evidence that ensures the necessary condition to achieve the theory in section 4.3.1. See the chapter 4 for a complete description of the theory. The condition (4.7) is the unique necessary restriction to achieve active shielding method. However, this is a mathematical relation, it means it cannot be measured. The empirical evidence proposed to compare a simulation using mathematical model that achieve the condition (4.7) with the measured data.

In order to obtain the mathematical model, [58] shows that the system identification method called output error is useful for a one dimensional acoustic system. It uses measured data to estimate the coefficients $a_{1,i}$, $a_{2,i}$, $b_{1,j}$ and $b_{2,j}$ for $i = 1, \cdots, N_a$ and $j = 1, \cdots, N_b$ of the next mathematical model:

$$\begin{aligned} y_1(k) &= a_{1,1}y_1(k-1) + \cdots + a_{1,N_a}y_1(k-N_a) + b_{1,1}u_1(k-1) + \cdots \\ &+ b_{1,N_b}u_1(k-N_b) \qquad (6.1) \\ y_2(k) &= a_{2,1}y_2(k-1) + \cdots + a_{2,N_a}y_2(k-N_a) + b_{1,1}u_2(k-1) + \cdots \\ &+ b_{1,N_b}u_2(k-N_b) \qquad (6.2) \\ y(k) &= y_1(k) + y_2(k) \qquad (6.3) \end{aligned}$$

Where N_a is the number of coefficients related to the actual and past input, N_b is number of coefficients related to the past outputs of the model. $u_1(k) := p(x_0, k\Delta_t)$ and $u_2(k) := p(x_{L+1}, k\Delta_t)$ are the input signals, y_1 and y_2 are state variables without physical meaning and $y(k)$ is the output. Notice that N_a and N_b are the order of the model. For this case, $y(k)$ is an estimation of $p(x_i, k\Delta_t)$. In order to simplify the notation, $y(x_i, k)$ indicates the pressure at location x_i and time $k\Delta_t$. Notice that i has different possible values between 1 and L. It means the procedure must be carried out L times, one by each possible value. The procedure to obtain the coefficients is detailed in [100].

The system in figure 4.2 does not have noise sources, which makes impossible to prove its behavior. For this reason, it is measured the system in scheme in figure 6.1. The difference consists of adding a sound source at the beginning and a surface at the end of the duct. Also, for this case, $L = 3$, $\Delta_x = 0.2$m. The distance between the source and x_0 is 0.2m. The distance between $x_L + 1$ and the surface is 0m. The sample frequency is 4410Hz. The system is identified using 22 seconds of audio. The order of the system is $N_a = 4$ and $N_b = 16$.

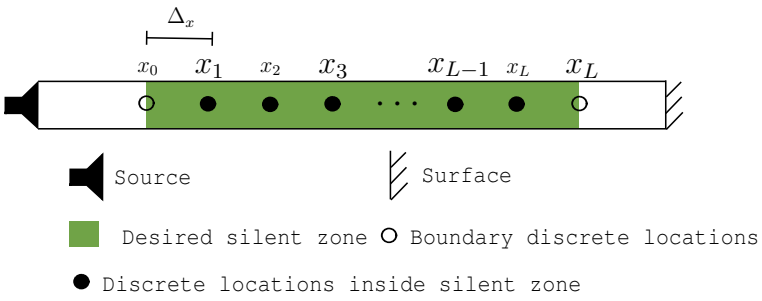

Figure 6.1: Scheme of acoustic measured system.

After obtaining the mathematical model using measured data, the model is compared with the measured data. Another measured data set is used to validate the condition (4.7). The parameter to quantify this comparison is called FIT, see equation (3.6). Measured and simulated output for the location x_1 is shown in figure 6.2. Both signals are very similar and is expected to achieve the condition (4.7). The FIT value obtained for the simulation of pressure at each location is:

$$\begin{aligned} FIT(x_1) &= 81.8514 \qquad (6.4) \\ FIT(x_2) &= 89.2338 \qquad (6.5) \\ FIT(x_3) &= 91.8943 \qquad (6.6) \end{aligned}$$

These FIT values are commonly accepted for a system identification procedure. For this reason, it can be assumed that the condition (4.7) is achieved.

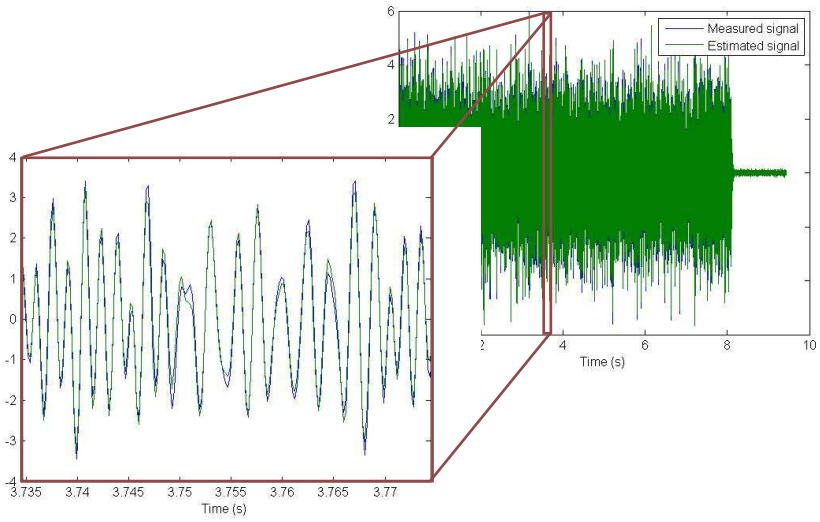

Figure 6.2: Estimated and measured signals for $p(x_1, t)$.

6.2 Validation of linear relation in 3D system

The difference regarding the section 6.1 is that, for this case, the discrete model is shown in Appendix C in equation (C.2). The concept is to use an identification system method using measured acoustic pressure $p(x_{i,j,l}, k+1)$ to estimate coefficients $\hat{\gamma}_{3,a}$, $\hat{\gamma}_{3,b}$ and $\hat{\gamma}_{3,c}$ of the discretized model of wave equation. Thus, the discrete model to be estimated is:

$$\begin{aligned} p(x_{i,j,l}, k+1) &= \hat{\gamma}_{3,a}\left[p(x_{i-1,j,l}, k) + p(x_{i+1,j,l}, k) + p(x_{i,j-1,l}, k)\right. \\ &+ \left. p(x_{i,j+1,l}, k) + p(x_{i,j,l-1}, k) + p(x_{i,j,l+1}, k)\right] \\ &+ \hat{\gamma}_{3,b} p(x_{i,j,l}, k) + \hat{\gamma}_{3,c} p(x_{i,j,l}, k-1) \end{aligned} \tag{6.7}$$

Notice that this model estimates the pressure at one location using the pressure of discrete locations around. It implies 6 input signals (two for each space axis). The model also needs 1 output signal, in the center. Furthermore, $\hat{\gamma}_{3,a}$, $\hat{\gamma}_{3,b}$ and $\hat{\gamma}_{3,c}$ are coefficients that have meaning in theoretical approach (see $\gamma_{3,a}$, $\gamma_{3,b}$ and $\gamma_{3,c}$ in Appendix C). However, in order to prove the hypothesis, with unknown damping coefficient, they have to be estimated.

The first step of the identification system procedure is to obtain measure data. The measurement set up is shown in figures 6.3 and 6.4. In figure 6.3, it is shown the sight from above to below. It means, the axis x_1 and x_2 . The microphones get the pressure signals, and two speakers, which are at the two source locations, reproduce the sound. The reference of the system is the center of the microphone array, elevated 1.07m from the floor. In this position of the axis x_1 and x_2 are 3 microphones located, but they have different height (position in axis x_3), as it is shown in figure 6.4. There are 30cm from the center to each microphone, setting a cross. Regarding the sources, in the experiment, first, one source is on and the other is off, then they exchange switch. Respect to the green sound source, it is located with a distance equal to 78cm in the axis x_1 , 1.6m in axis x_2 and -36cm in axis x_3 (negative value means below the axis). The second source location is the same height than first source location. Respect to the center of microphone array, it is

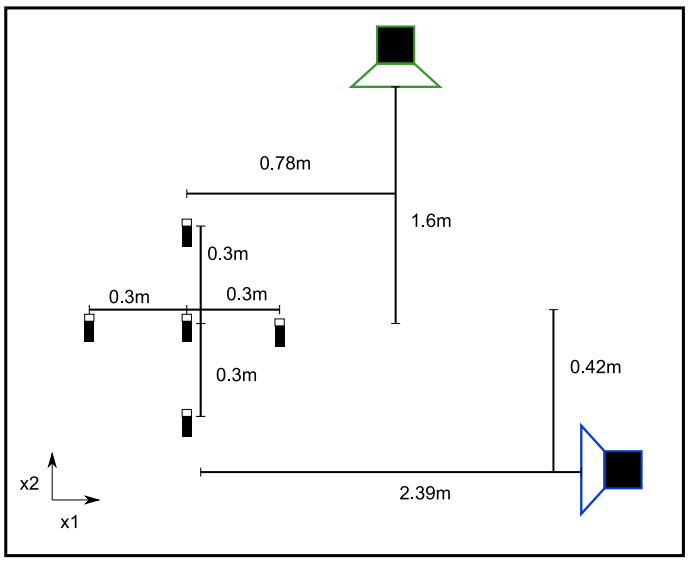

Figure 6.3: Plane cut of measurement scheme for 3 dimensional validation of model

2.39m and -0.42m for x_1 and x_2 axis respectively. The figure 6.5 shows a picture of the measurement. This locations are summarized in the table (6.1)

Element	Location $[\chi_1, \chi_2, \chi_3]$ (in meters)
Sensor 0 $(p(\chi_{i,j,l}, k))$	[0,0,0]
Sensor 1 $(p(\chi_{i+1,j,l}, k))$	[0.3,0,0]
Sensor 2 $(p(\chi_{i-1,j,l}, k))$	[-0.3,0,0]
Sensor 3 $(p(\chi_{i,j+1,l}, k))$	[0,0.3,0]
Sensor 4 $(p(\chi_{i,j-1,l}, k))$	[0,-0.3,0]
Sensor 5 $(p(\chi_{i,j,l+1}, k))$	[0,0,0.3]
Sensor 6 $(p(\chi_{i,j,l-1}, k))$	[0,0,-0.3]
Source 1	$[0.78, 1.6, -0.36]$
Source 2	$[2.39, -0.42, -0.36]$
Floor	$[\cdot, \cdot, -1.07]$

Table 6.1: Experimental set up locations for the three dimensional validation

Two sets have been measured, one for estimation procedure and the other for validation. The first set contains 7 seconds of audio, using noise filtered with a low pass filter at 250Hz. The second set contains 7 seconds of measurements of sinusoid signals for 63Hz, 80Hz, 100Hz, 125Hz, 160Hz and 200Hz. Additionally, another noise filtered measurement was contained in the validation set. All the measurement was carried out first with one source location, and then with the other, which implies that each set was measured twice.

The auto-regressive with exogenous model, shown in equation (B.3), contains the same form that equation (6.7). Thus, the procedure of the Output Error method described in Appendix B, allows to estimate the parameters $\hat{\gamma}_{3,a}$, $\hat{\gamma}_{3,b}$ and $\hat{\gamma}_{3,c}$.

The estimated values of coefficients are shown in the table 6.2. It is interesting the

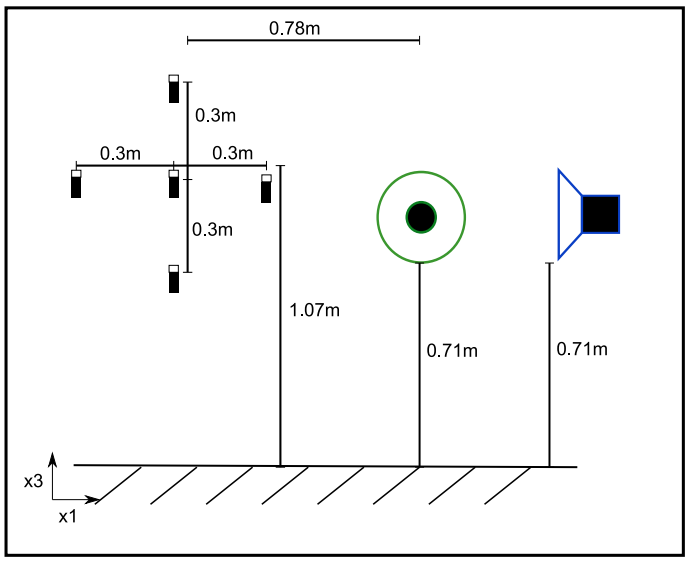

Figure 6.4: Plane cut of measurement scheme for 3 dimensional validation of model

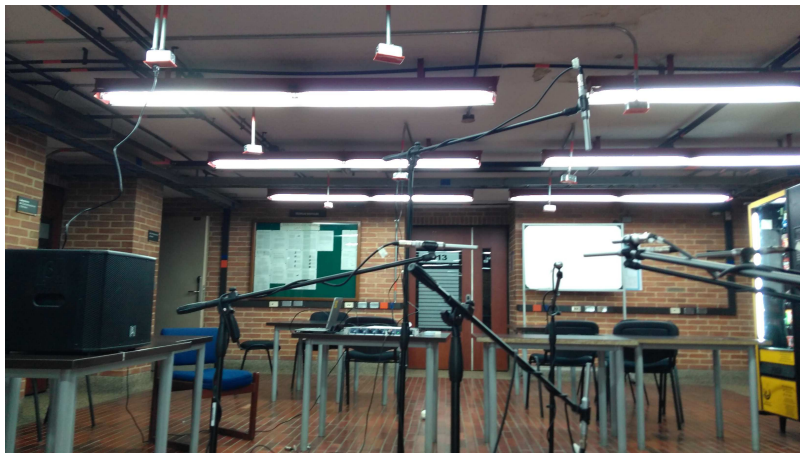

Figure 6.5: Plane cut of measurement scheme for 3 dimensional validation of model

similitude between the same parameter estimated using different source locations. Its value does not significantly vary. It is expected because the source location does not affects the model of the wave equation.

Regarding the validation set, it is used the FIT value to compare estimated and measured data. The estimation, obtained with each source position model, is compared with its corresponding measured validation data set. The acquired values are plotted in figures 6.6 and 6.7, for first and second source location respectively. The lower FIT value corresponds to the frequency at 160Hz, which is 75.21%. All other FIT values are between 82.67% and 88.50%. Moreover, the source location again does not show an affectation of the FIT, for both positions the FIT has similar values.

Another interesting result corresponds to compare the signal obtained with the model using the same source location to the one obtained using another source location. Specifically, the model obtained with using the training data with first location is validated using the data set obtained with the second source location. The opposite case is also carried out and all results are shown in the table 6.3. It

Coeficient	Source location 1	Source location 2
$\hat{\gamma}_{3,a}$	0.0042	0.0044
$\hat{\gamma}_{3,b}$	1.9683	1.9640
$\hat{\gamma}_{3,c}$	-0.9926	-0.9901

Table 6.2: Estimated cofficients of the discretized wave equation based on empirical evidence

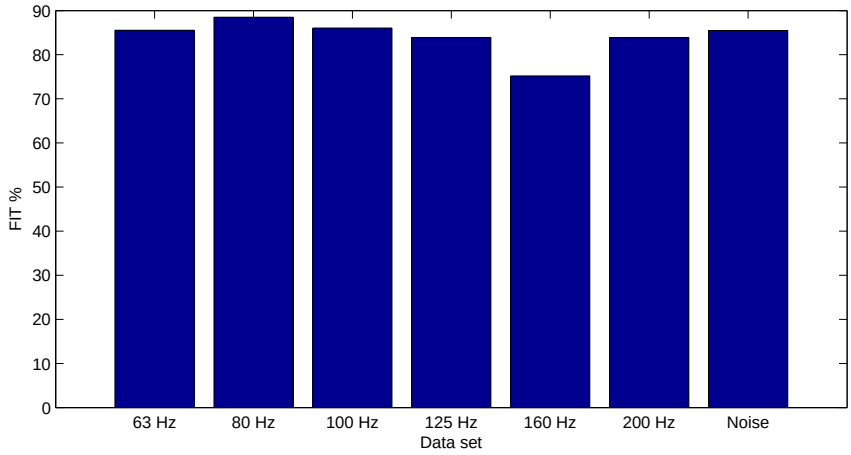

Figure 6.6: FIT obtained for the validation data sets using the location 1 for the estimation of the model

is important to remark that for all cases the FIT is very similar, with a difference lower than 2%. It confirms the statement inferred from table 6.2, the non affectation of the source location in the model.

	Source location 1 data set	Source location 2 data set
Source location 1 model	85.5048	86.1371
Source location 2 model	86.5867	86.9981

Table 6.3: FIT value for estimated data using models obtained with two locations.

Taking into account that the perfect estimation is the FIT equal to 100%, this estimation is acceptable and proves that empirically data also achieves the condition (4.7). Furthermore, the non-affectation of source location in the model is a property of the model in equation (B.3). This is the basis for active shielding method, which declares that pressure inside the silent zone can be controlled using only the pressure at boundary locations and source locations is redundant information because it affects pressure at boundaries.

6.3 Active shielding system validation scheme discussion

In previous sections, the condition in (4.7) was validated. It implies that the analysis in chapter 4 was completely based on assumptions which are achieved in real implementations. However, the complete system can be implemented to be proven.

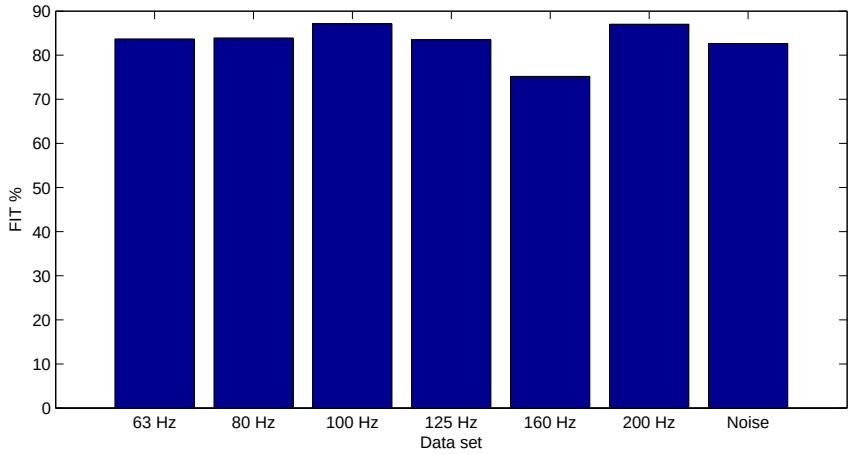

Figure 6.7: FIT obtained for the validation data sets using the location 2 for the estimation of the model

A general scheme to validate the active shielding system is the one simulated and exposed in figure 4.8, but the high number of sources and actuators could complicate this scheme. However, according to limitations they have not been implemented. The number of sensor in the simulation is 54, for $I = J = L = 3$, very high, which implies a high cost. Furthermore, inside a room, the controller implies an adaptive filter with a very high order. From section 3.3, it was expected at least an order equal to 500 for each location. Even though the decentralized control was taken into account in chapter 5, the time analysis was very restrictive for real implementation.

6.4 Conclusions

This chapter presented the empirical validation of the condition (4.7) for one and three dimensional systems. For a one dimensional system, an identification system method was applied to compare linear simulated and measured data. It was proven that there exists a linear relationship between boundaries and desired silent zone. On the other hand, the three dimensional system was not proven in the same way due to hardware limitations. Thus, it was validated the basic concept of the implicit control for active shielding, which is the discrete model of wave equation. The linear relationship between contiguous locations is an evidence of linear relationship between pressure at boundaries and inside of silent zone. The procedure was obtaining a model with the same form than discrete model of wave equation and compare with measured data. The results showed that empirical evidence FIT a higher value than 80%, except for 160Hz. This implies an acceptable linear model to represent the pressure at contiguous discrete locations. Furthermore, the model does not change when the source location changes and confirms the second location.

For future works, there is a possibility to locate boundaries of a room as boundaries of the desired silent zone, which reduces the sensors and actuators as well. This analysis also can produce a system for windows, doors or from half room to the other half.

Chapter 7

Concluding remarks and future work

This document shows a whole research which aims controlling the noise inside a desired silent zone without using elements that obstruct the path of any user inside. This work is focused on the active shielding method to be obtained using any control algorithm. Moreover, using techniques as active shielding requires massive multichannel control systems, which consequently requires high computational cost. In literature, distributed and decentralized control have been proposed, but not deeply analyzed in active noise control applications. Thus, this document dealt with the convergence of decentralized control algorithms.

In this work, the first step was to determine which class of control to use. The literature has reported non-linear control and linear control algorithms. They have been used to solve two problems: the non-linearity of the secondary path and non-causality of controller. With respecto to linearity, it was shown a high performance using simulation of an acoustic secondary path with linear models for a case study, comparing measured data with estimated output based on identification system methods. Regarding causality, an analysis of a one reflexion system yields to infer that if the distance between actuator and receiver is lower than the distance between primary source and receiver, then the controller is causal. This result was extrapolated to several reflexions using an approximation of the impulse response. Therefore, it is feasible to use linear active noise control inside rooms.

The main contribution was developed due to a new definition called implicit control. This concept produces a condition that determines when attenuating the pressure at one location also produces attenuation at another location. This was used with a discretization of wave equation to ensure that attenuating the boundaries at a desired silent zone is enough condition to attenuate pressure inside. For one dimensional system, simulations show that method works as the theoretical approach described. However, at two and three dimensional system, attenuation is not achieve inside the silent zone when the sensors are highly separated with respect to the wave length. Probably, the system cannot be described by the discretized model. Moreover, the limit frequency was obtained using a statistical estimation of a non-linear model.

In order to solve the computational cost due to high number of sources and sensors of active shielding, decentralized multichannel ANC problem was analyzed as a non-cooperative continuous game. The Nash equilibrium of this game is the

optimal solution for the decentralized control. It was found that Nash equilibrium of proposed scheme and optimal solution of the centralized control are the same, which remarkably implies that the same attenuation performance can be achieved using a decentralized scheme. A 32×32 active control system was simulated and results show that controllers independently converge to the Nash equilibrium.

Regarding empirical validation, condition (4.7) (linear relationship between pressures) for one and three dimensional systems was proven. An identification system method was applied to compare linear simulated and measured data. For the one dimensional system, the linear relationship was directly obtained. The Output Error method obtains FIT values higher than 80%. Three dimensional system was validated through the model that ensures the implicit control for the conditions of the active shielding. This is the discrete model of wave equation. The coefficients of discrete model was obtained using Output Error method. A comparison between measured and simulated data yields a FIT value higher than 80% for noise and all sinusoid signals, excepting for 160Hz. Then, it was found that a linear model explains the relation between the pressure at silent zone and boundaries locations, which confirms the condition (4.7). The model also has a specific characteristic regarding source location, that it does not affect the implicit control, because this information is implicit in pressure at boundaries. The experimental results confirm that coefficients obtained for two different source locations are similar and the FIT values have a lower difference to 2%.

The most important future work is to validate the proposed active shielding method. Even though the computational cost have some issues, this is not a limitation for open loop control systems when the noise signal is known. This characteristic reduces the problem to get all sensors, actuators and a method to reproduce the corresponding signals simultaneously.

Regarding the secondary path linearity, in chapter 3, it was not proven for all signals. Experiments obtains different behavior for impulsive noise. Thus, in order to expand the results in this thesis to another kind of noises, it is necessary to find non-linear models and controllers for the systems.

In linear systems, the active shielding implies high number of sensors and actuators, as it was shown in chapters 4 and 6. From this condition two problems appear. First one is how to reduce the number of sensors and actuators. A particular case is that the boundary of desired silent zone coincides with a surface of the room. Thus, if it is assumed that the noise does not come from outside the room, or flanking, the condition of zero pressure at this boundary can be expected without using control. Then, area of boundaries exposed to noise is lower than other case, which reduce number of sensors on it. This kind of systems also could allow to propose systems for active noise control for windows.

The second problem of the application of active noise control is the computational cost. A solution was analyzed in chapter 5. The theoretical game approach developed shows the possibility of obtaining the optimal centralized control using decentralized active noise control. Specifically, the frequency space has been demonstrated, but the optimization algorithm requires a Fourier transform and its application becomes difficult. On the other hand, the FxLMS algorithm was evaluated using the Nash Equilibrium, the conditions to obtain the minimum was very restrictive, different to the frequency space analysis. Furthermore, the convergence algorithm requires other conditions for obtaining the local minimum. This analysis

brings to anticipate that new algorithms that find the Nash Equilibrium will be a complete field of study.

The validation in chapter 6 of the discrete active shielding produces a new model very interesting. This model could be applied in any field of acoustics, because is very simple, the computational cost is very low and the accuracy with measured data is very high. However, the implementation is very far from obtaining a generalized discrete model. In future works, this model will be developed, including different distances for discrete locations and sample time. Moreover, this model can be complemented with the response of surfaces. This will complement the proposed analysis with boundaries of silent zone on surfaces.

Summarizing, this thesis developed an active shielding method which its implementation has several challenges to be solved. In the future works proposed in this chapter, it is expected new applications as windows, vehicles, different kind of noises, a more accurate new mathematical model based on measurements and more.

Appendix A

Multiple inverse impulse responses

The aim of this appendix is to show that it is possible to have more than one model that represents an inverse of the system. Let us begin with an analysis in discrete time, then a similar analysis in continuous time can be carried out.

Let $h(\tau)$ be the discrete impulse response of a system with discrete time τ. The inverse system with impulse response $h_{inv}(\tau)$ has to achieve the next equation:

$$\sum_{i=0}^{\kappa} h(i)h_{inv}(-i) = 1 \text{ if } \tau = 0 \tag{A.1}$$

$$\sum_{i=0}^{\kappa} h(i)h_{inv}(\tau - i) = 0 \text{ if } \tau \neq 0 \tag{A.2}$$

Where κ is the length of the impulse response (if it is infinite, $\kappa = \infty$).

Notice that this system of equations has more variables ($h_A(\tau - i)$ for each value of τ and i) than equations (one for each value of τ). Even, the number of variables η can be calculated as a functions of the number of equations Γ:

$$\eta = \Gamma + \kappa - 1 \tag{A.3}$$

The number of variables increases with Γ, then, while $\kappa > 1$ it always has infinite solutions.

For the case of continuous time t, with an impulse response $h(t)$ the same analysis can be carried out using the definition of the Riemann integral. The restriction of the inverse system is:

$$\int_a^b h(\psi)h_A(t-\psi)d\psi = \lim_{\Xi\to\infty} \frac{b-a}{\Xi}$$
$$+\sum_{\xi}^{\Xi} h(\frac{(a-b)\xi}{\Xi})h_A(-\frac{(a-b)\xi}{\Xi}) = 1 \text{ if } t = 0 \tag{A.4}$$

$$\int_a^b h(\psi)h_A(t-\psi)d\psi = \lim_{\Xi\to\infty} \frac{b-a}{\Xi}$$
$$+\sum_{\xi}^{\Xi} h(\frac{(a-b)\xi}{\Xi})h_A(-\frac{(a-b)\xi}{\Xi}) = 1 \text{ if } t \neq 0 \tag{A.5}$$

From (A.4), (A.5) and the discrete solution, it is evident that in continous time also has the same property. It has infinite inverse systems.

Appendix B

System identification methods

This section describes general form of system identification methods used in this work. For a deep description it is recommended [100]. The models are the next:

1. **Finite impulse response (FIR) filter:** This method finds a model assuming that the system can be represented through a FIR filter. Then, the estimation $\hat{y}_{fir}(n)$ of the output $y(n)$ of the system, at discrete time n, can be expressed as:

$$\hat{y}_{\text{fir}}(k) = \bar{w}_{\text{fir}}^T \bar{u}(k) \tag{B.1}$$

   where $\bar{w}_{\text{fir}} = [w_0, w_1, \cdots, w_{k-1}]^T$, w_i are the coefficients of the FIR filter, with $i = 1, \cdots, N_{\text{fir}}$; T denotes transpose; $\bar{u}(k) = [u(k), u(k-1), \cdots, u(k - N_{\text{fir}} + 1)]^T$; and $u(k)$ is the input of the system. This method gives as result the value of filter coefficients, ie. $\bar{w}_{\text{fir}}$.

2. **Autorregresive (AR):** This is a similar method to the FIR filter, the difference consists is that prediction of future values of the output based using previous values the same signal as follows:

$$\hat{y}_{ar}(k) = \bar{w}_{\text{ar}}^T \bar{y}(k-1) \tag{B.2}$$

   where $\bar{y}(k-1) = [y(k-1), \cdots, y(k-N_{\text{ar}})]^T$, for a N_{ar} order filter. This method also give the values of the coefficients $\bar{w}_{\text{ar}}$.

3. **Autorregresive with exogenous input (ARX):**

   Both previews models can be combined as a new mathematical model that can be expressed as:

$$\hat{y}_{arx}(k) = \bar{w}_{\text{fir}}^T \bar{u}(k) + \bar{w}_{\text{ar}}^T \bar{y}(k-1) \tag{B.3}$$

   The result of this identification is the values of the coefficient filters, $\bar{w}_{\text{fir}}$ and $\bar{w}_{\text{ar}}$. This minimum is produced to minimize the error of one step estimation using least squares.

4. **Output Error method (OE):**

   This method obtain the same model in equation (B.3) and also produce as result the coefficients $\bar{w}_{\text{fir}}$ and $\bar{w}_{\text{ar}}$. The difference consists on the optimization algorithm, which is focused on simulation, minimize not only based on one step estimation, but all future steps. The procedure used usually based on a gradient descent algorithm.

5. **N4SID:**

   The method N4SID is helpfully and commonly applied to find a model of the form:

$$\begin{aligned} x(k+1) &= \mathcal{A}_{n4s}x(k) + \mathcal{B}_{n4s}u(k) \\ y(k) &= \mathcal{C}_{n4s}x(k) + \mathcal{D}_{n4s}u(k) \end{aligned} \tag{B.4}$$

   where $x(k)$ is the state vector, and A_{n4s}, B_{n4s}, C_{n4s} and D_{n4s} are matrices to be found. For more details about the method, [101] is recommended.

6. **Least Mean Square (LMS) Filter:**

   The classic LMS algorithm can be applied to find a model of equation (B.1). Nevertheless, at this case, the optimization is not an analytical model, but the gradient descent concept is applied. More information about this filter is given in [96]. Then, the value of the filter weights $\bar{w}_{\text{LMS}}(k)$ can be updated as:

$$\bar{w}_{\text{LMS}}(k+1) = \bar{w}_{\text{LMS}}(k) - \alpha_{\text{LMS}}\bar{u}(k)e^*(k) \tag{B.5}$$

   Where α_{LMS} is the step size coefficient,$*$ is the complex conjugate operator, $e(k)$ is the estimation error, $\bar{u}(k) = [u(k), u(k-1), \cdots, u(k-N_{\text{LMS}}+1)]$ and k is the order of the system.

7. **Neural Networks:**

   The nonlinear identification is based on neural networks exposed in [41]. The proposed network contains one layer, the input to each neuron is $\bar{u}(n)$ and it is processed by the next function chosen as kernel:

$$\Phi_\eta(k) = \exp\left(-\frac{1}{\sigma_\eta^2}\,||\bar{u}(k) - t_\eta||_2^2\right) \tag{B.6}$$

   where σ_η and t_η are the width and the center of the Gaussian function. And the output is defined for η_m neurons as follows:

$$\hat{y}_{nn}(k) = \sum_{\eta=1}^{\eta_m} W_\eta \Phi_\eta(n) \tag{B.7}$$

   The coefficients W_η are the optimization variables in order to minimize the quadratic error of the estimation. The result of this optimization gives the model that represents the system. As it is common in neural network, the method to find the optimum is the gradient descent.

Appendix C

Active Shielding for a three dimensional system

Analogous to the analysis shown in the chapter 4, the three dimensional system obtains an active shielding method using implicit control. This case changes the wave equation, it uses $\nabla_{3D}(\cdot) := \frac{\partial^2 \cdot}{\partial x_1^2} + \frac{\partial^2 \cdot}{\partial x_2^2} + \frac{\partial^2 \cdot}{\partial x_3^2}$ instead $\nabla_{2D}(\cdot)$. Notice that the third axis added is called x_3, i.e.:

$$\nabla_{3D}(p(X,t)) - d\frac{\partial p(X,t)}{\partial t} - \frac{1}{c^2}\frac{\partial^2 p(X,t)}{\partial t^2} = 0 \tag{C.1}$$

Subsequently, discretizing equation (C.1) using finite difference method yields:

$$\begin{aligned} p(x_{i,j,l}, k+1) &= \gamma_{3,a}\left[p(x_{i-1,j,l},k) + p(x_{i+1,j,l},k) + p(x_{i,j-1,l},k) + p(x_{i,j+1,l},k)\right. \\ &+ \left. p(x_{i,j,l-1},k) + p(x_{i,j,l+1},k)\right] + \gamma_{3,b}p(x_{i,j,l},k) \\ &+ \gamma_{3,c}p(x_{i,j,l},k-1) \end{aligned} \tag{C.2}$$

With:

$$\gamma_{3,a} = \frac{2c^2\Delta_t^2}{\Delta_x^2\left(dc^2\Delta_t + 2\right)} \tag{C.3}$$

$$\gamma_{3,b} = \left[\frac{4\left(\Delta_x^2 - 3c^2\Delta_t^2\right)}{\Delta_x^2\left(dc^2\Delta_t + 2\right)}\right] \tag{C.4}$$

$$\gamma_{3,c} = \left[\frac{dc^2\Delta_t - 2}{\left(dc^2\Delta_t + 2\right)}\right] \tag{C.5}$$

Then, the vector that contains the whole discrete locations inside a cubic silent zone $z_{3D}(k)$ is:

$$\bar{Z}_{j,l}(k) := \left[p(x_{1,j,l},k) \quad p(x_{2,j,l},k) \quad \cdots \quad p(x_{I,j,l},k)\right]^T \tag{C.6}$$

$$\dot{Z}_l(k) := \left[\bar{Z}_{1,l}(k) \quad \bar{Z}_{2,l}(k) \quad \cdots \quad \bar{Z}_{J,l}(k)\right]^T \tag{C.7}$$

$$z_{3D}(k) := \left[\dot{Z}_1(k) \quad \dot{Z}_2(k) \quad \cdots \quad \dot{Z}_L(k)\right]^T \tag{C.8}$$

Also, the vector which contains the pressures at the boundary of this cube is:

$$\dot{u}_j(k) := \begin{bmatrix} \bar{Z}_{j,1}(k) & \bar{Z}_{j,2}(k) & \cdots & \bar{Z}_{j,L}(k) \end{bmatrix}^T \tag{C.9}$$

$$\tilde{u}_{i,l}(k) := \begin{bmatrix} p(x_{i,1,l},k) & p(x_{i,2,l},k) & \cdots & p(x_{i,J,l},k) \end{bmatrix}^T \tag{C.10}$$

$$\bar{u}_i(k) := \begin{bmatrix} \tilde{u}_{i,1}(k) & \tilde{u}_{i,2}(k) & \cdots & \tilde{u}_{i,L}(k) \end{bmatrix}^T \tag{C.11}$$

$$u_{3D}(k) := \begin{bmatrix} \dot{Z}_0(k) & \dot{Z}_{L+1}(k) & \dot{u}_0(k) & \dot{u}_{J+1}(k) & \bar{u}_0(k) & \bar{u}_{I+1}(k) \end{bmatrix}^T \tag{C.12}$$

The next equation relates the vectors $z_{3D}(k)$ and $u_{3D}(k)$

$$\begin{bmatrix} z_{3D}(k+1) \\ z_{3D}(k) \end{bmatrix} = \begin{bmatrix} A_{3D} & \hat{A}_{3D} \\ \mathbb{I}_{IJL} & \mathbb{O}_{IJL,IJL} \end{bmatrix} \begin{bmatrix} z_{3D}(k) \\ z_{3D}(k-1) \end{bmatrix} + \begin{bmatrix} B_{3D} \\ \mathbb{O}_{IJL,2IJ+2JL+2IL} \end{bmatrix} u_{3D}(k) \tag{C.13}$$

Where the matrices are Where $\hat{A}_{3D} = \gamma_{3,c}\mathbb{I}_{IJL}$ and:

$$A_{3D} = \begin{pmatrix} \dot{A} & \gamma_{3,a}\mathbb{I}_{IJ} & \mathbb{O}_{IJ,IJ} & \cdots & & \cdots & \mathbb{O}_{IJ,IJ} \\ \gamma_{3,a}\mathbb{I}_{IJ} & \dot{A} & \gamma_{3,a}\mathbb{I}_{IJ} & \mathbb{O}_{IJ,IJ} & \ddots & & \vdots \\ \mathbb{O}_{IJ,IJ} & \gamma_{3,a}\mathbb{I}_{IJ} & \dot{A} & \gamma_{3,a}\mathbb{I}_{IJ} & \ddots & \ddots & \vdots \\ \vdots & \mathbb{O}_{IJ,IJ} & \ddots & \ddots & \ddots & \mathbb{O}_{IJ,IJ} & \vdots \\ \vdots & \ddots & \ddots & \ddots & \ddots & \ddots & \mathbb{O}_{IJ,IJ} \\ \vdots & & \ddots & \mathbb{O}_{IJ,IJ} & \gamma_{3,a}\mathbb{I}_{IJ} & \dot{A} & \gamma_{3,a}\mathbb{I}_{IJ} \\ \mathbb{O}_{IJ,IJ} & \cdots & \cdots & \cdots & \mathbb{O}_{IJ,IJ} & \gamma_{3,a}\mathbb{I}_{IJ} & \dot{A} \end{pmatrix} \tag{C.14}$$

With:

$$\dot{A} = \begin{pmatrix} \bar{A} & \gamma_{3,a}\mathbb{I}_I & \mathbb{O}_{I,I} & \cdots & & \cdots & \mathbb{O}_{I,I} \\ \gamma_{3,a}\mathbb{I}_I & \bar{A} & \gamma_{3,a}\mathbb{I}_I & \mathbb{O}_{I,I} & \ddots & & \vdots \\ \mathbb{O}_{I,I} & \gamma_{3,a}\mathbb{I}_I & \bar{A} & \gamma_{3,a}I_I & \ddots & \ddots & \vdots \\ \vdots & \mathbb{O}_{I,I} & \ddots & \ddots & \ddots & \ddots & \vdots \\ \vdots & \ddots & \ddots & \ddots & \ddots & \ddots & \mathbb{O}_{I,I} \\ \vdots & & \ddots & \mathbb{O}_{I,I} & \gamma_{3,a}\mathbb{I}_I & \bar{A} & \gamma_{3,a}\mathbb{I}_I \\ \mathbb{O}_{I,I} & \cdots & \cdots & \cdots & \mathbb{O}_{I,I} & \gamma_{3,a}\mathbb{I}_I & \bar{A} \end{pmatrix} \tag{C.15}$$

And the tridiagonal matrix $\bar{A} = [a_{m,n}]$ defines its components as:

$$a_{m,n} = \begin{cases} \gamma_{3,a} & \text{if } m = n \\ \gamma_{3,b} & \text{if } [m+1 = n] \text{ and } [m-1 = n] \\ 0 & \text{otherwise} \end{cases} \tag{C.16}$$

Besides, the relation between $z_{3D}(k+1)$ and $u_{3D}(k)$ is given by:

$$B_{2D} = [B_1 \quad B_2 \quad B_3 \quad B_4 \quad B_5]] \tag{C.17}$$

where:

$$B_1 = \begin{bmatrix} \gamma_{3,a}\mathbb{I}_{LJ} & \mathbb{O}_{(IJ),(IJ)} \\ \mathbb{O}_{(IJ),(IJ)} & \mathbb{O}_{(IJ),(IJ)} \\ \vdots & \vdots \\ \mathbb{O}_{(IJ),(IJ)} & \mathbb{O}_{(IJ),(IJ)} \\ \mathbb{O}_{(IJ),(IJ)} & \gamma_{3,a}\mathbb{I}_{LJ} \end{bmatrix} \tag{C.18}$$

$$B_2 = \begin{bmatrix} \bar{B}_2 & \mathbb{O}_{(IJ),J} & \cdots & & \mathbb{O}_{(IJ),J} \\ \mathbb{O}_{(IJ),J} & \bar{B}_2 & \mathbb{O}_{(IJ),J} & \cdots & \mathbb{O}_{(IJ),J} \\ \vdots & \ddots & \ddots & \ddots & \vdots \\ \vdots & \ddots & \ddots & \bar{B}_2 & \mathbb{O}_{(IJ),J} \\ \mathbb{O}_{(IJ),J} & \cdots & \cdots & \mathbb{O}_{(IJ),J} & \bar{B}_2 \end{bmatrix} \tag{C.19}$$

$$\bar{B}_2 = \begin{bmatrix} \hat{B}_2 & 0_{I,1} & \cdots & & \mathbb{O}_{I,1} \\ \mathbb{O}_{I,1} & \hat{B}_2 & \mathbb{O}_{I,1} & \cdots & \mathbb{O}_{I,1} \\ \vdots & \ddots & \ddots & \ddots & \vdots \\ \vdots & \ddots & \ddots & \hat{B}_2 & \mathbb{O}_{I,1} \\ \mathbb{O}_{I,1} & \cdots & \cdots & \mathbb{O}_{I,1} & \hat{B}_2 \end{bmatrix} \tag{C.20}$$

$$\hat{B}_2 = \begin{bmatrix} \gamma_{3,a} \\ \mathbb{O}_{(I-1),1} \end{bmatrix} \tag{C.21}$$

$$B_3 = \begin{bmatrix} \bar{B}_3 & \mathbb{O}_{(IJ),J} & \cdots & & \mathbb{O}_{(IJ),J} \\ \mathbb{O}_{(IJ),J} & \bar{B}_3 & \mathbb{O}_{(IJ),J} & \cdots & \mathbb{O}_{(IJ),J} \\ \vdots & \ddots & \ddots & \ddots & \vdots \\ \vdots & \ddots & \ddots & \bar{B}_2 & \mathbb{O}_{(IJ),J} \\ \mathbb{O}_{(IJ),J} & \cdots & \cdots & \mathbb{O}_{(IJ),J} & \bar{B}_3 \end{bmatrix} \tag{C.22}$$

$$\bar{B}_3 = \begin{bmatrix} \hat{B}_3 & \mathbb{O}_{I,1} & \cdots & & \mathbb{O}_{I,1} \\ \mathbb{O}_{I,1} & \hat{B}_3 & \mathbb{O}_{I,1} & \cdots & \mathbb{O}_{I,1} \\ \vdots & \ddots & \ddots & \ddots & \vdots \\ \vdots & \ddots & \ddots & \hat{B}_3 & \mathbb{O}_{I,1} \\ \mathbb{O}_{I,1} & \cdots & \cdots & \mathbb{O}_{I,1} & \hat{B}_3 \end{bmatrix} \tag{C.23}$$

$$\hat{B}_3 = \begin{bmatrix} \mathbb{O}_{(I-1),1} \\ \gamma_{3,a} \end{bmatrix} \tag{C.24}$$

$$B_4 = \begin{bmatrix} \bar{B}_4 & \mathbb{O}4_{(IJ),I} & \cdots & & \mathbb{O}_{(IJ),I} \\ \mathbb{O}_{(IJ),I} & \bar{B}_4 & \mathbb{O}_{(IJ),I} & \cdots & \mathbb{O}_{(IJ),I} \\ \vdots & \ddots & \ddots & \ddots & \vdots \\ \vdots & \ddots & \ddots & \bar{B}_4 & \mathbb{O}_{(IJ),I} \\ \mathbb{O}_{(IJ),J} & \cdots & \cdots & \mathbb{O}_{(IJ),I} & \bar{B}_4 \end{bmatrix} \tag{C.25}$$

$$\bar{B}_4 = \begin{bmatrix} \gamma_{3,a}\mathbb{I}_I \\ \mathbb{O}_{J(I-1),I} \end{bmatrix} \tag{C.26}$$

$$B_5 = \begin{bmatrix} \bar{B}_5 & \mathbb{O}_{(IJ),I} & \cdots & & \mathbb{O}_{(IJ),I} \\ \mathbb{O}_{(IJ),I} & \bar{B}_5 & \mathbb{O}_{(IJ),I} & \cdots & \mathbb{O}_{(IJ),I} \\ \vdots & \ddots & \ddots & \ddots & \vdots \\ \vdots & \ddots & \ddots & \bar{B}_5 & \mathbb{O}_{(IJ),I} \\ \mathbb{O}_{(IJ),J} & \cdots & \cdots & \mathbb{O}_{(IJ),I} & \bar{B}_5 \end{bmatrix} \tag{C.27}$$

$$\bar{B}_5 = \begin{bmatrix} \mathbb{O}_{J(I-1),I} \\ \gamma_{3,a}\mathbb{I}_I \end{bmatrix} \tag{C.28}$$

Thereby, a space state model can be written to express the behavior of pressure at the discrete locations in the silent zone. It is shown that the condition (4.7) is achieved also for a three dimensional system. Thus, if the desired silent zone is a parallelepiped, it can be obtained by controlling the noise at discrete location in the boundaries of this parallelepiped while it can be discretized as it was shown in this section. Consequently, the restrictions are given only by the finite difference method, which basically relates the frequency with Δ_x.

Appendix D

Optimum controller description

In this article it is important to obtain the control signal at its maximum attenuation. The process to obtain the minimum attenuation at the sensor location is described below, similar as it is shown by [94]. It begins by describing the relation between the secondary source and error sensors signals, mathematically it is written as follows:

$$E_\iota(\omega) = D_\iota(\omega) + \sum_{j=1}^{\Lambda} H_{\iota,\lambda}(\omega)\nu_\lambda(\omega), \quad i = 1, \ldots, N, \tag{D.1}$$

Where $E_\iota(\omega) = F\{p(x_i, x_j, t)\}$ for two dimensional systems or $E_l(\omega) = F\{p(x_i, x_j, x_l, t)\}$ for three dimensional systems; ι expresses a different combination of i, j or i, j, l at boundary locations and its maximum value is the number of discrete locations at boundary of silent zone; $D_\iota(\omega)$ is the noise due to the primary source at sensor ι location; $H_{\iota,\lambda}(\omega)$ is the secondary path from the secondary source λ to the sensor ι; $\nu_\lambda(\omega)$ is the sound emitted by the secondary source λ; and Λ is the number of secondary sources. Equation (D.1) can be written in matrix form as:

$$E(\omega) = D(\omega) + H(\omega)\nu(\omega). \tag{D.2}$$

With $E(\omega) = [E_1(\omega), E_2(\omega), \ldots, E_\Lambda(\omega)]^T$, $D(\omega) = [D_1(\omega), D_2(\omega), \ldots, D_\Lambda(\omega)]^T$, and $\nu(\omega) = [\nu_1(\omega), \nu_2(\omega), \ldots, \nu_\Lambda(\omega)]^T$ and defining the matrix:

$$H(\omega) = \begin{bmatrix} H_{1,1}(\omega) & H_{1,2}(\omega) & \cdots & H_{1,\Lambda}(\omega) \\ H_{2,1}(\omega) & H_{2,2}(\omega) & & H_{2,\Lambda}(\omega) \\ \vdots & \vdots & \ddots & \vdots \\ H_{\Lambda,1}(\omega) & H_{\Lambda,2}(\omega) & \cdots & H_{\Lambda,\Lambda}(\omega) \end{bmatrix} \tag{D.3}$$

Notice that it is assumed the number of sensors equal to Λ, it implies H to be a square matrix, which will be useful below. The control signal is obtained with the aim to minimize the energy of the sensors signals. It means:

$$\nu^*(\omega) = \underset{\nu(\omega)}{\operatorname{argmin}}\, E^{\mathcal{H}}(\omega)E(\omega) = -(H^{\mathcal{H}}(\omega)H(\omega))^{-1}H^{\mathcal{H}}(\omega)D(\omega), \tag{D.4}$$

Simplifying this result with the properties of square matrices, the control signal becomes:

$$\nu^*(\omega) = -H(\omega)^{-1}D(\omega), \tag{D.5}$$

Appendix E

Error of the optimum controller description

In appendix D, the optimal control signal for feedback scheme is obtained, see equation (E.1). This appendix shows the error signal obtained when this controller is applied. Furthermore, this result is extended for feed-forward control scheme.

$$\begin{aligned} U_C^*(\omega) &= \underset{U(\omega)}{\operatorname{argmin}} J_C \\ &= -(H^{\mathcal{H}}(\omega)H(\omega))^{-1}H^{\mathcal{H}}(\omega)D(\omega), \end{aligned} \tag{E.1}$$

where the subscript C refers to the centralized feedback control scheme. This solution simplifies to

$$U_C^*(\omega) = \underset{U(\omega)}{\operatorname{argmin}} J_C = -H(\omega)^{-1}D(\omega) \tag{E.2}$$

in the square case, i.e. with $M = N$.

Substituting the last expression in Equation (5.3) immediately yields $E(\omega) = 0$.

The feed-forward scheme with centralized control usually focuses on minimizing the energy of all sensed signals. Thus, the value of $W_i(\omega)$ is the decision variable of the optimization problem as follows:

$$\begin{aligned} \bar{W}_C^*(\omega) &= \underset{\bar{W}(\omega)}{\operatorname{argmin}} J_C = \underset{\bar{W}(\omega)}{\operatorname{argmin}} E^{\mathcal{H}}(\omega)E(\omega) \\ &= -(H^{\mathcal{H}}(\omega)H(\omega))^{-1}H^{\mathcal{H}}(\omega)H_p(\omega) \end{aligned} \tag{E.3}$$

where the superscript $\mathcal{H}$ indicates the Hermitian transpose operator and:

$$\bar{W}_C^*(\omega) = [W_1^*(\omega), W_2^*(\omega), \cdots, W_J^*(\omega)]^T \tag{E.4}$$

Replacing $\bar{W}_C^*(\omega)$ and $\bar{U}_{FFC,i}^*(\omega)$ and equation (5.8) in equation (5.3) yields:

$$\begin{aligned} E(\omega) &= H_p(\omega)X(\omega) + \left(H(\omega)\ \left[-(H^T(\omega)H(\omega))^{-1}H^T(\omega)H_p(\omega)\right]X(\omega)\right) \\ &= \mathcal{O}_{J,1} \end{aligned} \tag{E.5}$$

Where $\mathcal{O}_{J,1}$ is a column vector with size J.

Bibliography

[1] J. S. Vipperman, E. R. Bauer, and D. R. Babich, "Survey of noise in coal preparation plants," *The Journal of the Acoustical Society of America*, vol. 121, no. 1, pp. 197–205, 2007.

[2] M. Alayrac, C. Marquis-Favre, S. Viollon, J. Morel, and G. L. Nost, "Annoyance from industrial noise: Indicators for a wide variety of industrial sources," *The Journal of the Acoustical Society of America*, vol. 128, no. 3, pp. 1128–1139, 2010.

[3] Y. Huang and M. J. Griffin, "The effects of sound level and vibration magnitude on the relative discomfort of noise and vibration," *The Journal of the Acoustical Society of America*, vol. 131, no. 6, pp. 4558–4569, 2012.

[4] S. M. Kuo and D. R. Morgan, "Active noise control: a tutorial review," *Proceedings of the IEEE*, vol. 87, pp. 943–973, Jun 1999.

[5] L. Paul, "Process of silencing sound oscillations," June 9 1936. US Patent 2,043,416.

[6] D. Guicking, "On the invention of active noise control by paul lueg," *The Journal of the Acoustical Society of America*, vol. 87, no. 5, pp. 2251–2254, 1990.

[7] P. de Heering, "Comments on 'on the invention of active noise control by paul lueg' [j. acoust. soc. am. 87, 2251-2254 (1990)]," *The Journal of the Acoustical Society of America*, vol. 93, no. 5, pp. 2989–2989, 1993.

[8] S. Rao, *Engineering Optimization: Theory and Practice*. Wiley Interscience, Wiley, 1996.

[9] J. W. Parkins, S. D. Sommerfeldt, and J. Tichy, "Narrowband and broadband active control in an enclosure using the acoustic energy density," *The Journal of the Acoustical Society of America*, vol. 108, no. 1, pp. 192–203, 2000.

[10] Y. C. Park and S. D. Sommerfeldt, "Global attenuation of broadband noise fields using energy density control," *The Journal of the Acoustical Society of America*, vol. 101, no. 1, pp. 350–359, 1997.

[11] J. W. Parkins, S. D. Sommerfeldt, and J. Tichy, "Error analysis of a practical energy density sensor," *The Journal of the Acoustical Society of America*, vol. 108, no. 1, pp. 211–222, 2000.

[12] A. Gonzalez, A. Albiol, and S. Elliott, "Minimisation of the maximum error signal in active control," in *Acoustics, Speech, and Signal Processing, 1997. ICASSP-97., 1997 IEEE International Conference on*, vol. 1, pp. 387–390 vol.1, 1997.

[13] P. M. Joplin and P. A. Nelson, "Active control of low-frequency random sound in enclosures," *The Journal of the Acoustical Society of America*, vol. 87, no. 6, pp. 2396–2404, 1990.

[14] R. L. Clark and D. G. Cole, "Active damping of enclosed sound fields through direct rate feedback control," *The Journal of the Acoustical Society of America*, vol. 97, no. 3, pp. 1710–1716, 1995.

[15] H. C. Geng, Z. S. Rao, and Z. S. Han, "New modeling method and mechanism analyses for active control of interior noise in an irregular enclosure using piezoelectric actuators," *The Journal of the Acoustical Society of America*, vol. 113, no. 3, pp. 1439–1447, 2003.

[16] B. S. Cazzolato and C. H. Hansen, "Active control of sound transmission using structural error sensing," *The Journal of the Acoustical Society of America*, vol. 104, no. 5, pp. 2878–2889, 1998.

[17] S.-M. Kim and M. J. Brennan, "Active control of harmonic sound transmission into an acoustic enclosure using both structural and acoustic actuators," *The Journal of the Acoustical Society of America*, vol. 107, no. 5, pp. 2523–2534, 2000.

[18] N. Tanaka and K. Kobayashi, "Cluster control of acoustic potential energy in a structural/acoustic cavity," *The Journal of the Acoustical Society of America*, vol. 119, no. 5, pp. 2758–2771, 2006.

[19] T. Kaizuka and N. Tanaka, "Radiation clusters and the active control of sound transmission into a symmetric enclosure," *The Journal of the Acoustical Society of America*, vol. 121, no. 2, pp. 922–937, 2007.

[20] A. Montazeri and J. Poshtan, "Modeling of coupling of loudspeakers for anc system in a confined space," in *Electronic Design, 2008. ICED 2008. International Conference on*, pp. 1–7, 2008.

[21] A. Montazeri, J. Poshtan, and M. Poshtan, "Analysis of the behavior of coupled loudspeakers in a mimo anc system in an enclosure," in *Control Applications (CCA), 2010 IEEE International Conference on*, pp. 228–233, 2010.

[22] T. Pàmies, J. Romeu, M. Genescà, and A. Balastegui, "Sound radiation from an aperture in a rectangular enclosure under low modal conditions," *The Journal of the Acoustical Society of America*, vol. 130, no. 1, pp. 239–248, 2011.

[23] B. Xu and S. D. Sommerfeldt, "A hybrid modal analysis for enclosed sound fields," *The Journal of the Acoustical Society of America*, vol. 128, no. 5, pp. 2857–2867, 2010.

[24] J. Yuan, "A relaxed condition for "perfect" cancellation of broadband noise in 3d enclosures," *The Journal of the Acoustical Society of America*, vol. 107, no. 6, pp. 3235–3244, 2000.

[25] K. Zhou and J. Doyle, *Essentials of Robust Control*. Prentice Hall Modular Series f, Prentice Hall, 1998.

[26] D. Kirk, *Optimal Control Theory: An Introduction*. Dover Books on Electrical Engineering Series, Dover Publications, 2004.

[27] X. H. Yang, J. Van Niekerk, K. S. Parwani, A. Packard, and B. Tongue, "Attenuation of structurally generated interior noise through active control," in *American Control Conference, 1993*, pp. 1–7, 1993.

[28] B. Fang, A. Kelkar, and S. Joshi, "Modelling and control of acoustic-structure interaction in 3-d enclosures," in *Decision and Control, 2002, Proceedings of the 41st IEEE Conference on*, vol. 1, pp. 873–878 vol.1, 2002.

[29] A. Sampath, B. Balachandran, R. Mehra, and R. Prasanth, "Active control of noise in a three-dimensional enclosure using indirect adaptive control," in *Control Applications, 1997., Proceedings of the 1997 IEEE International Conference on*, pp. 848–853, 1997.

[30] F. Liu, B. Fang, and A. Kelkar, "Lqg-based robust broadband control of acoustic-structure interaction in 3-d enclosure," in *American Control Conference, 2003. Proceedings of the 2003*, vol. 1, pp. 803–808 vol.1, 2003.

[31] S. Lane and R. Clark, "Active control of a reverberant enclosure using an approximate constant volume velocity source," in *American Control Conference, 1998. Proceedings of the 1998*, vol. 4, pp. 2606–2610 vol.4, 1998.

[32] T. Yucelen and F. Pourboghrat, "Active noise blocking: Non-minimal modeling, robust control, and implementation," in *American Control Conference, 2009. ACC '09.*, pp. 5492–5497, 2009.

[33] M. De Diego, A. Gonzalez, and C. Garcia, "On the performance of a local active noise control system," in *Acoustics, Speech, and Signal Processing, 1999. Proceedings., 1999 IEEE International Conference on*, vol. 2, pp. 885–888 vol.2, 1999.

[34] J. Landaluze, I. Portilla, J. Pagalday, A. Martínez, and R. Reyero, "Application of active noise control to an elevator cabin," *Control Engineering Practice*, vol. 11, no. 12, pp. 1423 – 1431, 2003. Award winning applications-2002 IFAC World Congress.

[35] S. M. Kuo and J. Tsai, "Residual noise shaping technique for active noise control systems," *The Journal of the Acoustical Society of America*, vol. 95, no. 3, pp. 1665–1668, 1994.

[36] S. D. Sommerfeldt and T. O. Samuels, "Incorporation of loudness measures in active noise control," *The Journal of the Acoustical Society of America*, vol. 109, no. 2, pp. 591–599, 2001.

[37] L. J. Eriksson, "Development of the filtered-u algorithm for active noise control," *The Journal of the Acoustical Society of America*, vol. 89, no. 1, pp. 257–265, 1991.

[38] B. Wu and M. Bodson, "Direct adaptive cancellation of periodic disturbances for multivariable plants," in *Decision and Control, 2002, Proceedings of the 41st IEEE Conference on*, vol. 3, pp. 3079–3084 vol.3, 2002.

[39] B. Wu and M. Bodson, "Direct adaptive cancellation of periodic disturbances for multivariable plants," *Speech and Audio Processing, IEEE Transactions on*, vol. 11, no. 6, pp. 538–548, 2003.

[40] C. X. Tan and H. Tachibana, "Nonlinearity-tolerated active noise control using an artificial neural network," in *Applications of Signal Processing to Audio and Acoustics, 1997. 1997 IEEE ASSP Workshop on*, pp. 4 pp.–, 1997.

[41] R. Bambang, L. Anggono, and K. Uchida, "Dsp based rbf neural modeling and control for active noise cancellation," in *Intelligent Control, 2002. Proceedings of the 2002 IEEE International Symposium on*, pp. 460–466, 2002.

[42] A. Montazeri and J. Poshtan, "Design of a mimo neuro-controller for anc system with loudspeaker nonlinearity in enclosure," in *Signal Processing and Communications, 2007. ICSPC 2007. IEEE International Conference on*, pp. 1415–1418, 2007.

[43] A. Montazeri, J. Poshtan, and M. Jahed-Motlagh, "Evaluating the performance of a nonlinear active noise control system in enclosure," in *Industrial Electronics Society, 2007. IECON 2007. 33rd Annual Conference of the IEEE*, pp. 2484–2488, 2007.

[44] S. Elliott, I. Stothers, and P. Nelson, "A multiple error lms algorithm and its application to the active control of sound and vibration," *Acoustics, Speech and Signal Processing, IEEE Transactions on*, vol. 35, no. 10, pp. 1423–1434, 1987.

[45] S. Elliott, C. Boucher, and P. Nelson, "The behavior of a multiple channel active control system," *Signal Processing, IEEE Transactions on*, vol. 40, no. 5, pp. 1041–1052, 1992.

[46] S. Elliott and C. Boucher, "Interaction between multiple feedforward active control systems," *Speech and Audio Processing, IEEE Transactions on*, vol. 2, no. 4, pp. 521–530, 1994.

[47] A. Montazeri, J. Poshtan, and M. H. Kahaei, "Optimal placement of loudspeakers and microphones in an enclosure using genetic algorithm," in *Control Applications, 2003. CCA 2003. Proceedings of 2003 IEEE Conference on*, vol. 1, pp. 135–139 vol.1, 2003.

[48] D. Li and M. Hodgson, "Optimal active noise control in large rooms using a "locally global" control strategy," *The Journal of the Acoustical Society of America*, vol. 118, no. 6, pp. 3653–3661, 2005.

[49] S. Elliott and A. David, "A virtual microphone arrangement for local active sound control," in *1st international conference on motion and vibration control*, 2011.

[50] J. Garcia-Bonito, S. J. Elliott, and C. C. Boucher, "Generation of zones of quiet using a virtual microphone arrangement," *The Journal of the Acoustical Society of America*, vol. 101, no. 6, pp. 3498–3516, 1997.

[51] A. Roure and A. Albarrazin, "The remote microphone technique for active noise control," *Proceedings of Active 1999, Fort Lauderdale*, pp. 1233–1244, 1999.

[52] C. D. Petersen, R. Fraanje, B. S. Cazzolato, A. C. Zander, and C. H. Hansen, "A kalman filter approach to virtual sensing for active noise control," *Mechanical Systems and Signal Processing*, vol. 22, no. 2, pp. 490 – 508, 2008.

[53] D. J. Moreau, J. Ghan, B. S. Cazzolato, and A. C. Zander, "Active noise control in a pure tone diffuse sound field using virtual sensing," *The Journal of the Acoustical Society of America*, vol. 125, no. 6, pp. 3742–3755, 2009.

[54] D. P. Das, D. J. Moreau, and B. S. Cazzolato, "A nonlinear active noise control algorithm for virtual microphones controlling chaotic noise," *The Journal of the Acoustical Society of America*, vol. 132, no. 2, pp. 779–788, 2012.

[55] C. D. Kestell, B. S. Cazzolato, and C. H. Hansen, "Active noise control in a free field with virtual sensors," *The Journal of the Acoustical Society of America*, vol. 109, no. 1, pp. 232–243, 2001.

[56] J. M. Munn, B. S. Cazzolato, C. D. Kestell, and C. H. Hansen, "Virtual error sensing for active noise control in a one-dimensional waveguide: Performance prediction versus measurement (l)," *The Journal of the Acoustical Society of America*, vol. 113, no. 1, pp. 35–38, 2003.

[57] J. Yuan, "Virtual sensing for broadband noise control in a lightly damped enclosure," *The Journal of the Acoustical Society of America*, vol. 116, no. 2, pp. 934–941, 2004.

[58] R. Quintana, L. Piroddi, and D. Patino, "Virtual sensing at low computational cost for active noise control," *INTER-NOISE and NOISE-CON Congress and Conference Proceedings*, vol. 250, no. 4, pp. 2989–2997, 2015.

[59] N. Miyazaki and Y. Kajikawa, "Head-mounted active noise control system with virtual sensing technique," *Journal of Sound and Vibration*, vol. 339, pp. 65 – 83, 2015.

[60] H. Lim, S. V. Utyuzhnikov, Y. W. Lam, and L. Kelly, "Potential-based methodology for active sound control in three dimensional settings," *The Journal of the Acoustical Society of America*, vol. 136, no. 3, pp. 1101–1111, 2014.

[61] M. Jessel and G. Mangiante, "Active sound absorbers in an air duct," *Journal of Sound and Vibration*, vol. 23, no. 3, pp. 383 – 390, 1972.

[62] G. Canevet, "Active sound absorption in an air conditioning duct," *Journal of Sound and Vibration*, vol. 58, no. 3, pp. 333 – 345, 1978.

[63] S. Uosukainen, "Modified jmc method in active control of sound," *Acta Acustica united with Acustica*, vol. 83, no. 1, pp. 105–112, 1997.

[64] S. Ise, "A principle of sound field control based on the kirchhoff-helmholtz integral equation and the theory of inverse systems," *Acta Acustica united with Acustica*, vol. 85, no. 1, pp. 78–87, 1999.

[65] N. Epain and E. Friot, "Active control of sound inside a sphere via control of the acoustic pressure at the boundary surface," *Journal of Sound and Vibration*, vol. 299, no. 3, pp. 587 – 604, 2007.

[66] M. L. Munjal and L. J. Eriksson, "An analytical, one dimensional, standing wave model of a linear active noise control system in a duct," *The Journal of the Acoustical Society of America*, vol. 84, no. 3, pp. 1086–1093, 1988.

[67] B. Kwon and Y. Park, "Active window based on the prediction of interior sound field: experiment for a band-limited noise," in *Inter-Noise 2011*, 2011.

[68] H. Lim, S. V. Utyuzhnikov, Y. W. Lam, and A. Turan, "Multi-domain active sound control and noise shielding," *The Journal of the Acoustical Society of America*, vol. 129, no. 2, pp. 717–725, 2011.

[69] J. Loncaric, V. S. Ryaben'kii, and S. V. Tsynkov, "Active shielding and control of noise," *SIAM Journal on Applied Mathematics*, vol. 62, no. 2, pp. 563–596, 2001.

[70] V. Ryaben'kii and S. Utyuzhnikov, "Differential and finite-difference problems of active shielding," *Applied Numerical Mathematics*, vol. 57, no. 4, pp. 374 – 382, 2007.

[71] V. Ryaben'kii, S. Tsynkov, and S. Utyuzhnikov, "Inverse source problem and active shielding for composite domains," *Applied Mathematics Letters*, vol. 20, no. 5, pp. 511 – 515, 2007.

[72] A. Loghmani, M. Danesh, M. K. Kwak, and M. Keshmiri, "Active structural acoustic control of a smart cylindrical shell using a virtual microphone," *Smart Materials and Structures*, vol. 25, no. 4, p. 045020, 2016.

[73] J. Bay, *Fundamentals of Linear State Space Systems*. Electrical Engineering Series, WCB/McGraw-Hill, 1999.

[74] S. J. Elliott, "Distributed control of sound and vibration," *Noise Control Engineering Journal*, vol. 53, no. 5, pp. 165–180, 2005.

[75] S. Spors and H. Buchner, "Efficient massive multichannel active noise control using wave-domain adaptive filtering," in *Communications, Control and Signal Processing, 2008. ISCCSP 2008. 3rd International Symposium on*, pp. 1480–1485, March 2008.

[76] K. D. Frampton, O. N. Baumann, and P. Gardonio, "A comparison of decentralized, distributed, and centralized vibro-acoustic control," *The Journal of the Acoustical Society of America*, vol. 128, no. 5, pp. 2798–2806, 2010.

[77] R. Scattolini, "Architectures for distributed and hierarchical model predictive control - a review," *Journal of Process Control*, vol. 19, no. 5, pp. 723 – 731, 2009.

[78] S. J. Elliott, P. Gardonio, T. C. Sors, and M. J. Brennan, "Active vibroacoustic control with multiple local feedback loops," *The Journal of the Acoustical Society of America*, vol. 111, no. 2, pp. 908–915, 2002.

[79] E. Bianchi, P. Gardonio, and S. Elliott, "Smart panel with multiple decentralized units for the control of sound transmission. part iii: control system implementation," *Journal of Sound and Vibration*, vol. 274, no. 1-2, pp. 215 – 232, 2004.

[80] L. Zhang, J. Tao, and X. Qiu, "Performance analysis of decentralized multichannel feedback systems for active noise control in free space," *Applied Acoustics*, vol. 74, no. 1, pp. 181 – 188, 2013.

[81] W. P. Engels, O. N. Baumann, S. J. Elliott, and R. Fraanje, "Centralized and decentralized control of structural vibration and sound radiation," *The Journal of the Acoustical Society of America*, vol. 119, no. 3, pp. 1487–1495, 2006.

[82] S. Spors, H. Buchner, and R. Rabenstein, "Eigenspace adaptive filtering for efficient pre-equalization of acoustic mimo systems," in *Signal Processing Conference, 2006 14th European*, pp. 1–5, Sept 2006.

[83] N. V. George and G. Panda, "A particle-swarm-optimization-based decentralized nonlinear active noise control system," *IEEE Transactions on Instrumentation and Measurement*, vol. 61, pp. 3378–3386, Dec 2012.

[84] T. Li, Z. Wang, J. Li, and Y. Ma, "Distributed vibration control of tensegrity structure," *Journal of Vibration and Control*, vol. 19, no. 5, pp. 720–728, 2013.

[85] M. Yuan, J. Qiu, H. Ji, W. Zhou, and R. Ohayon, "Active control of sound transmission using a hybrid/blind decentralized control approach," *Journal of Vibration and Control*, vol. 21, no. 13, pp. 2661–2684, 2015.

[86] M. Yuan, R. Ohayon, and J. Qiu, "Decentralized active control of turbulent boundary induced noise and vibration: a numerical investigation," *Journal of Vibration and Control*, vol. 22, no. 18, pp. 3821–3839, 2016.

[87] M. Latos and K. Stankiewicz, "Studies on the effectiveness of noise protection for an enclosed industrial area using global active noise reduction systems," *Journal of low frequency noise, vibration and active control*, vol. 34, no. 1, pp. 9 – 20, 2015.

[88] J. Tao, S. Wang, X. Qiu, and J. Pan, "Performance of an independent planar virtual sound barrier at the opening of a rectangular enclosure," *Applied Acoustics*, vol. 105, pp. 215 – 223, 2016.

[89] N. V. George and G. Panda, "Advances in active noise control: A survey, with emphasis on recent nonlinear techniques," *Signal Processing*, vol. 93, no. 2, pp. 363 – 377, 2013.

[90] D. P. Das and G. Panda, "Active mitigation of nonlinear noise processes using a novel filtered-s lms algorithm," *IEEE Transactions on Speech and Audio Processing*, vol. 12, pp. 313–322, May 2004.

[91] K. Chen, R. Paurobally, J. Pan, and Q. X., "Adaptive feedback noise control with leaky felms algorithm," *INTER-NOISE and NOISE-CON Congress and Conference Proceedings*, 2014.

[92] A. J. Antunes, R. C. Leal-Toledo, O. T. da Silveira Filho, and E. M. Toledo, "Finite difference method for solving acoustic wave equation using locally adjustable time-steps," *Procedia Computer Science*, vol. 29, pp. 627 – 636, 2014.

[93] B. Hamilton and S. Bilbao, "Optimised 25-point finite difference schemes for the three-dimensional wave equation," in *International conference on acoustics ICA 2016*, 2016.

[94] S. J. Elliott and J. Cheer, "Modeling local active sound control with remote sensors in spatially random pressure fields," *The Journal of the Acoustical Society of America*, vol. 137, no. 4, pp. 1936–1946, 2015.

[95] F. Vega-Redondo, *Economics and the Theory of Games*. Cambridge University Press, 2003.

[96] B. Widrow, J. McCool, M. Larimore, and C. Johnson, "Stationary and nonstationary learning characteristics of the lms adaptive filter," *Proceedings of the IEEE*, vol. 64, no. 8, pp. 1151–1162, 1976.

[97] D. Morgan, "An analysis of multiple correlation cancellation loops with a filter in the auxiliary path," *IEEE Transactions on Acoustics, Speech, and Signal Processing*, vol. 28, pp. 454–467, Aug 1980.

[98] J. Daafouz and J. Bernussou, "Parameter dependent lyapunov functions for discrete time systems with time varying parametric uncertainties," *Systems & Control Letters*, vol. 43, no. 5, pp. 355 – 359, 2001.

[99] R. Quintana and D. Patino, "Shielding the source," in *International Conference on Acoutics, ICA 2016*, 2016.

[100] L. Ljung, *System Identification - Theory For the User*. Upper Saddle River, N.J.: PTR Prentice Hall, 2 ed., 1999.

[101] S. Miranda and C. Garcia, "Subspace identification using the integration of moesp and n4sid methods applied to the shell benchmark of a distillation column," in *Proceedings of the 9th Brazilian Conference on Dynamics Control and their Applications*, 2010.